UNIVERSITY OF SOUTHAMPTON

FACULTY OF ENGINEERING AND APPLIED SCIENCE

Department of Ship Science

FORCES ON A CYLINDER IN A VORTEX FLOW FIELD

by

Brian Ward BSc

A Thesis Submitted for the Degree of MPhil

1993

UNIVERSITY OF SOUTHAMPTON

ABSTRACT

FACULTY OF ENGINEERING AND APPLIED SCIENCE

SHIP SCIENCE

Master of Philosophy

FORCES ON A CYLINDER IN A VORTEX FLOW FIELD

by

Brian Ward BSc

1993

This thesis makes a study into submarine manoeuvring research and in particular the prediction of forces on a turning submarine. A history of the subject is given, and experiment and theoretical methods are described.

A lengthy experiment to examine the flow around an appended body of revolution in a water channel is described. Flow and pressure measurements are presented. Conclusions made state that an appendage acts as a spoiler to the flow when attached to a body of revolution in flow. This arrangement causes an asymmetry in the flow pattern and subsequently an asymmetry in the pressure distribution.

A simple computer model is described but predictions with experiment results are poor.

Contents

Acknowledgements

The following peoples' contributions towards completion of this thesis were appreciated.

Mr P A Wilson of the Ship Science Department at the University of Southampton who supervised my studies.

Dr A R J M Lloyd of DRA Haslar who initiated the experiments described in this thesis.

Mr M Risk who set up the experiment and advised on the design of the traverse rig used.

Mr E Denness who assisted with rigging the model and instrumentation during the experiments.

Mr B Dawson who assisted with rigging the model.

Mr D Ball, Mr A Hunt and Mr W Wallace of the DRA Haslar drawing office who designed the model and managed the contractors who designed the traverse rig.

Mr A Dacombe who provided the computer acquisition system used and wrote part of the software.

Mr M Smith who assisted with software problems during the experiment and wrote part of the software.

Mrs E Kent who traced many of the figures.

Miss P Miles the librarian who provided many of the references used in this thesis.

Mr B Briscoe who allowed me more time in the facility.

The DRA Haslar workshop who manufactured the model.

Mr P Wilson and the photographic section who produced all the photographs.

Mrs K Greenaway and Mr P Goddard who photocopied the thesis.

Dr B Taylor of Department of Mathematical Studies at the University of Portsmouth whose unpublished work was a valuable source of reference.

Notation

Roman

a_c Aspect ratio

$$\frac{2S}{c}$$

A Maximum cross-sectional area of hull or area of appendage — m^2

c Chord length — m

C_L Lift coefficient :

$$\frac{L}{\frac{1}{2}\rho U^2 A}$$

C_P Prismatic coefficient of hull :

$$\frac{V}{AL}$$

C'_P Pressure coefficient :

$$\frac{P}{\frac{1}{2}\rho U^2}$$

D Diameter of body of revolution — m

F_N Froude number

$$\frac{V}{\sqrt{gL}}$$

F'_Y Side force per unit length/$0.5\rho U^2 L$: positive to starboard

F'_Z Downward force per unit length/$0.5\rho U^2$: positive down

g Acceleration due to gravity — m/s^2

k_{cn} Factor to allow for effects of viscous vortex core in nth vortex

k_{cin} Factor to allow for effects of viscous vortex core in nth image vortex

k_1, k_2 Lamb's added mass coefficients for a prolate ellipsoid

K Calibration factor for Freestone probe

L Length of hull — m

or lift on hydroplane — kN

m Mass of hull — tonnes

M Total pitch moment : positive bow up — kNm

or Munk moment

M′ Non dimensional pitch moment

$$\frac{M}{\frac{1}{2}\rho U^2 L^3}$$

M'_w Non dimensional linear pitch moment/ heave velocity coefficient for hull

$M'_{w|w|}$ Non dimensional second order pitch moment/ heave velocity coefficient for hull

N'_v Yaw moment due to yaw velocity

P Pressure — Nm^{-2}

q Velocity normal to specific point on hull — m/sec

r Radius from body axis to position of probe — m

r′ Non dimensional rate of turn or turn parameter :

$$\frac{L}{S}$$

r_* Core radius of vortex — m

R Radius of model at cross-section — m

R_e	Reynold's number : $\frac{UD}{\nu}$	
R_F	Reduction factor for strength of deck vortex	
S	Arm radius ; radius of turn or Span of hydroplane	m
S_1	Spanwise location of fin vortex from root of hydroplane	m
S_D	Longitudinal point of separation -deck side of body	m
S_K	Longitudinal point of separation -keel side of body	m
U	Flow velocity	m/sec
v	Velocity in y direction : positive to starboard	m/sec
v_s	Local lateral velocity of hull section : positive to starboard	m/sec
V	Volume of hull	m^3
w	Complex conjugate velocity of fluid in transverse plane relative to hull	m/sec
or	Velocity in z direction	m/sec
w_s	Local vertical velocity of hull section : positive down	m/sec
x	Longitudinal distance from nose of body : positive aft	m
x'	Non dimensional distance from nose to body : $\frac{x}{L}$	
y	Lateral distance from body centre :	mm

y_{max} y location of maximum vorticity : positive starboard — mm

y_t Lateral scale on traverse rig : positive starboard — mm

Y'_v Non dimensional side force/ lateral velocity coefficient for hull

z Vertical distance from body centre — mm

z_{max} z location of maximum vorticity — mm

Z Total force in z direction : positive down — kN

Z' Non dimensional Z force

$$\frac{Z}{\frac{1}{2}\rho U^2 L^2}$$

Z'_w Non dimensional linear heave force/ heave velocity coefficient for hull

$Z'_{w|w|}$ Non dimensional second order heave force/ heave velocity coefficient for hull

Greek

α Angle of incidence : positive nose to starboard, body incidence relative to channel axis, appendage incidence relative to body axis — deg

α' Angle of local transverse velocity $\alpha'=\tan^{-1}[w_s/-v_s]$ — deg

δ Radius of Freestone probe — m

θ Angle of strut — deg

θ_p Angular location of pressure tapping 0 degrees pointing up, positive clockwise looking forward — deg

ζ	Complex co-ordinate of a point in the transverse plane	m
ζ_n	Complex co-ordinate of centre of nth real vortex	m
ζ_x	Streamwise vorticity	rad/sec
ρ	Mass density of water	tonnes/m^3
υ	Kinematic viscocity	m^2/sec
Γ	Circulation	m^2/sec
Γ_θ	Circulation density	m^2/s/rad
Γ_D	Circulation from body - deck side : positive clockwise looking forward	m^2/sec
Γ_F	Circulation from fin positive clockwise looking forward	m^2/sec
Γ_K	Circulation from body - keel side : positive clockwise looking forward	m^2/sec
ΔP	Pressure difference	N/m^2

Preface

Introduction

The submarine has played an important part in naval fleets during the 20th century. The importance of a good knowledge of the stability and manoeuvring performance of a submersible was greatly increased when high speed streamlined vessels were introduced in the early 1960s. A comprehensive account of the history of submersibles is given in Horton [1]. Arentzen and Mandel [2] contain a wealth of information with particular reference to American submarines.

This thesis makes a study of submarine manoeuvring research and in particular the prediction of forces on a turning submarine.

Chapter 1 deals with the manoeuvring of submarines and the importance of this property.

Chapter 2 gives a historical review of research into forces on bodies of revolution and simulation methods of submarine manoeuvring.

Chapter 3 describes experimental estimates of forces on bodies and Chapter 4 describes the alternative theoretical methods that have been used.

Chapter 5 describes a series of lengthy experiments conducted at DRA Haslar during 1990 and 1991 where the measured vortex flow and pressure distributions around an appended and unappended body of revolution, were obtained.

Chapter 6 describes the analysis and comments on the experiment results.

Chapter 7 describes a simple computational method of estimating the forces on an appended body of revolution making use of semi-empirical techniques and classical

theory. A comparison is made between the estimates and experiment results of chapter 5.

Conclusions are made in chapter 8 and suggestions for future work are made.

Chapter 1

Introduction to Submarine Manoeuvring

The role of the submarine is well established as one of the most important naval ship types in existance today. Not only does the submarine contribute to maintaining a naval presence, but it contributes towards peaceful pursuits through oceanographic research and has a potential for commercial utilisation.

British submarine design developed in a similar way to that of the United States after the Second World War had ended. The first British nuclear submarine Dreadnought (launched 1960) was greatly influenced by American design experience. The Americans have developed submarines for different roles; the most important of these has been the Polaris 'boats' which have been the main deterent since the 1960's being used as the launch pad of ballistic missiles. Similar developments took place in the Soviet Union during the Cold War period of 1945 until the late eighties. HMS Vanguard (Figure 1), built by Vickers was launched from Barrow-in-Furness during 1992 and is the first of class of the Trident submarines.

Submarines can now operate undetected for long periods in waters dominated by enemy air and surface forces. If the submarine goes too deep it will collapse: if it comes to the surface it will be detected by the enemy. However the submarine can only operate in a layer that is several times deeper than its own length. Consequently accurate depth control is vitally important to allow lateral and vertical manoeuvrablity in tactical situations.

Modern vessels are capable of high speeds and can turn in only a few boat-lengths. Diving depths have increased but these are still only measured in a few hull-lengths so manoeuvres in the vertical plane are extremely restricted. Restrictions are more critical at high speeds as the submarine may have to recover in an emergency say if

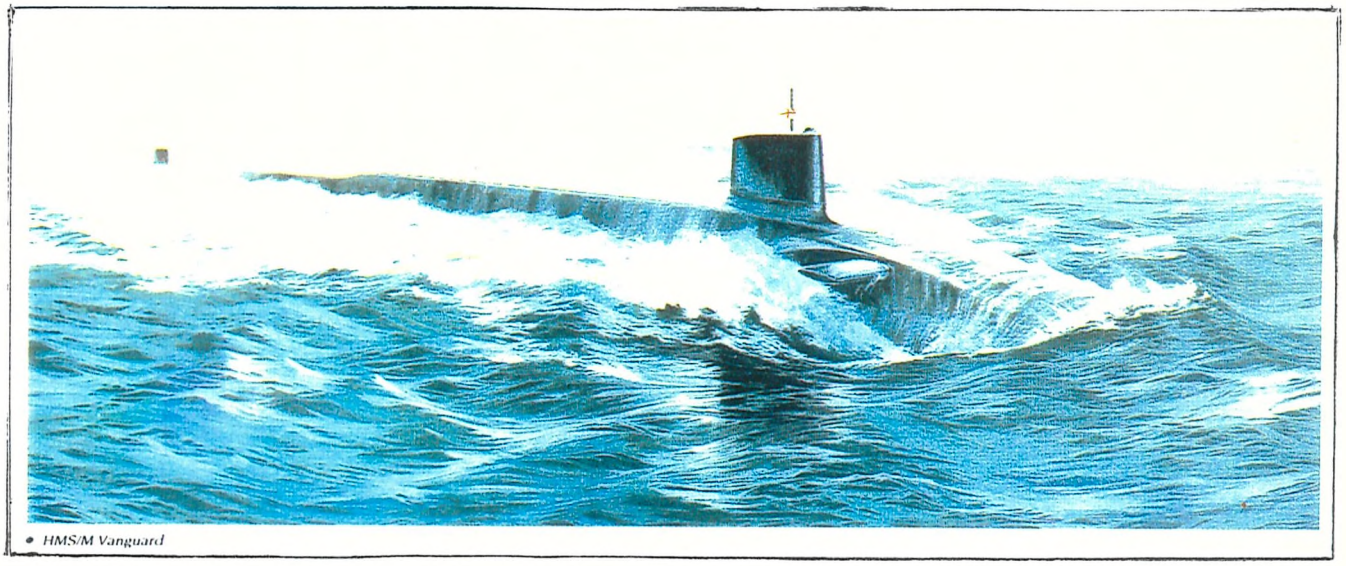

FIG.1 HMS VANGUARD

hydroplanes were to jam. Before construction of a new vessel starts it is necessary to ensure that it will have satisfactory static and dynamic stability and that its controls will give the desired responsiveness. Analytical information about the vessel's dynamics is also required in order to design an automatic pilot that is capable of simultaneously controlling depth and course. When the vessel enters service it is necessary to advise the crew on the limits of safe manoeuvring in the form of maximum control surface deflections for any combination of speed and depth. This is often termed the vessels operating envelope. Within the specified limits for example the vessel must be able to recover from a jammed hydroplane emergency. Maximum rudder deflection for any approach speed must be known to ensure that transient roll angles and depth excursions are within safe limits. Roll angles must be constrained to keep the submarine stable. As an aid to training and research a good mathematical model is required in order to provide a simulator.

In the vertical (& horizontal) plane there are basically four performance criteria as noted in Arentzen and Mandel [2] as;

1. Ability to maintain constant depth or course with minimum plane movement and minimum depth (course) error.
2. Ability to enter into a manoeuvre as rapidly as possible.
3. Ability to exit from a manoeuvre as rapidly as possible.
4. Ability to return to equilibrium as quickly as possible when the control surfaces are reduced to zero positions.

An additional performance criterion required only in the horizontal plane, is the ability to execute a steady-turning manoeuvre with a minimum tactical diameter, advance, transfer, loss of speed, and with minimum cross-coupled motions such as roll. This is necessary as the submarine might be chased by an enemy submarine therefore responsiveness is required in most situations.

A detailed knowledge of the hydrodynamic forces is

therefore necessary for the submarine designer who needs to be able to predict the submerged manoeuvring, stability and control characteristics of a new submarine design at an early stage for comparison with the required design principals. This has led to theoretical and experimental work to determine hydrodynamic forces acting on submarines and hence the prediction of the subsequent manoeuvre.

Chapter 2

Historical Review

2.1 Theoretical Estimates of Forces on a Body

The traditional submarine hull shape is not unlike a body of revolution with a rounded nose and pointed tail. Hence the work covered in the area of the prediction of forces on circular bodies is of interest to the scientist and engineer involved in the study of submarine dynamics. The following sections look at various methods of estimating forces on a body of revolution.

2.2 The Estimation of Forces on a Body of Revolution

Work regarding forces on bodies of revolution emerged with the advent of the airship. Interest subsided with the Hindenburg disaster. Following the Second World War submarine development progressed without too much experimental work taking place. Much experimental data on circular bodies has in the past been concerned with missiles (blunt bodied) which are not directly appropriate and applicable to submarines.

Munk [3] applied Lamb's classical theory [4] to airship hulls in the 1920's. This method has tended to overpredict forces on submarine type bodies probably because they are not ellipsoids due to the pointed tail. This theory deals only with potential flow and does not account for any viscous effects. It is probable that empirical corrections could be used to overcome these problems ; however, there are a multitude of other problems associated with shapes that diverge significantly from ellipsoids.

Von Karman [5] conducted a similar investigation. His theoretical methods involved the use of sources, sinks and doublets to calculate the potential flow around the body. These methods are described further in chapter 4.

Nonweiler (referenced in Spencer [6]) attempted a more detailed estimation of the effect of boundary layer over the stern of a submarine hull. From airship experiment results he arrived at a formula applicable to turbulent flow as follows.

$$Z_w = -\frac{1.5D}{(R_e)^{\frac{1}{5}}L} \qquad (2.1)$$

Lotz [7] developed a method in which sources and sinks are placed upon the surface of the rotational symmetric body. Her method was developed by Smith and Pierce [8] and subsequently by Hess and Smith [9]. This method is universally known as the 'panel method' and is more accurate in the calculation of potential flow but requires the evaluation of very involved simultaneous integral equations which can be computationally intensive.

The separated flow that exists on a submarine during high speed turns say, has a significant effect on the hydrodynamic forces and moments and the manoeuvring performance. This has posed a large problem for the theoretical treatment in attempting to determine the forces on the hull. The most obvious solution is to use an empirical estimate derived from model experiments (Mackay [10], Van den Pol [11]).

Van den Pol [11] used Von Karman's method to estimate forces on a body of revolution. The trajectory and strength of the vortex pair are then computed using experiment data on the separation line as a boundary condition and the resulting 'viscous' contribution to the local normal force is added to the potential flow result.

Discrete vortex methods have been developed by Mendenhall et al [12] and Tinker [13]. Tinker has shown predictions of forces and moments to be good but the methods are highly computational.

Work in the computational fluid dynamics (CFD) area is progressing towards solutions of the Navier-Stokes equations using highly computational mathematical techniques. This work typically involves the use of super computers which are used to perform the rigorous numerical methods required at a fast computational speed. Figure 2 shows a velocity-contour plot from a Reynolds-Average Navier-Stokes (RANS) solution. The complete flow field, including the effect of wall and support struts, is solved using computational fluid dynamics techniques. This figure appeared on the cover of Reference 14 and was contributed by the David Taylor Research Centre (now Ship Hydromechanics Department, Carderock Division, Naval Surface Warfare Center).

The rapid technological expansion that was taking place in the area of submarine stability and control in the late 1950's initiated a program of in-house research at DTRC (David Taylor Research Centre) in the United States. This research led ultimately to what are now considered to be standard equations of motion for submarines presented by Gertler and Hagen [15] and subsequently revised by Feldman [16]. The decision made at that time was to develop general equations of motion for six degrees of freedom which could be used in conjuction with coefficients (described in Chapter 3) which relate forces to velocities and accelerations obtained from *scale* model experiments. Below is an example of one of these equations and details of the terms and notation can be found in Feldman [16].

This in turn led to the development of computer programs which used these standard equations of motion to simulate submarine manoeuvres. The input data required for these computer programs are the hydrodynamic coefficients. This is known as the conventional derivative approach to predicting submarine manoeuvres.

Numerical simulation avoids lengthy programmes of model tests and provides data during the early design process. A number of designs can be tried out using computer

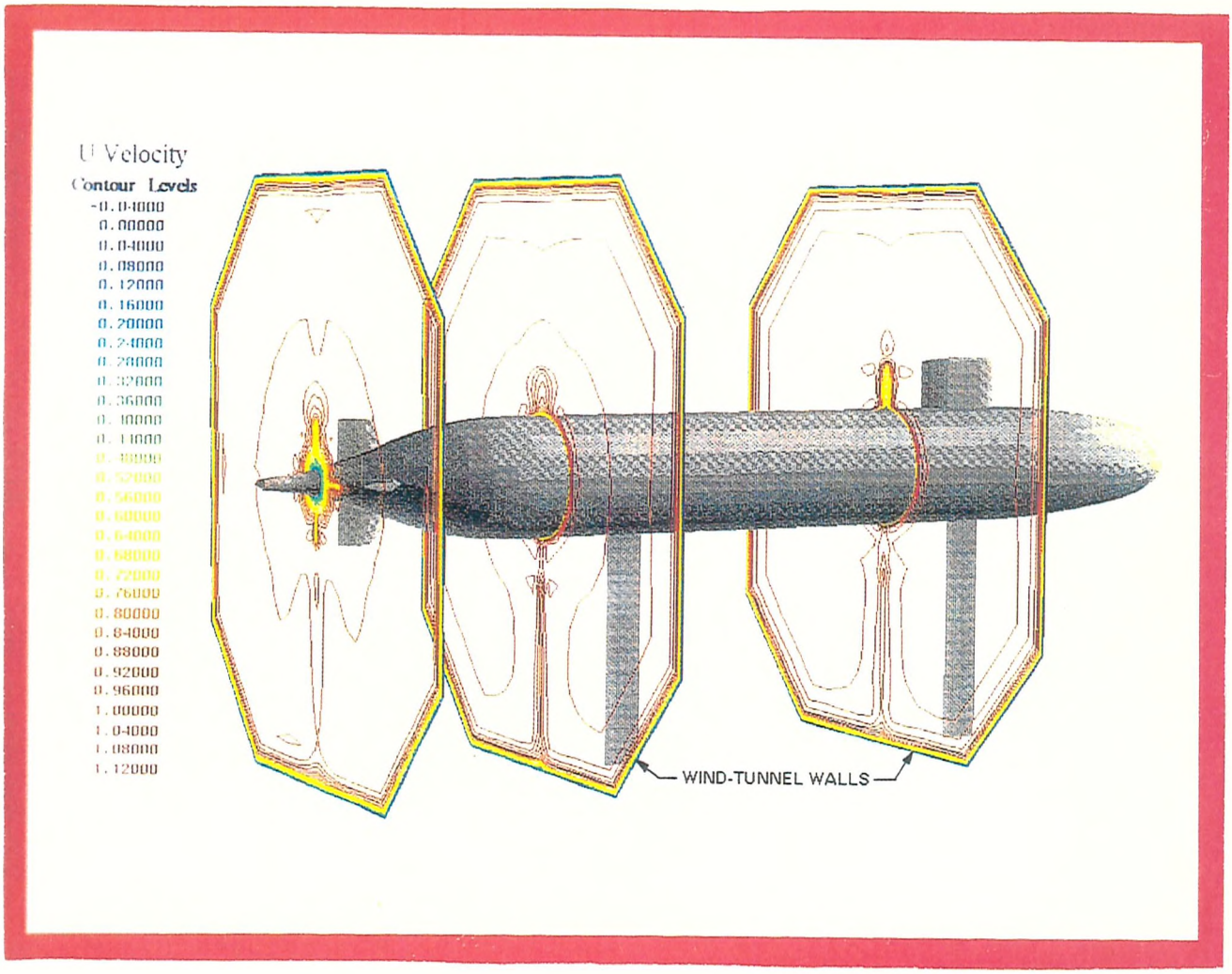

FIG.2 A SUBMARINE HULL IN A WIND TUNNEL
A CFD APPROACH

NORMAL FORCE EQUATION

$$m\left[\dot{w} - uq + vp - z_G(p^2 + q^2) + x_G(rp - \dot{q}) + y_G(rq + \dot{p})\right] =$$

$$+ \frac{\rho}{2} \ell^4 Z_{\dot{q}}' \dot{q}$$

$$+ \frac{\rho}{2} \ell^3 \left[Z_{\dot{w}}' \dot{w} + Z_q' uq + Z_{vp}' vp\right]$$

$$+ \frac{\rho}{2} \ell^2 \left[Z_*' u^2 + Z_w' uw\right]$$

$$+ \frac{\rho}{2} \ell^2 \left[Z_{|w|}' u|w| + Z_{ww}' |w(v^2 + w^2)^{1/2}|\right]$$

$$+ \frac{\rho}{2} \ell^2 \left[Z_{\delta s}' u^2\delta_s + Z_{\delta b}' u^2\delta_b + Z_{\delta s\eta}' u^2\delta_s \left(\eta - \frac{1}{C}\right) C\right]$$

$$- \frac{\rho}{2} C_d \int_{\ell} b(x)\, w(x) \left\{[w(x)]^2 + [v(x)]^2\right\}^{1/2} dx$$

$$+ \frac{\rho}{2} \ell \bar{C}_L \int_{x_2}^{x_1} v(x)\, \bar{v}_{FW}(t - \tau[x])\, dx$$

$$+ (W - B) \cos\Theta \cos\phi$$

simulation and once a good design has been apparently achieved then the model testing phase can take place. This allows the designer to try out *unusual* designs such as that shown in Figure 3 where there are three hydroplanes at the stern and four at the front rather than the conventional two bow planes, two stern planes and two rudders.

2.3 Predictions of Submarine Manoeuvres without Model Experiments

As previously stated, the conventional derivative based mathematical model requires hydrodynamic derivatives often obtained by the lengthy and expensive process of model experiments. More recent simulation methods avoid this

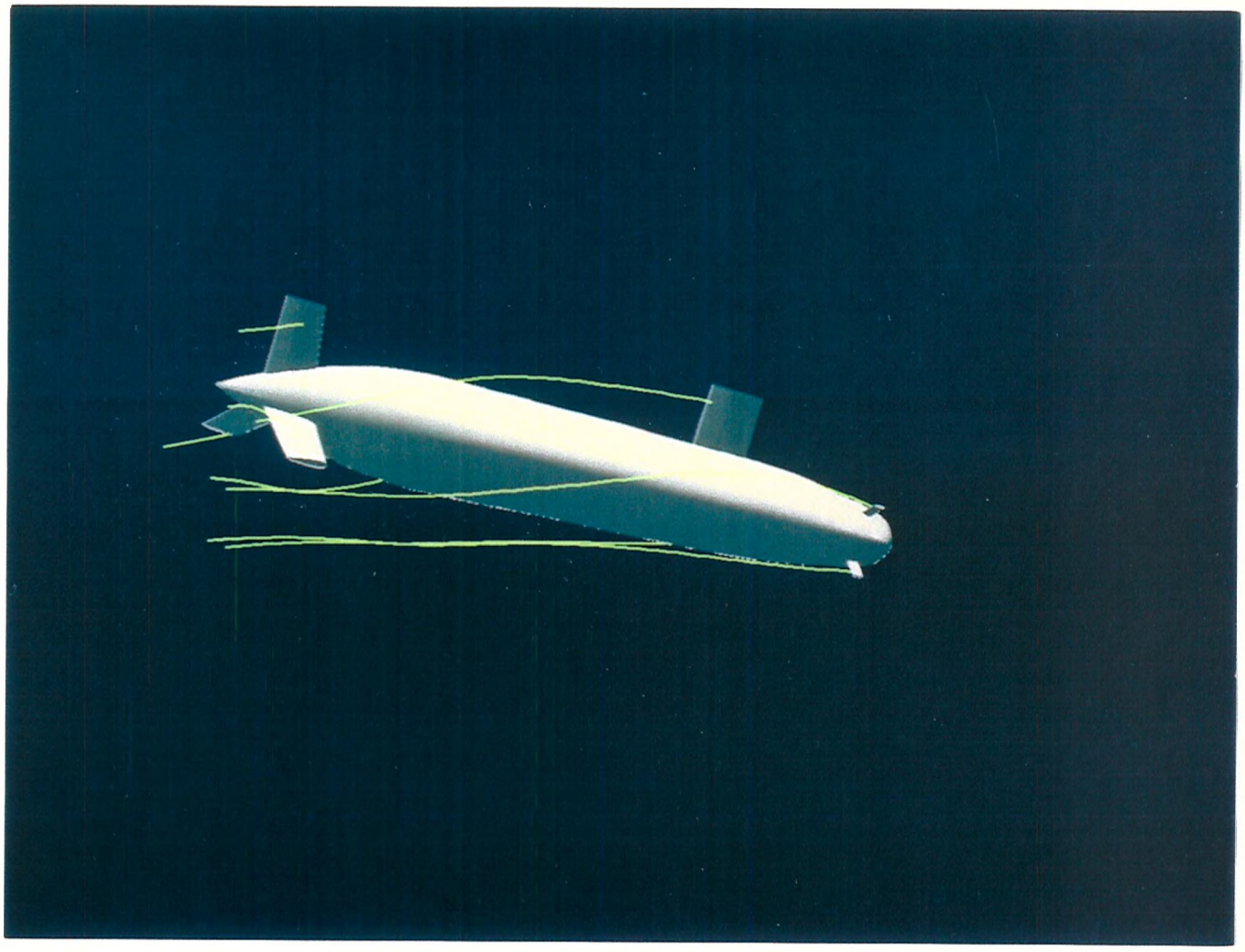

FIG.3 UNCONVENTIONAL SUBMARINE CONFIGURATION

lengthy programme of model tests and can provide data during the early design process.

Bohlmann [17,18] uses the standard equations of motion together with ancillary analytic methods to predict the coefficients (in particular Slender Body Theory as described in Newman [19]). In comparison with 47 measured PMM values; 37 predicted values deviated by 20% and 30 less than 10%. During his presentation at the 'RINA 1991 Symposium on Naval Submarines' he stated that the Feldman equations should be modified further.

MacKay [10,20] has used a panel method to predict forces on a submarine but the method is computationally intensive. The naval architect needs to assess the manoeuvring characteristics of an early design within a reasonable time which makes SUBSIM developed by Lloyd [21,22] a more attractive proposal.

2.4 SUBSIM - a model for the prediction of submarine manoeuvres

SUBSIM is a mathematical model developed by Lloyd [21,22] which predicts deeply submerged submarine manoeuvres using a knowledge of the submarine hull and appendage dimensions together with details of mass, inertias, BG etc. No ad hoc model test data is required and the model can therefore be used to predict submarine manoeuvring characteristics during the early stages of a design.

Lloyd opted for a quick empirical approach to calculate the forces and moments on the hull. These are calculated by functions which relate the forces to the fineness ratio and prismatic coefficient. These functions were derived from model experiments on bodies of revolution conducted by DTRC. Examples of other experiments used to gather empirical data in order to derive functions to enhance the program are described in Ward [23].

Glauert's lifting line theory [24] is used to compute forces generated by the submarines' appendages (hydroplanes, rudders and bridge fin), with an empirical correction derived from Whicker and Fehlner's formula [25]. Glauert's theory tends to over predict lift on aspect ratios less than three which is the range that submarine appendages lie within. Hence the need for Whicker's formula which was derived from low aspect ratio hydroplanes.

The out-of-plane forces on the hull due to appendage vortices and their interaction with body vortices are calculated by Blasius' Theorem detailed in Chapter 4.

The continually changing hydrodynamic forces and moments acting on the submarine during the course of a manoeuvre are calculated directly from a knowledge of the surrounding flow field. The flow model and the resulting forces and moments are updated at successive intervals of time. Calculated accelerations derived from the forces and moments are numerically integrated to give velocities. Velocities are then integrated numerically to give displacements. Displacements are resolved from the body axes to earth axes to give the next position of the submarine in space during the manoeuvre.

The flow around a manoeuvring submarine is dominated by vortices which are shed from the appendages and the hull (Figure 4). The body vortices are affected by incidence and rate of turn of the submarine. The SUBSIM computer program makes use of empirical formulae to represent the positions and strengths of body vortices.

If a body is at a moderate angle of incidence the boundary layer on the leeward surface separates as shown in Figure 4. Vorticity shed from the boundary layer is convected away and coalesces to form a diffuse pair of vortices with cores almost parallel to the body axis. The strength of the vortices i.e. the circulation, increases towards the tail of the body as more vorticity is added as the flow separates along the hull. A graphical

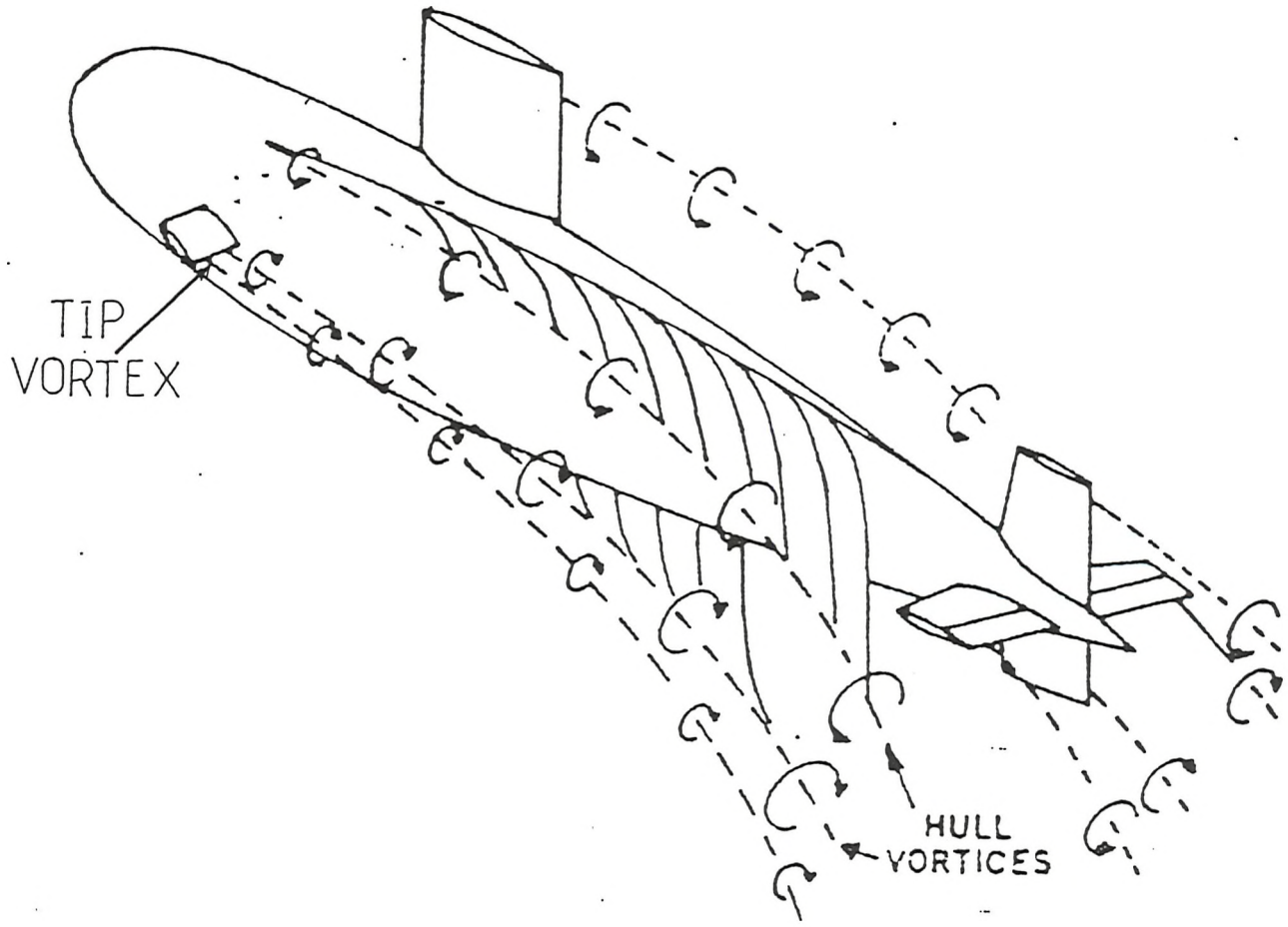

FIG.4 VORTICES AROUND A SUBMARINE

representation of how discrete vortices around the body are modelled in SUBSIM is shown in Figure 5. Note how the strength changes along the length of the body.

Determination of the point of separation on bodies of revolution has been a problem in fluid dynamics for sometime. The use of an empirical estimate from experiment results has tended to be the more common solution for the determination of the separation point.

More recent work conducted in support of the SUBSIM simulation program is described in this thesis and also in papers by Ward and Wilson [26,27]. These papers can be found in Appendix 3.

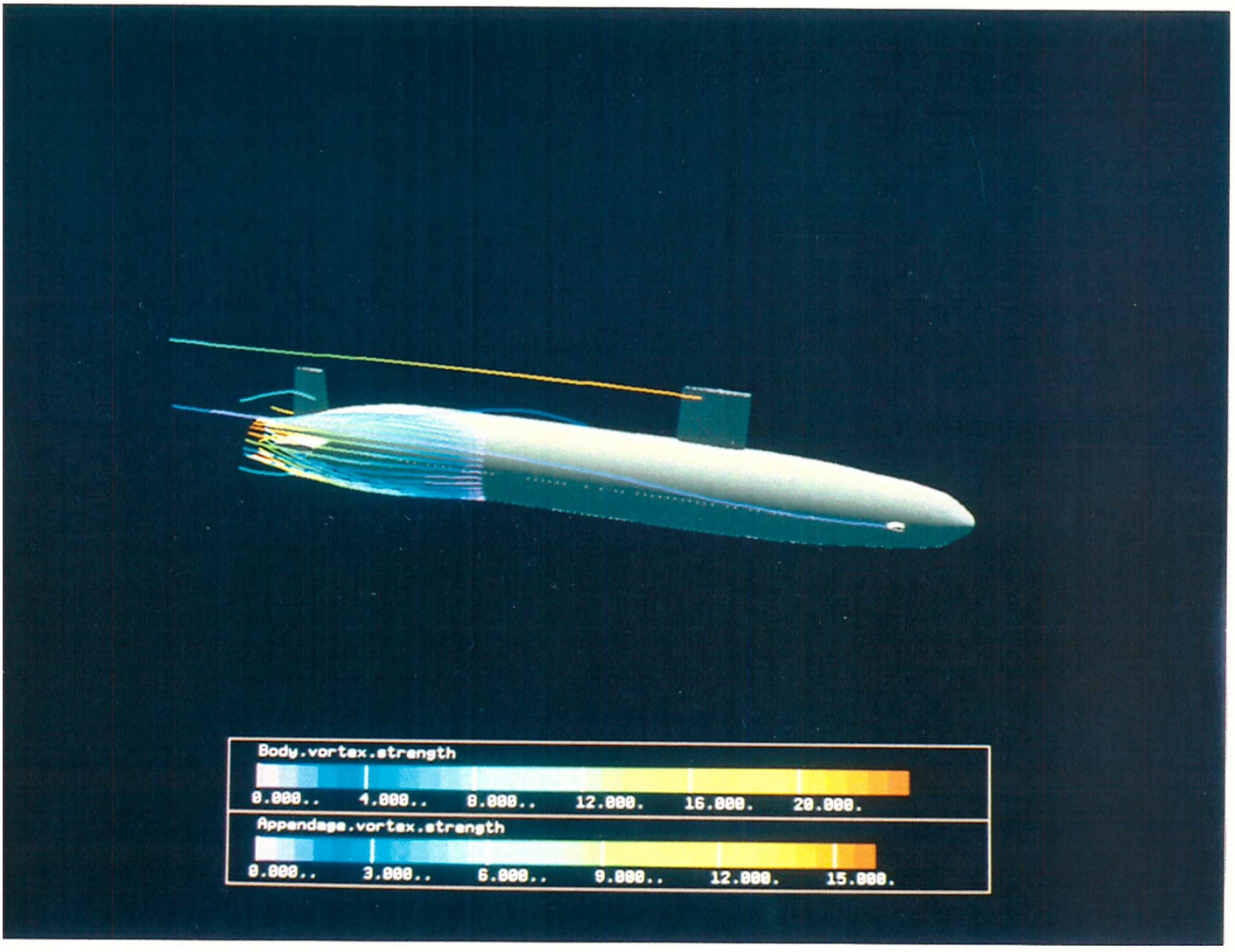

FIG.5 MODELLING OF BODY VORTICES IN SUBSIM

Chapter 3

Experimental Estimates of Forces on a Body

3.1 Experimental Determination of Derivative Values

There are basically two types of experiment that can be conducted, one involving free-running models, and the other using constrained models. Free-running models are controlled remotely and are used in a large manoeuvring basin or in lakes. Contrained models are fixed to a carriage and towed down a tank.

Scale model tests (Burcher [28], Gertler [29]) in a towing tank (using a constrained model set-up or a planar motion mechanism (Booth [30])) or on a rotating arm have been used to measure the hydrodynamic forces for any arbitrary submerged body-appendage configuration. Curve fitting techniques are then used to estimate the required coefficients.

Free-running models have been used for many years to perform standard manoeuvres e.g. zig-zag, spiral and pull-out, and also to determine parameters describing overall performance e.g. turning circle diameters (Burcher [28]).

3.2 Scale effects

Whatever the type of experiment being conducted a significant problem is the scale effect. When working with models certain conditions must be fulfilled in order so that the results can be applied to the full-scale submarine. If a submarine is completely immersed in water then a typical force acting on the vessel will depend on the relative velocity U, the size of the vessel (specified by a typical linear dimension such as the length L), the density of the fluid ρ, the kinematic viscocity υ, and, if near to the surface where waves may be formed, g the acceleration due to gravity.

R_c the Reynolds number, and F_N as the Froude number. It is obvious that, for the same fluid at the same temperature, to satisfy the invariance of the Reynolds number, the ratio of model speed to full-scale speed must be the same as the ratio of their linear dimensions. Thus in experiments with a one-tenth scale model the corresponding model speed should be ten times that of the full-scale submarine. For present purposes only deeply submerged submarines are being considered, and Froude number is of little consequence; the effect of any difference in Reynolds number is of much greater significance.

3.3 The Viscous Effect

It is obviously practically impossible to undertake all experiments with scale models at the correct Reynolds number. Consequently the majority of experiments are carried out at a somewhat lower full scale Reynolds number, the resultant effect on the validity of the results is to some extent still unknown. However, it is generally accepted that quite large variations in the Reynold's number can be tolerated, provided certain precautions are taken which are discussed below.

An important effect associated with the Reynold's number is the variation in the flow pattern around the body. At low Reynold's number, boundary layer separation usually takes place while the flow is still laminar. Above a certain critical Reynold's number the transition to turbulent flow in the boundary layer occurs before separation, and as a consequence of this the separation point moves aft along the body. Various estimates for this critical Reynold's number have been given, but it probably lies around 1.0×10^6 (Lamont [31]) where R_c is based on diameter. Model tests should be run at a Reynolds number greater than this critical value. This would ensure a more realistic flow pattern, and for a typical submarine a model with diameter 0.5 metres would require a towing speed of at least 2.28 m/s to achieve a Reynolds number of 1.0×10^6.

The turbulent boundary layer could be artificially stimulated by using wires or pins on the model at the appropriate point. This method, although extensively used, is open to critisism on the grounds that even if the turbulence is stimulated in the right place, it is not necessarily the same as naturally induced transition. Jones-Bell [32] referenced in Hoerner[33] demonstrated how the drag coefficient of a spheroid varies as a function of the diameter of a wire ring applied for stimulation. The results suggest, however, that some consideration must be given to degree and consequences of turbulence stimulation in model testing. The wires or pins are usually placed at five percent of the total length from the nose of the model. Figure 6 shows a close-up of pins on the nose of a body of revolution model.

3.4 Experimental Determination of Derivatives with Respect to a Linear Velocity

The experimental facility most widely used for ship and submarine model experiments is the long towing tank; of which a number have been built in many countries. A scaled model is fixed below a carriage which runs on rails at either side of the tank (Figure 7). Early experiments were chiefly concerned with measuring the resistances of models.

Strain gauges are fixed at known positions within the model. When the gauge is under strain a voltage is produced. The gauges are subjected to various levels of strain by placing loads on the strain gauge 'post'. By plotting voltage against load a calibration factor can be calculated.

When a number of measurements of downward force Z' say at various angles of pitch have been made, it is possible that regression curves to be fitted to the results. Z' is plotted against $\sin\alpha$ i.e. non dimensional downward velocity w/U. From this we can arrive at coefficients Z_w (the linear term) and $Z_{w|w|}$ (a first non-linear term). These coefficients can then be used in the equations of motion to determine

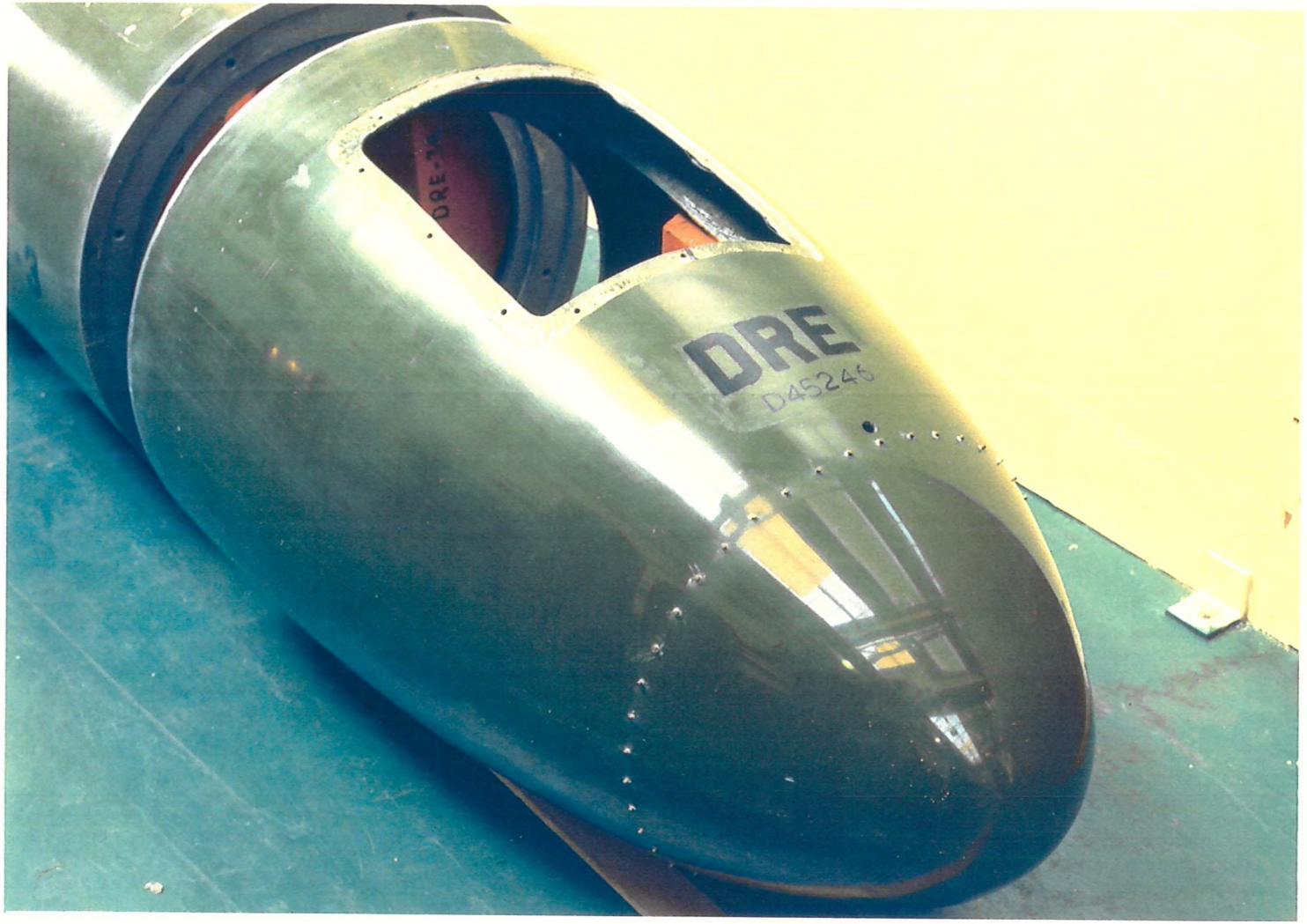

FIG.6 TURBULENCE PINS ON THE NOSE OF A MODEL

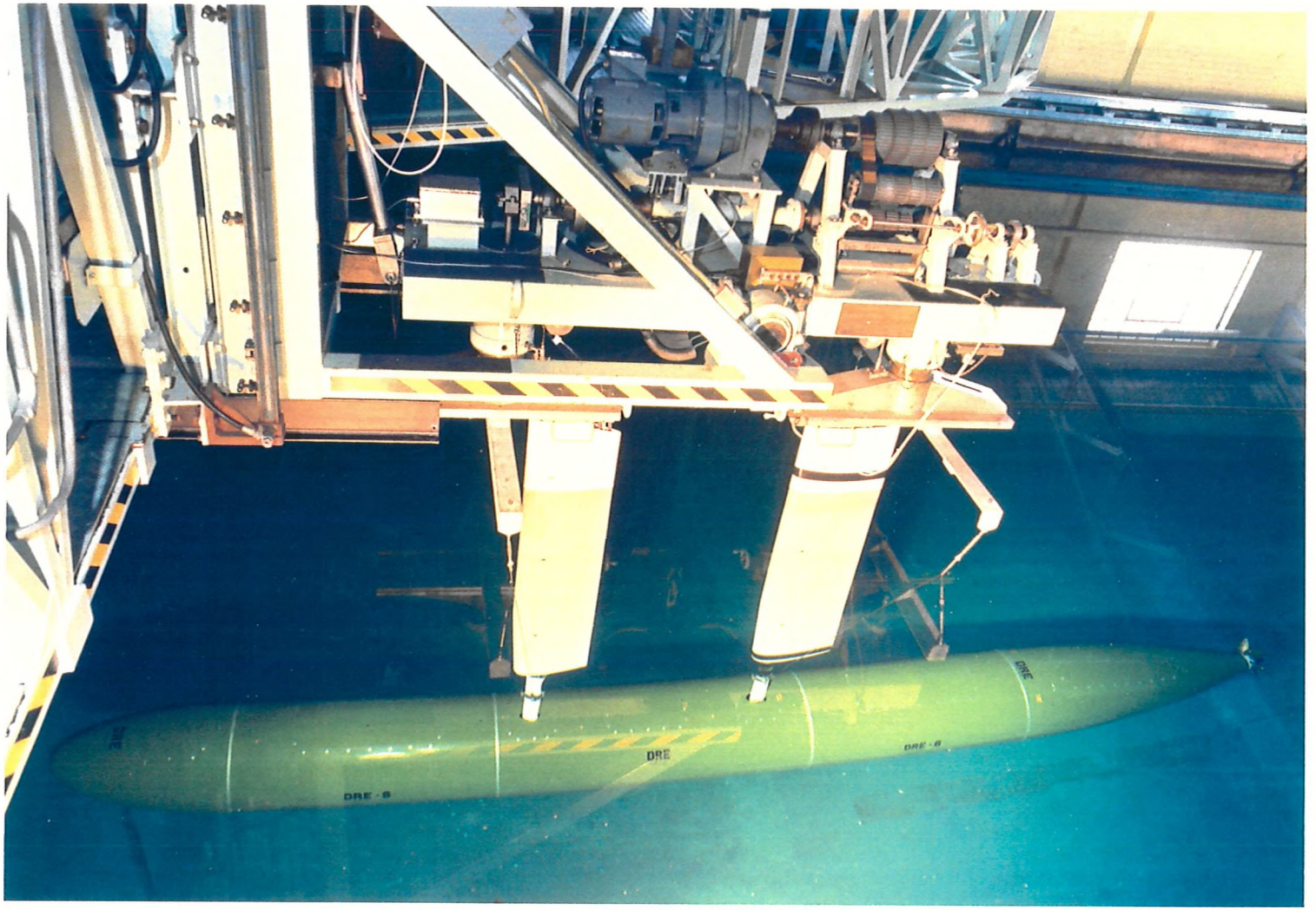

FIG.7 TOWING TANK - MODEL PITCHED DOWN

the total force acting on the body for a particular speed and angle of incidence.

3.5 Experimental Determination of Derivatives with Respect to Angular Velocity

The most realistic way to obtain the rotational or curvature derivatives is to tow the models in a curved path. A number of large tanks have now been built in which it is possible to conduct experiments of this nature. A rotating arm is used whereby models can be attached at various radii. Various angular velocities and radii of attachment are used and by measuring the hydrodynamic forces the derivatives can be calculated in a similar manner as previously described. A rotating arm experiment is shown in Figure 8.

3.6 Experimental Determination of Derivatives using an Oscillator Mechanism

In the methods described above particular velocities were applied and the actual hydrodynamic forces are measured. These are termed direct methods. The technique where an oscillator mechanism is used to produce this model movement is an indirect procedure. The Planar Motion Mechanism tows the model and simultaneously oscillates the model at a particular frequency and amplitude. From the experiment results the dynamic coefficients can be derived by analysis. This method has been used quite extensively in both aircraft and submarine investigations. It is the only method so far used to obtain experimental values of the acceleration derivatives.

The submarine model is suspended from the towing carriage of the long towing tank (Figure 9). It is suspended by two struts each of which can be oscillated sinusoidally in the vertical plane while the model is being towed through the water. The phases and amplitudes of the oscillations of the strut can be adjusted, and it is possible for the model to be in pure pitching motion, pure

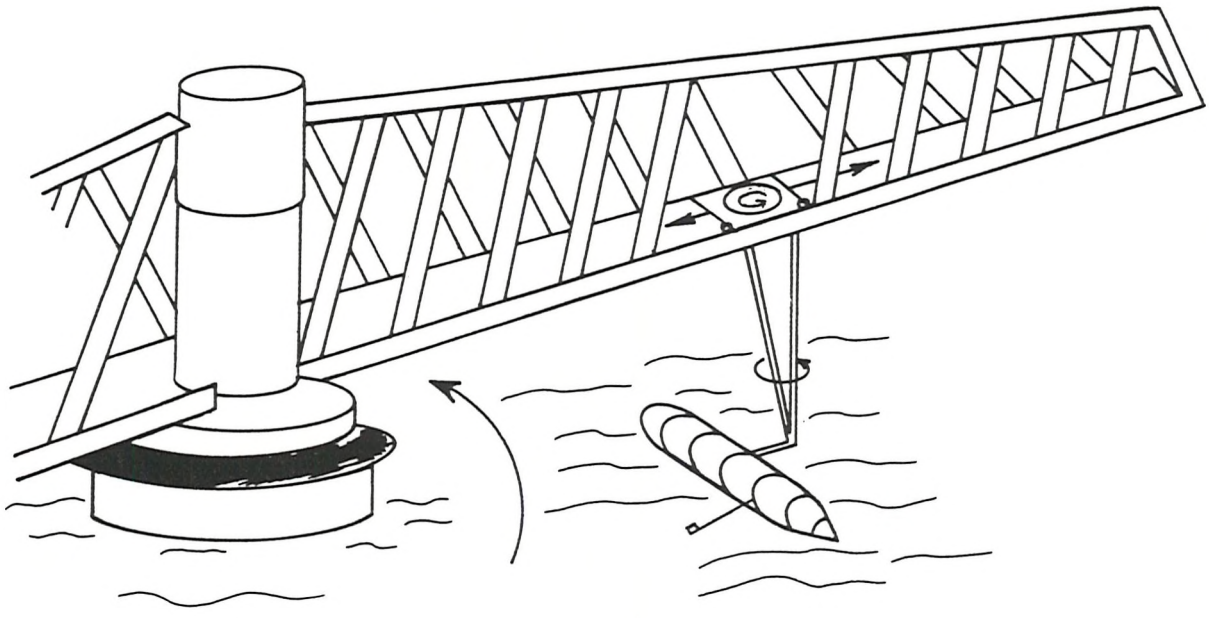

FIG.8 ROTATING ARM EXPERIMENT

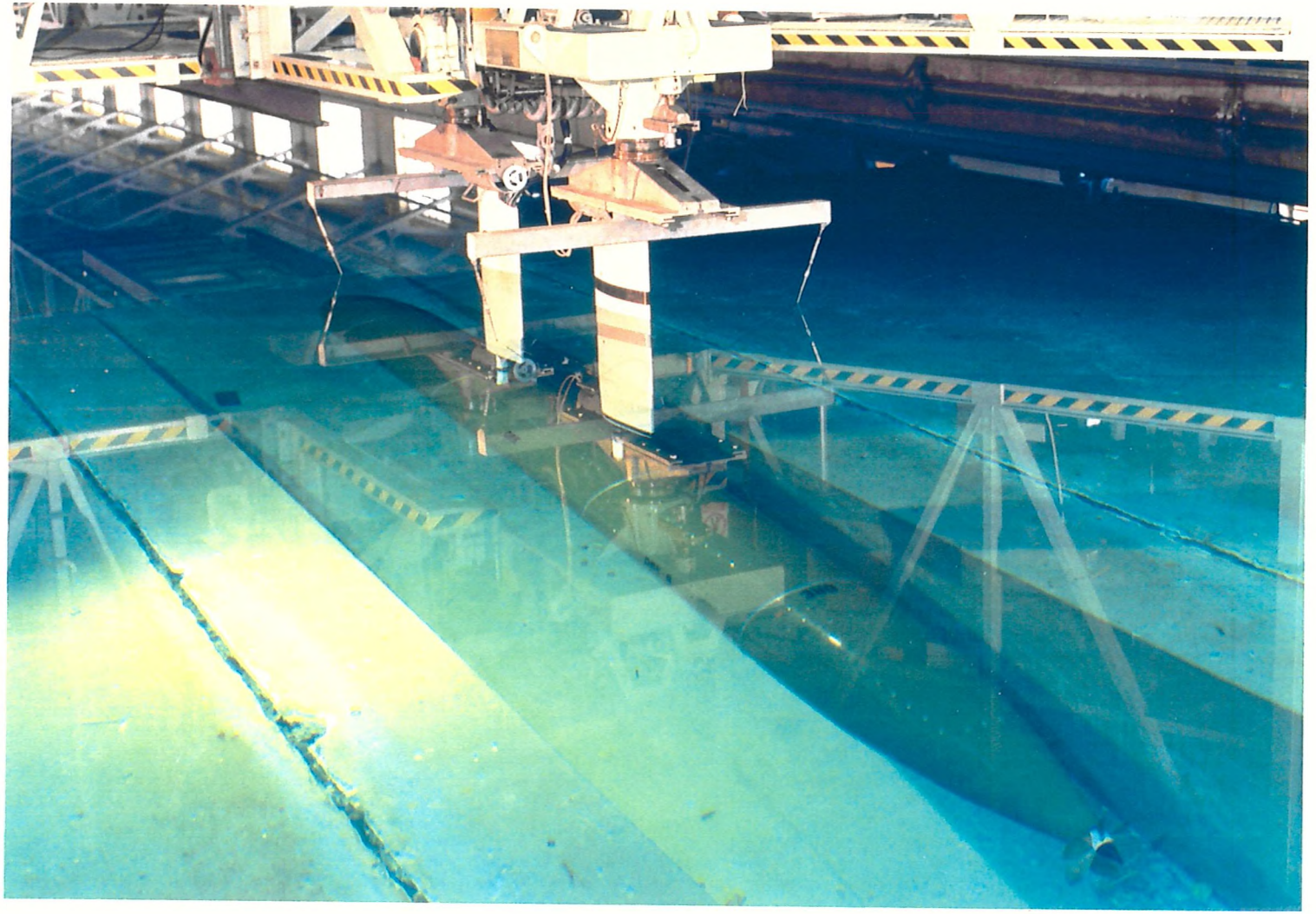

FIG.9 PMM ARRANGEMENT - MODEL MOVING OUT OF DOCK

heaving motion, or perhaps a combination of pitching and heaving.

As stated by Burcher [28], model testing has its deficiencies due to scale effects but if a design performs well overall in a tank it should perform well at sea and conversely a consistently bad performance in a tank will probably imply a poor performance at sea.

Predictions using derivatives from model experiments are never entirely accurate and free running models and system identification techniques (Tinker et al [34]) have been used in parallel to overcome this problem. Systems identification takes the opposite approach in measuring the motion that a free running model experiences when for example a particular rudder deflection is made. A transfer function then determines the force which would have created such a response.

Model testing has its place in the design process but the method is time consuming and costly.

Chapter 4

Theoretical Methods

4.1 Munk's Slender Body Theory

An early work applying classical theories to airship hulls was that of Munk [3] published in 1924. Munk presented the general theory of the aerodynamic forces on airship hulls, a theory which was used in the study of the forces experienced by the airship ZR-1. The airship was considered in the first instance to be without tail fins (i.e. barehull), and proceeding on a straight course at an angle of incidence α. The calculated force and moment on the hull should thus give derivatives for the bare hull, Z'_w and M'_w in the vertical plane, and Y'_v and N'_v in the horizontal plane.

When a slender, axially-symmetric body moves in a straight line through an ideal fluid, with an angle of incidence α, it experiences a destabilizing pitching moment, with the total aerodynamic lift on the body equal to zero. The moment is often called the Munk moment and is often expressed by

$$M=mU^2(k_2-k_1)\sin 2\alpha \qquad (4.1)$$

where k_1 and k_2 are added mass coefficients for transverse and axial motions, respectively
m is mass of the fluid displaced by the body
U is the forward speed.

The actual magnitudes of the longitudinal and transverse added masses of elongated surfaces of revolution can be studied by means of exact computations made by Lamb with ellipsoids of revolution of different ratio of elongation. The variables obtained by Lamb [4] from a closed solution of the potential flow about ellipsoids of revolution are contained in Table 1. For bodies of a shape

reasonably similar to ellipsoids it can be approximately assumed that (k_2-k_1) has the same value as for an ellipsoid of the same L/D ratio.

In the non dimensional derivative terminology the relation 4.1 could be written:

$$M'_w(\text{bare hull})=m'(k_2-k_1) \qquad (4.2)$$

and since the lift force is zero:

$$Z'_w(\text{bare hull})=0 \qquad (4.3)$$

Munk also obtained the force distribution along the hull such that the transverse (or lift) force on an element dx is given:

$$dz=\frac{1}{2}\rho U^2 \frac{dA}{dx} dx \sin\alpha \qquad (4.4)$$

where dA/dx is the rate of change of cross-sectional area, with respect to length along the body.

It is obvious that the assumption of an ideal fluid leads to quite serious discrepancies, since it is well-known that an airship hull at an angle of incidence will be subject to a lift force, albeit small. The 'Munk Moment' has also been found to overestimate (often by some 30 per cent) the moment measured by experimental methods. Munk himself observed these facts, and suggested that the estimation of the lift acting over the rear half of the hull was the most in error, due to the presence of shed body vortices.

Table 1

L/D	k_1	k_2
1.0	0.5	0.5
2.0	0.209	0.702
3.99	0.082	0.86
6.01	0.045	0.918
8.01	0.029	0.945
9.97	0.021	0.96
∞	0	1.0

4.2 Von Karman's Method

Von Karman [5] conducted similar investigations on the bare hull of the ZR-III, assuming equivalent circular cross-sections at all stations. His theoretical methods involved the use of sources and sinks, or doublets along the axis of symmetry. The results were a little closer to experimental values than those of Munk, but there is still a discrepancy of the force distribution at the stern. Von Karman claimed to have obtained better agreement by assuming the existance of a vortex trail, as in airfoil theory, and calculating the effects of the vortices on the lift. He concluded that the method could only be applied in 'the exeptional case when the analytical continuation of the potential function, free from singularities in the space outside the body, can be extended to the axis of symmetry without encountering singular spots'. However, he added that 'even in cases for which this method offers no accurate solution, the potential in the surrounding space can be ascertained to any desired degree of approximation by increasing the fineness of division of the line sources'.

4.3 Blasius' Theorem

It is well-known that a vortex induces a force on a circular cylinder. The force can be evaluated by using Blasius' theorem. This method is used in the SUBSIM computer program.

Consider a vortex of strength K, and consequent circulation $2\pi K$, at a point (c,0) in the presence of a circular cylinder $|z|=a$ where $a<c$.

The complex potential for the vortex and its image is obtained by Milne-Thomson's circle theorem namely

$$w=-iK \ln(z-c)+iK \ln(z-a^2/c) \qquad (4.5)$$

In this analysis an image vortex at the centre of the cylinder has not been included. This is consistent with the assumption that there will be a non-zero circulation around the cylinder because the vortex has been shed from the body.

The force per unit length is obtained by Blasius' theorem so that

$$Y+iX=-\frac{\rho}{2}\int_{|z|=a}\left(\frac{dw}{dz}\right)^2 dz \qquad (4.6)$$

$$Y+iX=-\frac{\rho}{2}\int_{|z|=a}\left(-\frac{iK}{z-c}+\frac{iK}{z-\frac{a^2}{c}}\right)^2 dz \qquad (4.7)$$

This integral can be evaluated by the calculus of residues so that

$$Y+iX=-\frac{\rho}{2}2\pi i\left(\frac{-2K^2i^2}{\frac{a^2}{c}-c}\right) \tag{4.8}$$

since the integrand has only one singularity inside the contour. Hence

$$X=\frac{2\pi\rho K^2c}{c^2-a^2} \tag{4.9}$$

$$Y=0 \tag{4.10}$$

Blasius' formulae also provides an expression for the moment namely

$$M=Re\left(-\frac{\rho}{2}\int_{|z|=c} z\left(\frac{dw}{dz}\right)^2dz\right) \tag{4.11}$$

$$M=Re\left(-\frac{\rho}{2}2\pi i\frac{2K^2a^2}{c\left(\frac{a^2}{c}-c\right)}\right) \tag{4.12}$$

$$M=0 \tag{4.13}$$

As a result it is concluded that the cylinder is attracted towards the vortex by a force of magnitude

$$Y=\frac{2\pi\rho k^2c}{c^2-a^2} \tag{4.14}$$

Consider a number of vortices of strengths $k_1, k_2, \ldots . k_n$ at $z_1, z_2, \ldots . z_n$ where $z_1, \ldots z_n$ are all complex.

It follows that

$$W=\sum_{i=1}^{n}\left(-iK_r\ln(z-z_r)+iK_r\ln(z-\frac{a^2}{z_r})\right) \qquad (4.15)$$

and so

$$Y+iX=-\frac{\rho}{2}\int_{|z|=a}\left(\sum_{r=1}^{n}\left(-\frac{iK_r}{z-z_r}+\frac{iK_r}{z-\frac{a^2}{z_r}}\right)^2 dz \qquad (4.16)$$

$$Y+iX=-\rho\pi i\sum_{r=1}^{n}(\textit{residue at } z-\frac{a^2}{z_r}) \qquad (4.17)$$

It follows by considering the relevent terms that

$$Y+iX=-\rho\pi i\left(\sum_{r=1}^{n}\sum_{s=1}^{n}\frac{2K_rK_s}{\frac{a^2}{z_r}-z_s}-\sum_{r=1}^{n}\sum_{s=1}^{n}\frac{2K_rK_s}{\frac{a^2}{z_r}-\frac{a^2}{z_s}}\right) \qquad (4.18)$$

Now the second double sum is in fact zero since it involves pairs of terms with opposite signs. Hence

$$Y+iX=2\rho\pi i\sum_{r=1}^{n}\sum_{s=1}^{n}\frac{K_rK_sz_r}{z_rz_s-a^2} \qquad (4.19)$$

Blasius' theorem has been used in SUBSIM to predict the out-of-plane forces, however, no improvement resulted in predictions of depth change in the turn. This was not because Blasius' theorem is a poor method but probably due to the modelling of the vortices which were considered to be symmetrical pairs. It is known that this is not the case in reality and therefore a set of experiments were devised in order to examine the distribution of circulation around an appended body of revolution.

Chapter 5

Experiments

5.1 Previous Experiments To Investigate Vortex Flow

5.1.1 A summary

Lloyd [35,36] described experiments to measure vortex strengths and positions. The aim was to acquire data from which empirical estimates of vorticity could be derived. The author [37] became involved in the subsequent analysis of experiments which measured body vortices in curved flow.

The experiments were conducted on the rotating arm facility (Figure 8) in the manoeuvring tank at DRA Haslar (formerly ARE Haslar). They were performed by the Wolfson Unit for Marine Technology and Industrial Aerodynamics (University of Southampton) working under contract.

A 5 metre body of revolution was used with fineness ratio L/D of 8.5. A Freestone probe (Figure 10) was used to measure vorticity. A more detailed description of the probe is given later in this chapter. The probe was mounted on a stayed circular strut which could be positioned at one of three locations along the length of the model (x'=0.7, 0.85, 0.925). The probes' radial and angular location could be adjusted.

The model was towed in a circular path by the rotating arm. Runs were conducted at various angles of incidence. The position of the model along the arm was varied to give different angular rates. Speed was constant throughout the experiment at 2.5 m/s.

Measurements were taken at 10 degree angular intervals (taking 0 degrees with the strut parallel to the surface of the tank on the leeward side of the model and 90 degrees with the probe vertical above the model) and at 25 mm radial steps from the body surface.

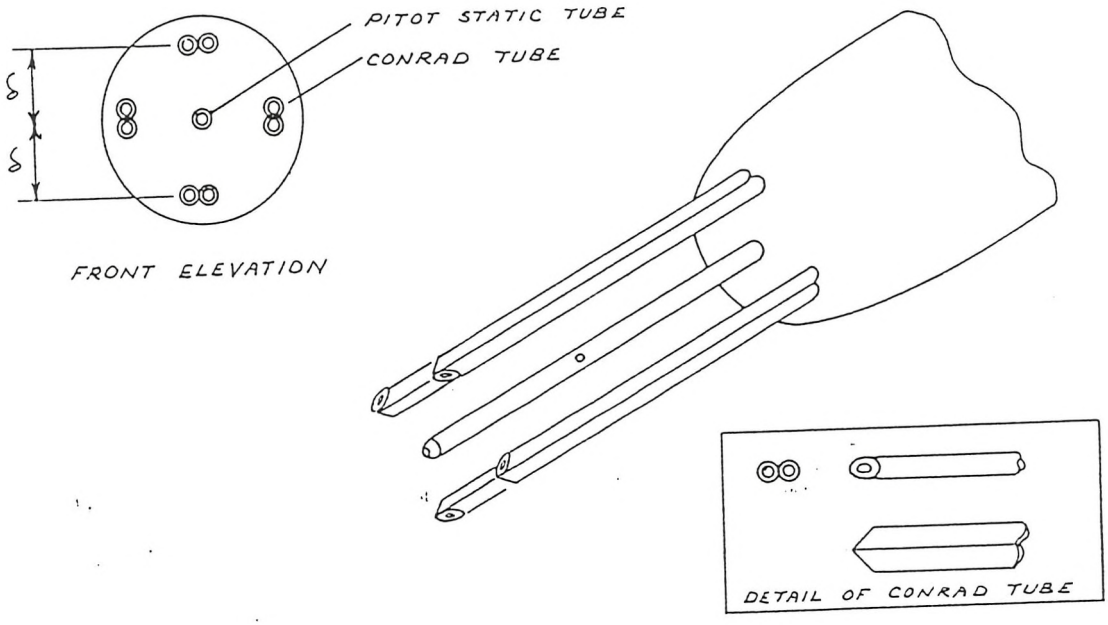

FIG.10 FREESTONE PROBE

The raw data was faired to a more expected form as can be seen in Figure 11. This fairing is explained in Ward [23] which appears in Appendix 3.

The vorticity data was analysed by the author and values for vortex centres, core radii, circulation density and total circulation were calculated for all conditions.

The local circulation density is

$$\Gamma_\theta = \int_0^\infty \zeta_x r dr \qquad (5.1)$$

A graph of circulation density against angle was plotted for each experiment condition and an example is shown in Figure 12. An empirical curve was derived from all results. This gave circulation density as a function of strut angle, angle of incidence, turn parameter and longitudinal position along the hull. Other equations were derived to determine positions of vortices and core radii. Figure 13 shows a representation of the flow as two symmetrical sets of vortices.

The empirical equations derived from the model experiments are described in Ward [37]. Figure 5 shows the modelling of the discrete body vortices, note that the vortices start to be shed longitudinally at $x'=0.65$. This of course would not happen in reality but for convenience it was assumed that vortex strengths were small below this value. The strength of the body vortices increases with longitudinal position.

5.1.2 Validation

The equations were incorporated into the SUBSIM computer program. The modified program was then validated by comparing predictions of submarine manoeuvres with full-scale trials results. These trials results consisted of

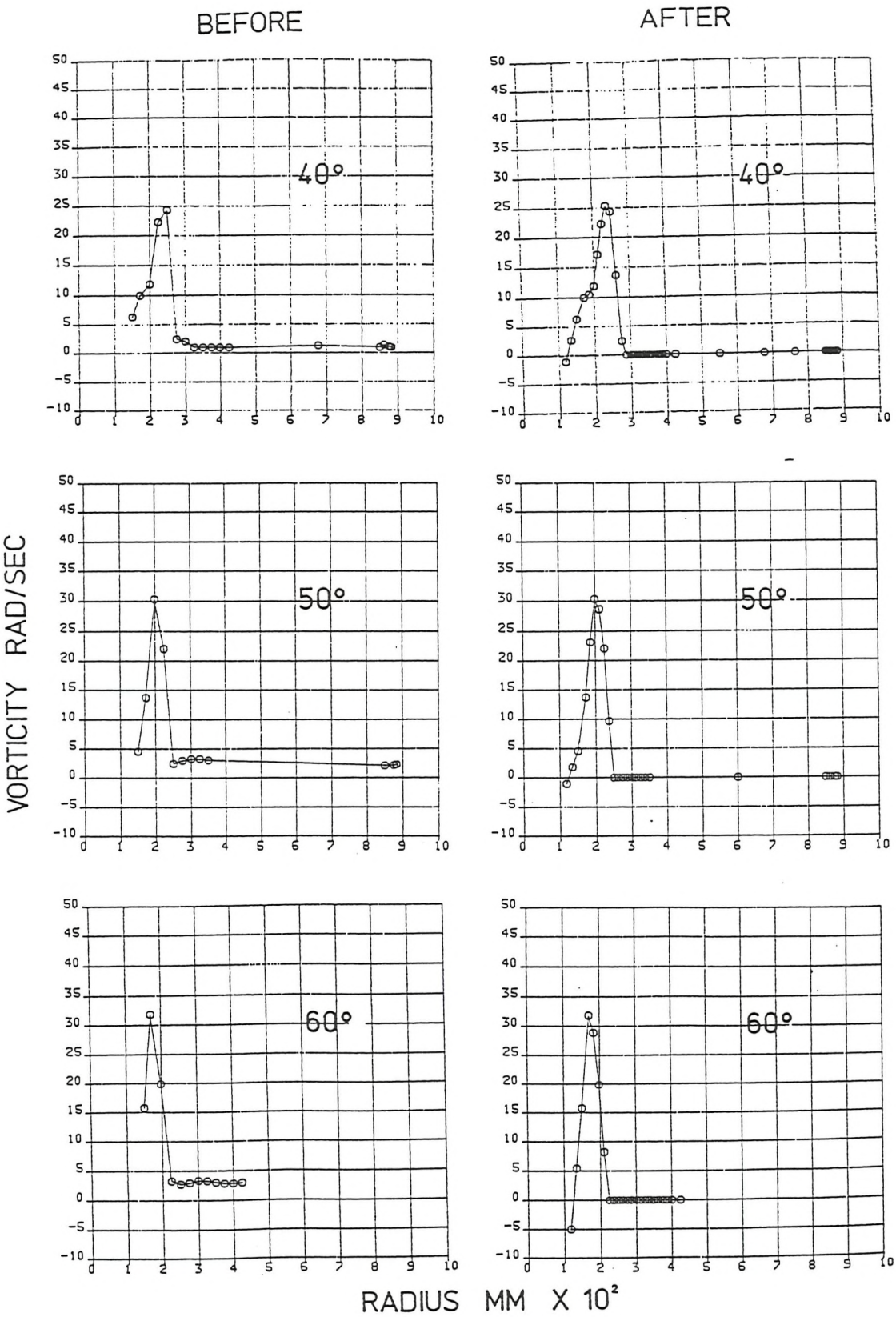

FIG.11 VORTICITY TRAVERSES - BEFORE AND AFTER FAIRING
(X'=0.925, r'=0.3, α=7.5)

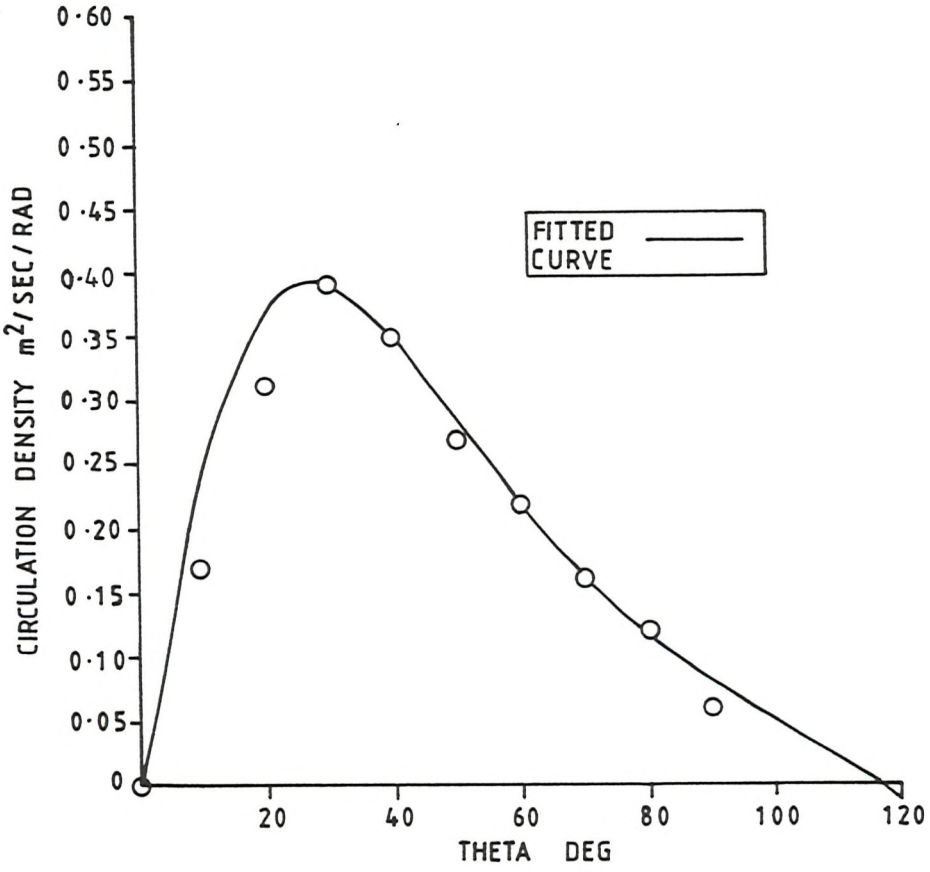

FIG.12 CIRCULATION DENSITY AGAINST STRUT ANGLE
(X' =0.925,r' =0.4,α=5 DEGREES)

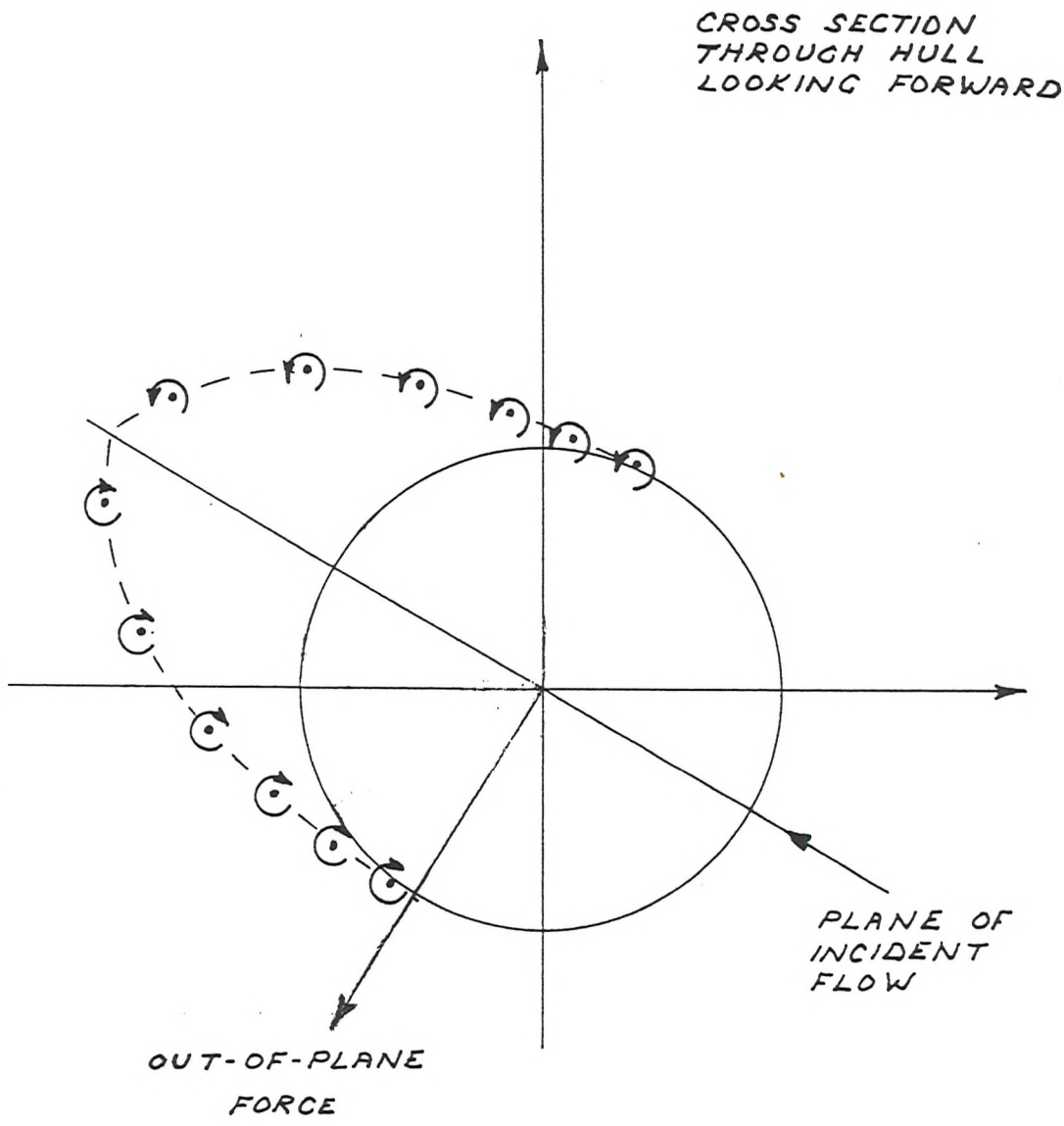

FIG.13 LOCATION OF BODY VORTICES AND DEFINITION OF OUT-OF-PLANE FORCE

deeply submerged submarine manoeuvres where the submarine is moving forward at a constant speed and the rudders are ramped over to a fixed angle. The validation used results of various RN submarine trials and covered a range of speeds and rudder deflections. Figure 14 is typical of a turning circle prediction where control deflections have been replicated exactly as on the trial. It can be seen that the trajectory in the lateral plane, heading and speed loss in the turn simulations are all very good. However, there are problems in predicting depth change during turns.

The reason for poor prediction of depth change in the turn is almost certainly due to unsatisfactory estimation of the out-of-plane force (Figure 13). This force is related to body vortices and as noted earlier the vortices are modelled as symmetrical pairs. This modelling would be correct in dealing with an unappended body of revolution as was the case in the experiments described above. In reality, if a change in separation point occurred on one side of the body then an asymmetry would occur in the force. This phenomenon occurs in the presence of an appendage. On a submarine the most forward appendages are the bow hydroplanes and the bridge fin. The bow hydroplanes are relatively small in relation to the submarine hull but bridge fins are usually substantial. This has caused some problems in the prediction of submarine manoeuvres. Mackay [10,20] has looked at the problem using a panel method and has found good agreement between predictions and experiment data.

To investigate this problem a series of dedicated experiments were planned and conducted by the author, and are described next.

5.2 Experiments to Measure Vorticity and Pressure around an Appended Body of Revolution

5.2.1 Introduction

Of all the forces and moments that are generated on the

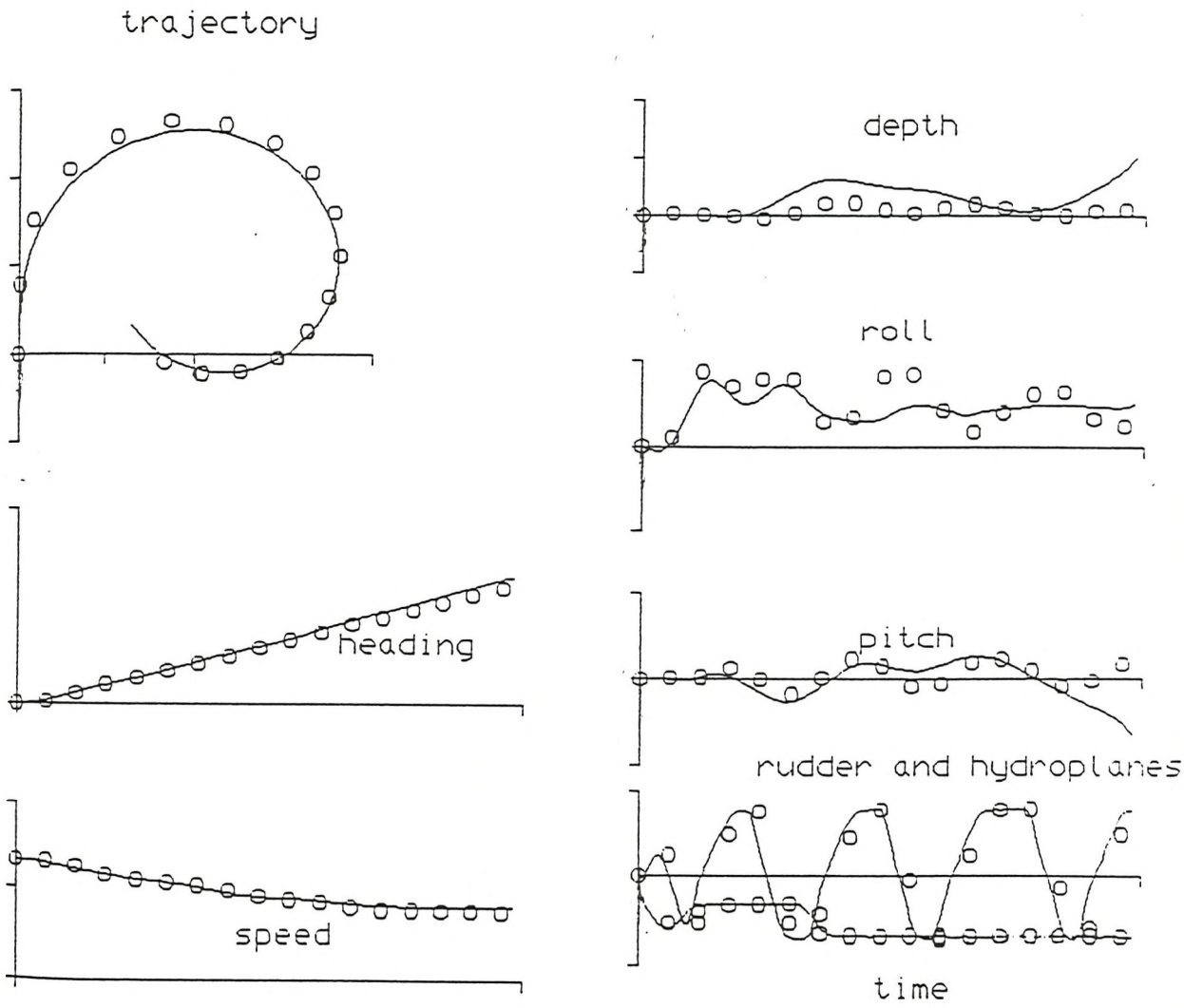

FIG. 14 COMPUTER PREDICTION OF SUBMARINE TURNING CIRCLE

body in submerged flow, the out-of-plane force is vital. It was believed that the out-of-plane force on the submarine body is influenced by the bridge fin vortex and the effect it has on the total circulation around the body. Experiments described below examine the interaction of the bridge fin vortex (Figures 15 and 16) on the body vortices. The subsequent effect on the total circulation due to this bridge fin vortex on pressure around the body is examined.

Various experiments to measure flow velocities on appended bodies of revolution have been conducted in recent years mostly using laser doppler techniques. Kaplan [38] used laser doppler velocimetry techniques to map the flow field about a body of revolution. The data showed the body vortices increased with strength along the hull. When the fin was attached the body vortices no longer displayed the deck-keel symmetry of the unappended model. The strength of the tip vortex, shed from the fin, remained constant along the length of the model. Reed [39] use laser techniques to measure velocity contours around a body of revolution with a fin. The conclusions made, highlighted the problem in acquiring satisfactory data.

The experiments were planned with the following aims;
a. To gather data.
b. To examine the interaction between vorticity and pressure.

5.2.2 Model Design

The model (Figures 17 and 18) was a simple teardrop body of revolution and made of glass-reinforced plastic. The nose and tail shape were chosen as they are representative of modern submarine practice. The fineness ratio defined as, L/D of 8, (also chosen to be representative of a modern submarine) with an overall length of 1.0 metres. Table 2 gives the distribution of diameter. It can be seen that there is an extensive parallel middle body. Metal rings were positioned at four stations flush with the surface of the hull each with 36

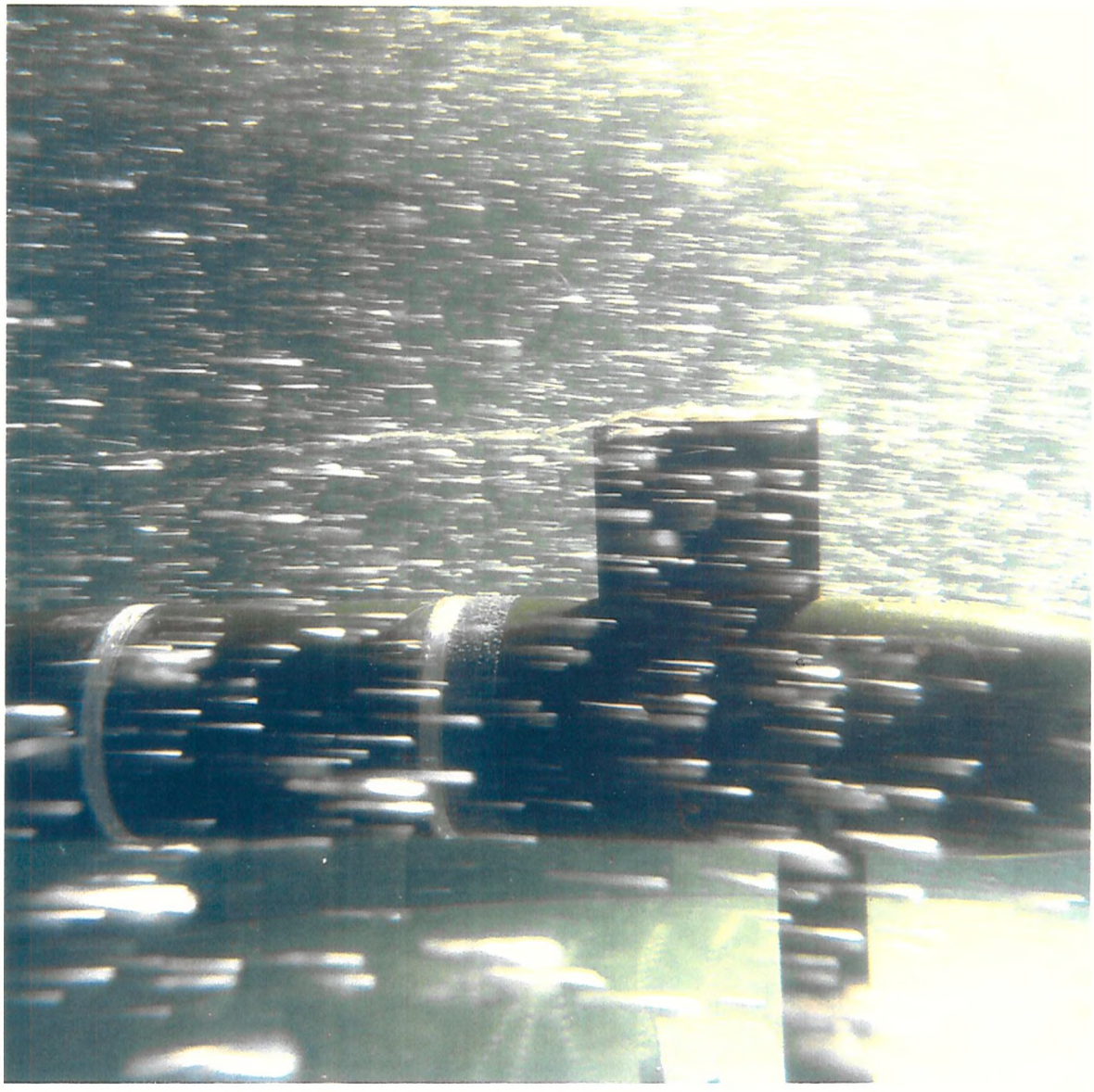

FIG.15 BRIDGE FIN VORTEX

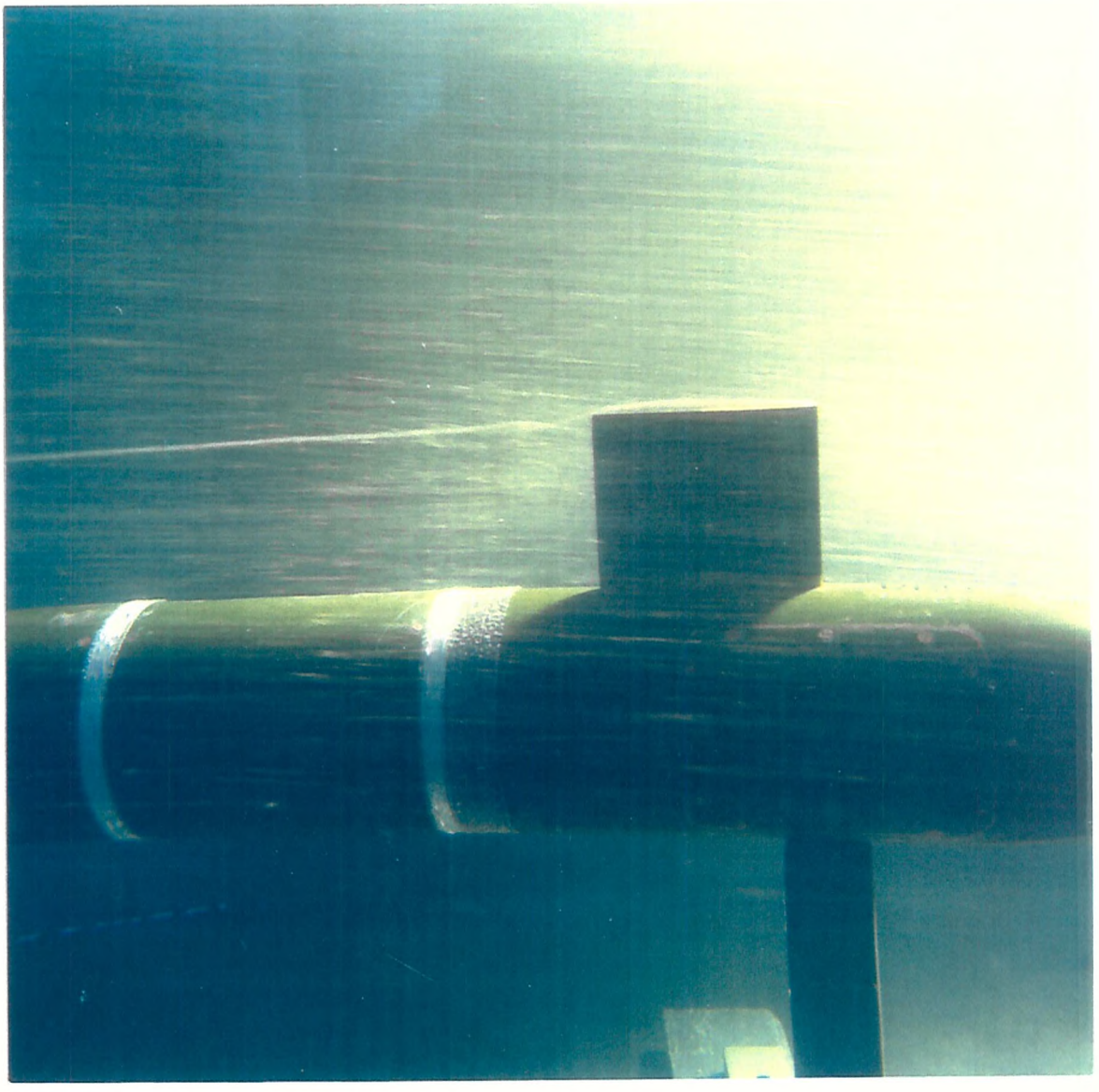

FIG.16 BRIDGE FIN VORTEX - SLOW EXPOSURE

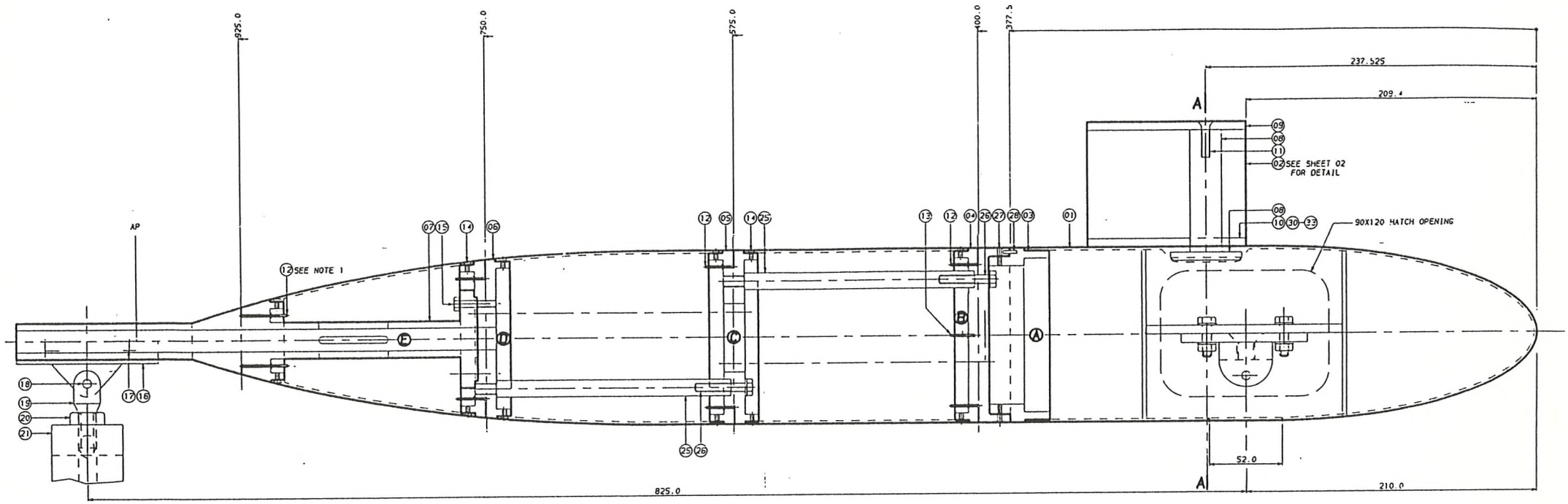

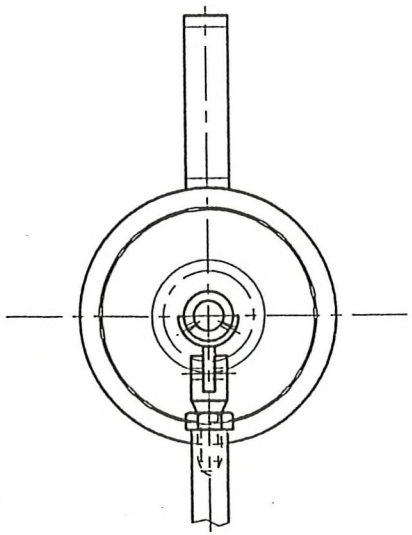

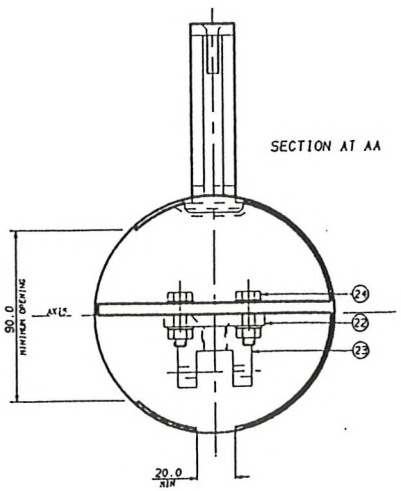

FIG.17 MODEL DRAWING

LENGTH OVERALL 1000.0
MAX DIAMETER 125.0

NOTES

1. ALL TUBE ADAPTORS TO BE ARALDITED INTO POSITION PRIOR TO FINAL ASSEMBLY.

MATERIAL	TOLERANCE AS STATED OR	CONTRACTOR M.O.D. (PE) HASLAR	CHANGE 01 ISSUE 01
FINISH	SURFACE ROUGHNESS	TITLE GENERAL ARRANGEMENT	SECURITY CLASSIFICATION UNCLASSIFIED
DIMS. IN mm	SCALE 1:1	PUNCH CARD TITLE	CONTRACTOR'S DRAWING NUMBER
			SERVICE DRAWING NUMBER/SHEET NUMBER ARE 90 D45314

DRAWN A.HUNT
CHECKED
CERT'D

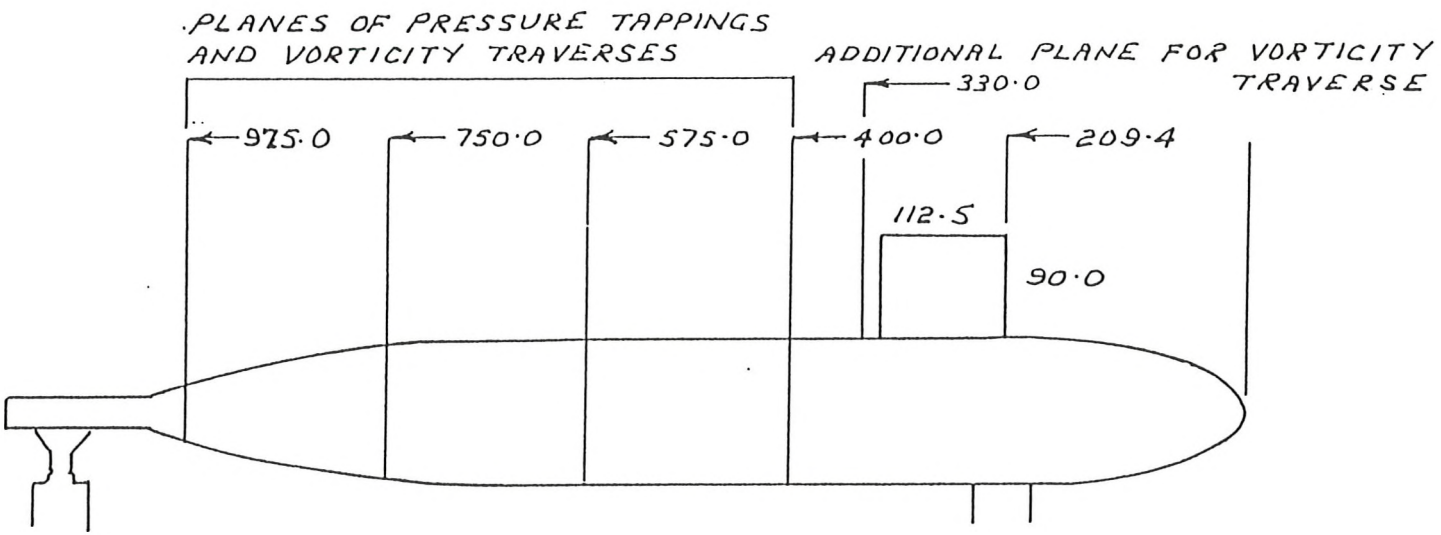
PLANES OF PRESSURE TAPPINGS
AND VORTICITY TRAVERSES
ADDITIONAL PLANE FOR VORTICITY
TRAVERSE
330·0
975·0
750·0
575·0
400·0
209·4
112·5
90·0
DIMENSIONS IN mm

FIG.18 MODEL

Table 2

MODEL DRN

x (metres)	Diameter (metres)
0.00	0.0
0.05	0.085
0.10	0.110
0.15	0.122
0.20	0.125
0.25	0.125
0.30	0.125
0.35	0.125
0.40	0.125
0.45	0.125
0.50	0.125
0.55	0.125
0.60	0.125
0.65	0.125
0.70	0.121
0.75	0.113
0.80	0.101
0.85	0.084
0.90	0.061
0.95	0.033
1.00	0.0

pressure tappings drilled accurately at 10 degree intervals. The positions of the pressure tappings along the model length can be seen in Figure 18. The model had a detachable fin and modelled as a NACA 0020 wing of aspect ratio 1.6.

The fin position is slightly more forward than in conventional submarines. The position was chosen so as more of the cylindrical part of the model hull and all of the tail section would be aft of the fin and therefore subject to its effect.

Positions of stations were chosen to give a good distribution along the hull. The value of $x'=0.925$ was chosen as the Wolfson Unit (Lloyd [36]) had carried out many of their measurements at this station and it was felt that both sets of data could be pooled together.

5.2.3 The Freestone Probe

In this experiment the Freestone probe (Figure 10) was again chosen to measure vorticity as it had been used with previous success at Haslar (Lloyd [35,36]).

The Freestone probe (Figure 19,20 and 21) is a robust instrument that is relatively easy to use, and as such provides an easy data collection device. The probe consists of four pairs of yaw meters whose faces are chamfered at an angle of 45 degrees. One of each pair leads via a manifold to one side of a pressure transducer, the other of the pair to the opposite side. This arrangement produces a pressure difference which is proportional to the streamwise vorticity.

Freestone [40] showed that streamwise vorticity is given, to first order, by

$$\zeta_x = \frac{\delta w}{\delta y} - \frac{\delta v}{\delta z} \qquad (5.2)$$

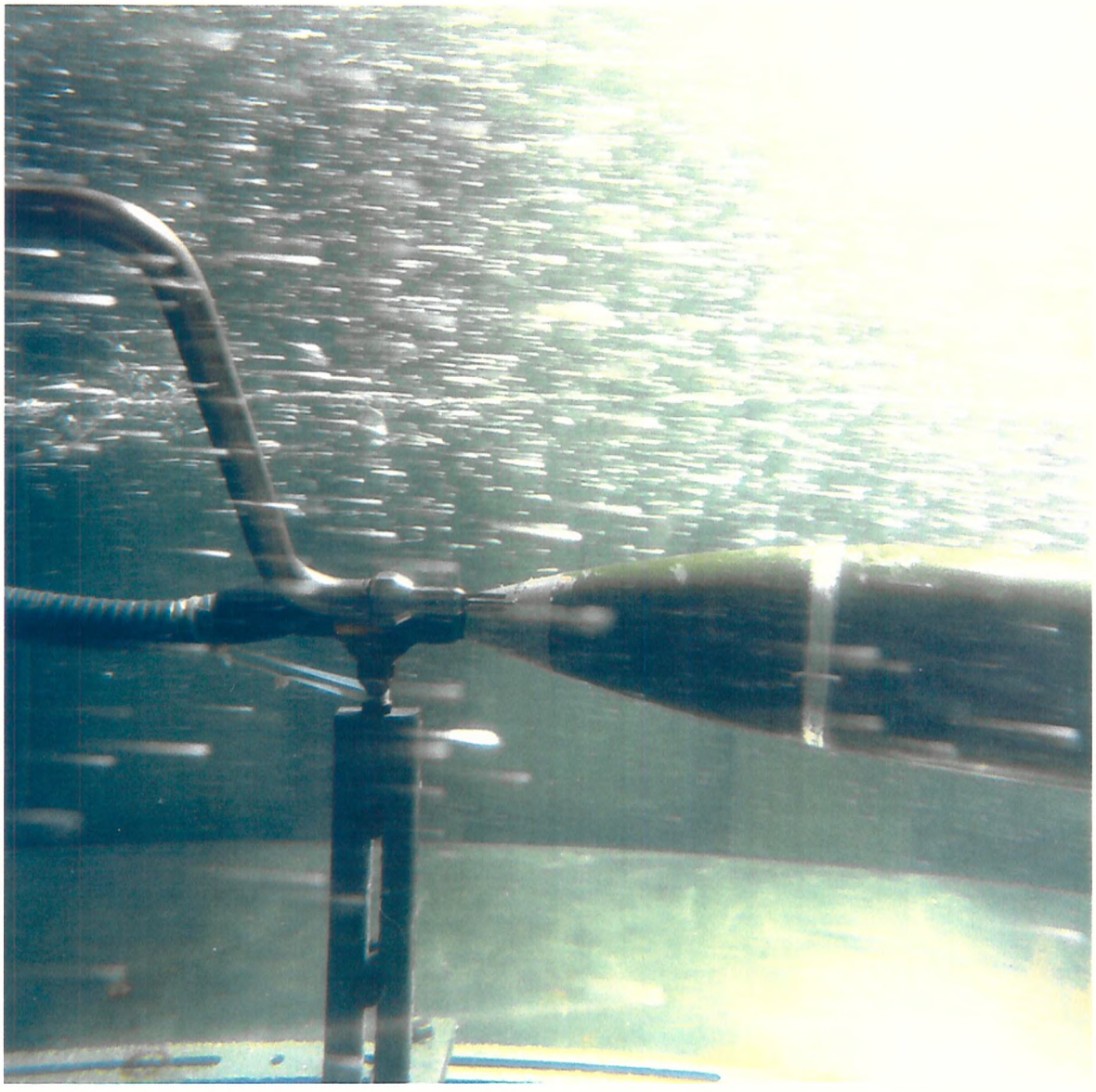

FIG.19 FREESTONE PROBE AT REAR OF MODEL
FIN VORTEX IS VISIBLE

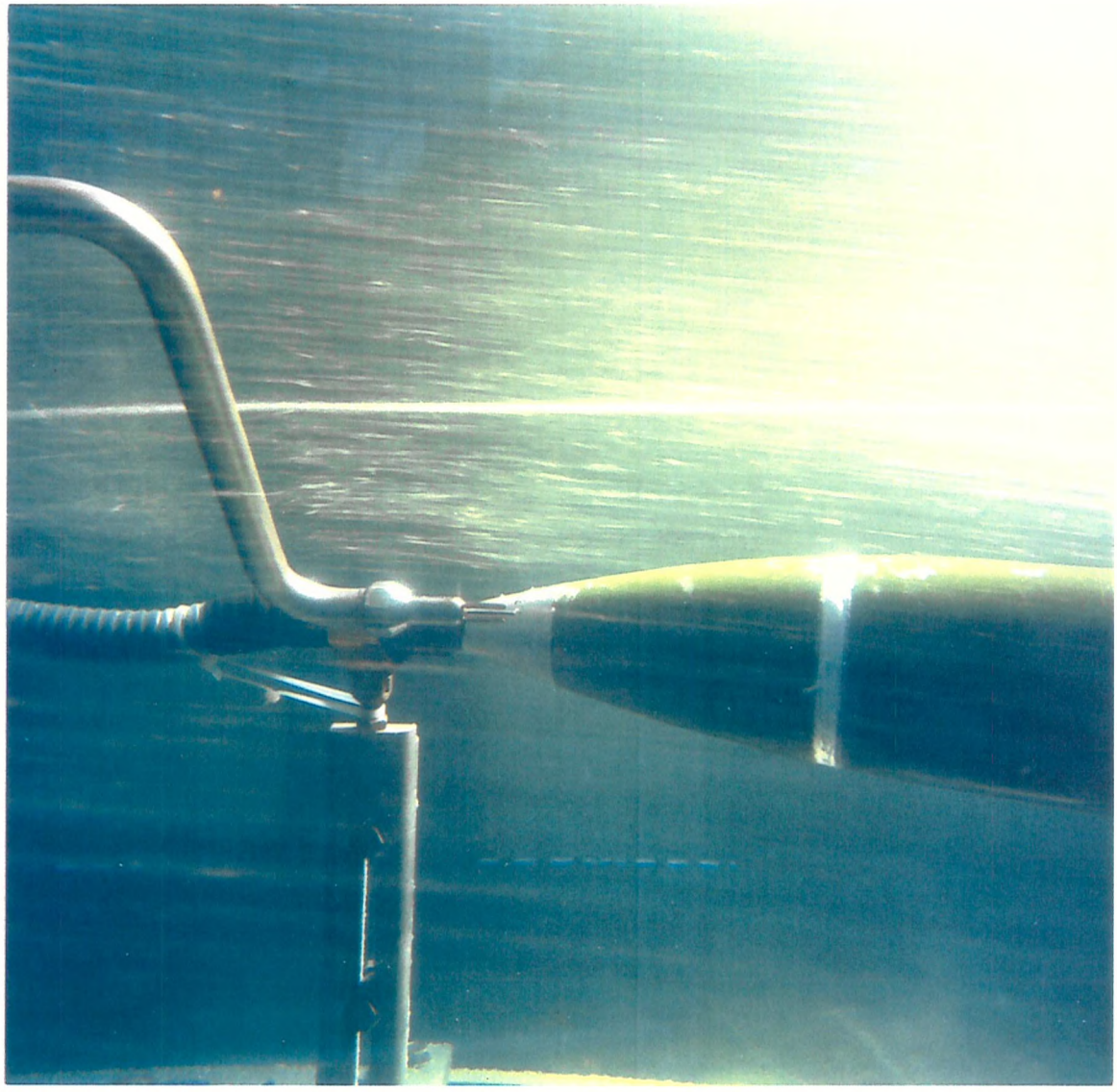

FIG.20 VORTEX AT REAR OF MODEL - SLOW EXPOSURE

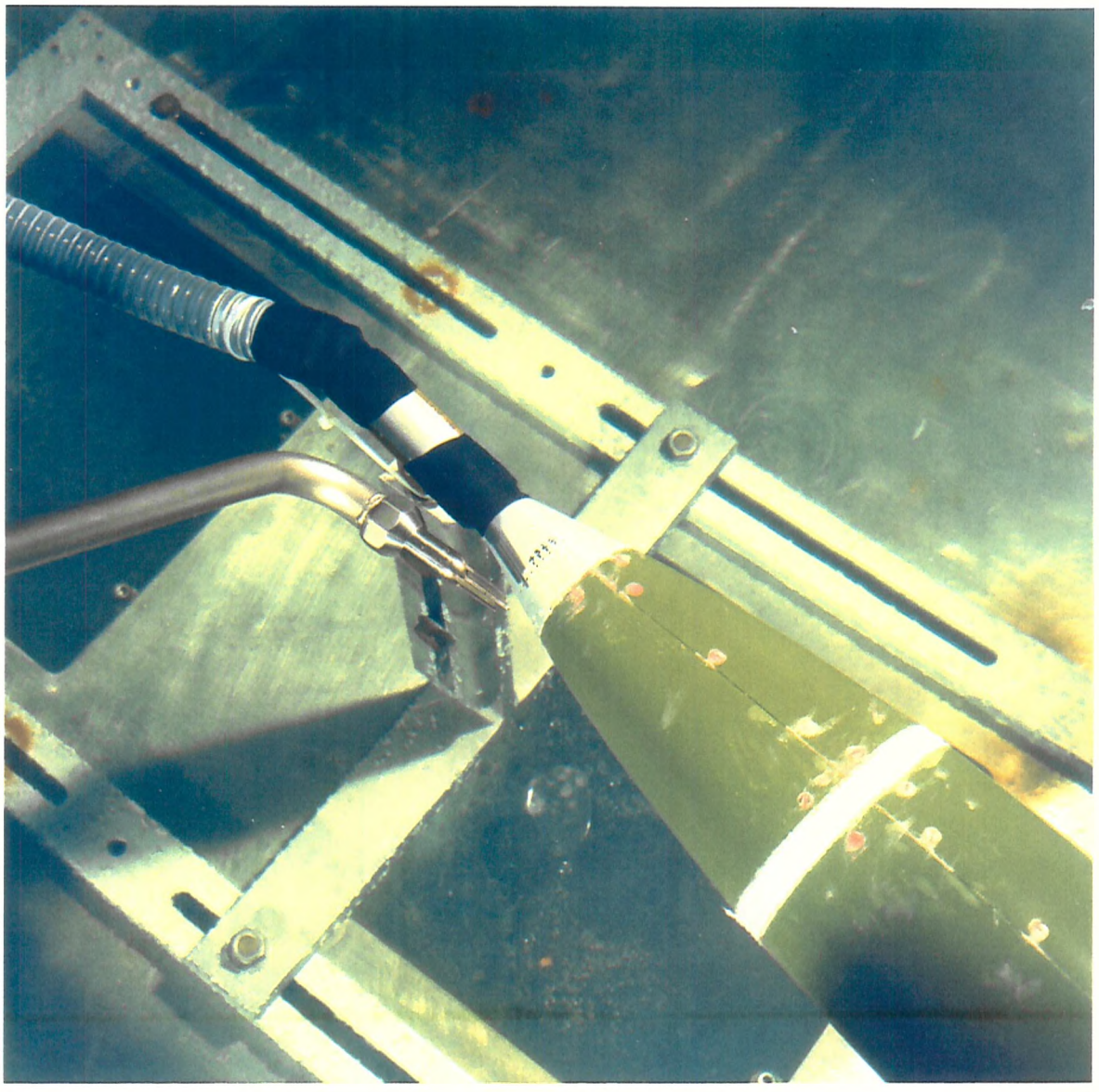

FIG.21 FREESTONE PROBE AT REAR OF MODEL - TOP VIEW

$$\zeta_x = \frac{\Delta W}{2\delta} - \frac{\Delta V}{2\delta} \tag{5.3}$$

$$\zeta_x = \frac{\Delta \Sigma PU}{\frac{1}{2}\rho U^2 2K\delta} \tag{5.4}$$

where δ is the 'radius' of the probe. $\Delta\Sigma P$ is the difference of the 'sum of the odd numbered pressures' and the 'sum of the even numbered pressures' i.e.

$$\Delta \sum P = \sum_{i\ \text{odd}} P_i - \sum_{i\ \text{even}} P_i \tag{5.5}$$

All odd numbered tubes are connected to a common plenum chamber and likewise for the even numbered tubes. In this case the pressure difference between the two plena is

$$\Delta \sum P = \Delta \sum \frac{P}{4} \tag{5.6}$$

hence equation (5.4) becomes using (5.5),(5.6)

$$\zeta_x = \frac{\Delta P 2U}{\frac{1}{2}\rho U^2 K\delta} \tag{5.7}$$

A pitot static tube is fitted in the centre of the tube so that dynamic pressure and velocity can be measured simultaneously with vorticity.

The calibration of such Freestone probes is long and tedious therefore no attempt was made to calculate a value of K specific to this experiment. From previous work a calibration factor of K of 2.47 was used (Drummond [41]).

5.2.4 Experiment Facility

The Circulating Water Channel at DRA Haslar was chosen because it is easy to use. This facility is a general purpose facility in which a wide range of experiments can be conducted. The test section has a width of 1.4 m, a length of 5 m and a maximum depth of 0.84 m. The maximum water speed is 5.5 m/s. The drive system is a toothed belt driven impeller. A large 75 kw motor is used for high speeds and a small 1.5 kw motor for low speeds say for flow visualisation studies. It is particularly suited to the visual observation of flow phenomena. It also provides a capability for the conduct of preliminary experiments, or the development of special equipment, prior to carrying out tests in larger facilities. It is self-operable i.e. it requires no driver as a large towing tank does. It has more flexibility regarding testing time as it is not a dedicated facility for say surface ship or submarine experiments.

5.2.5 Experiment Procedure

The experiment was conducted in two stages during 1990 and 1991. The model was tested at various conditions to explore the relationship between the vortex characteristics, angle of incidence and pressure distribution at particular cross-sections along the body. All angles of incidence were measured with the model's nose to starboard. Speed was kept constant at 2.5 m/s throughout the experiments using a pitot static tube. Measurements of freestream velocity using laser doppler velocimetry techniques during the second stage showed the flow to be rising at about 8 degrees hence the model is slightly pitched. The model remained fixed in pitch throughout both sets of experiments; in effect trim of +8 degrees.

A traverse rig (Figures 22 and 23) was specially designed for this experiment and used to position the Freestone probe. The traverse rig consists of a large frame which is bolted to the top of the walls of the open

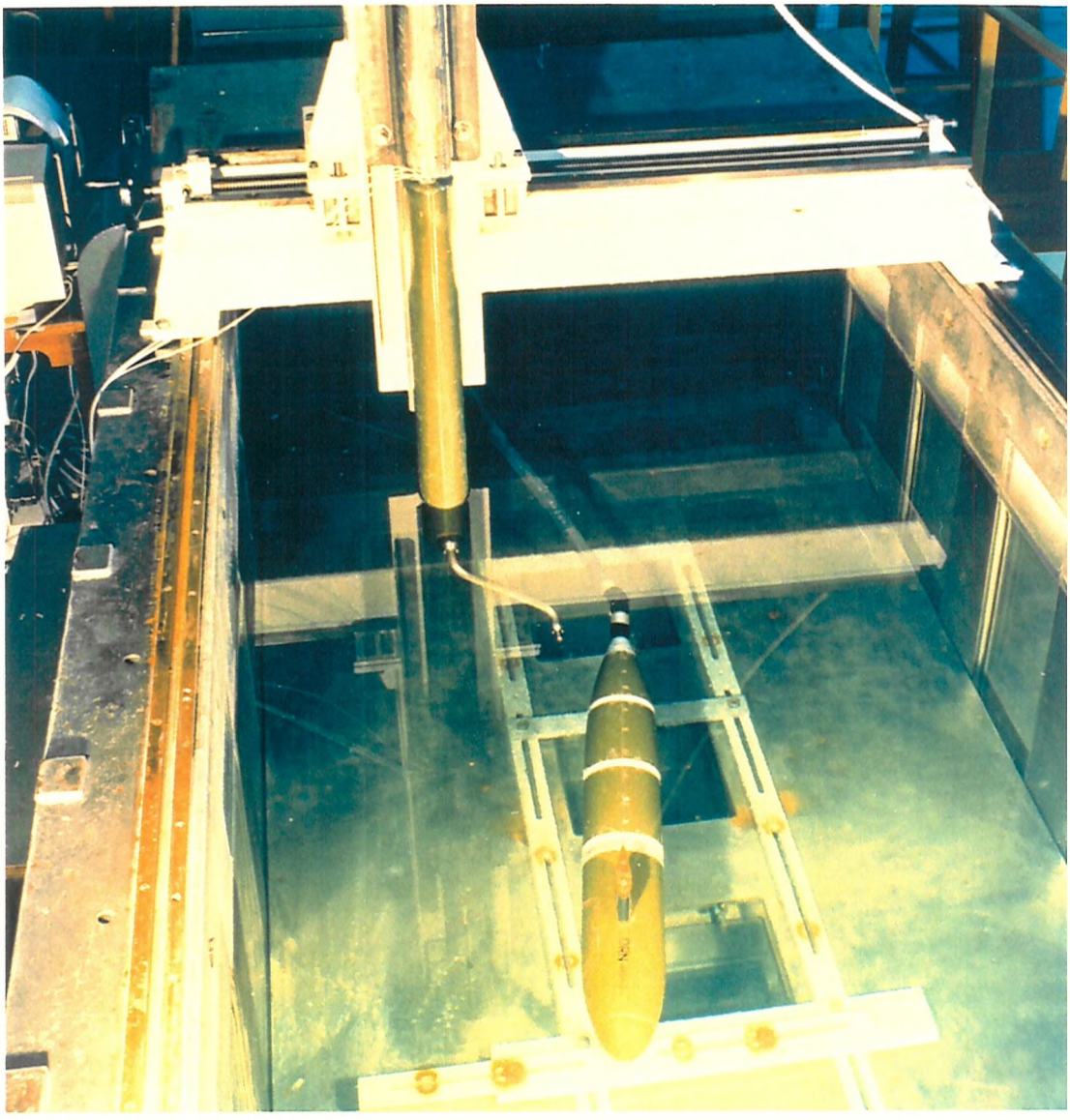

FIG.22 TRAVERSE RIG AND MODEL IN CIRCULATING WATER CHANNEL

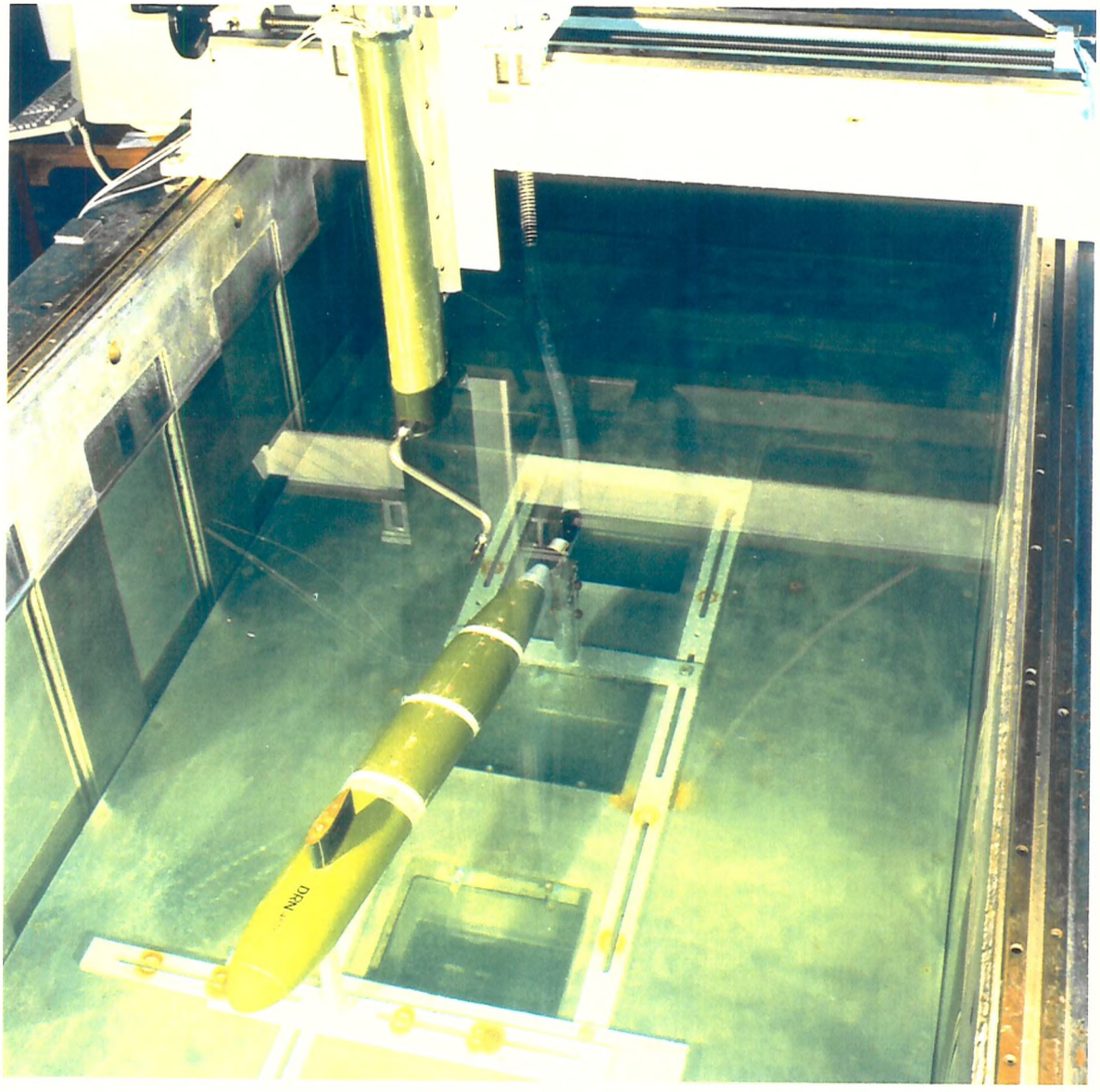

FIG.23 TRAVERSE RIG AND MODEL IN CIRCULATING WATER CHANNEL

Circulating Water Channel. The frame supports a large strut part of which protrudes into the water. On the end of this large strut is a smaller dog-legged strut which holds the probe. Cavities exist through the struts and nylon tubes are attached to the probe through these cavities. The tubes lead to pressure transducers outside of the channel. The larger strut can move vertically or horizontally along the frame which enables the probe to be positioned at any y,z co-ordinate in the channel. The rig is robust and no significant vibration was noted during the experiment.

For the second stage of the experiment the rig was controlled by stepper motors that gave 0.5 mm positional accuracy. A single computer program was also used during the second stage to control the rig, acquire data and perform the arithmetic operations to calculate vorticity.

5.2.6 Calibration of Instrumentation

The pressure difference from the vorticity probe was measured on a 100 mb transducer. This transducer was calibrated by inputing known pressures and measuring the voltage levels. By fitting a least squares line to the plot of pressure against volts (Figure 24) a calibration factor of 20.39 was calculated.

The pitot static tube in the centre of the Freestone probe was also connected to a 100 mb transducer. This was calibrated by varying the flow velocity in the empty channel and plotting volts against velocity (Figure 25). The line was quadratic and it was decided to fit a quadratic curve through the data for values greater than 0.5 volts and a least squares line below 0.5 volts. The equation is noted in the DATS program in Appendix 1.

The pressure transducer in the Scanivalve had a maximum of 1 bar. One side was exposed to atmospheric pressure and the other side to a known pressure. Again pressure was plotted against volts (Figure 26) and a calibration factor of 67.2 was calculated.

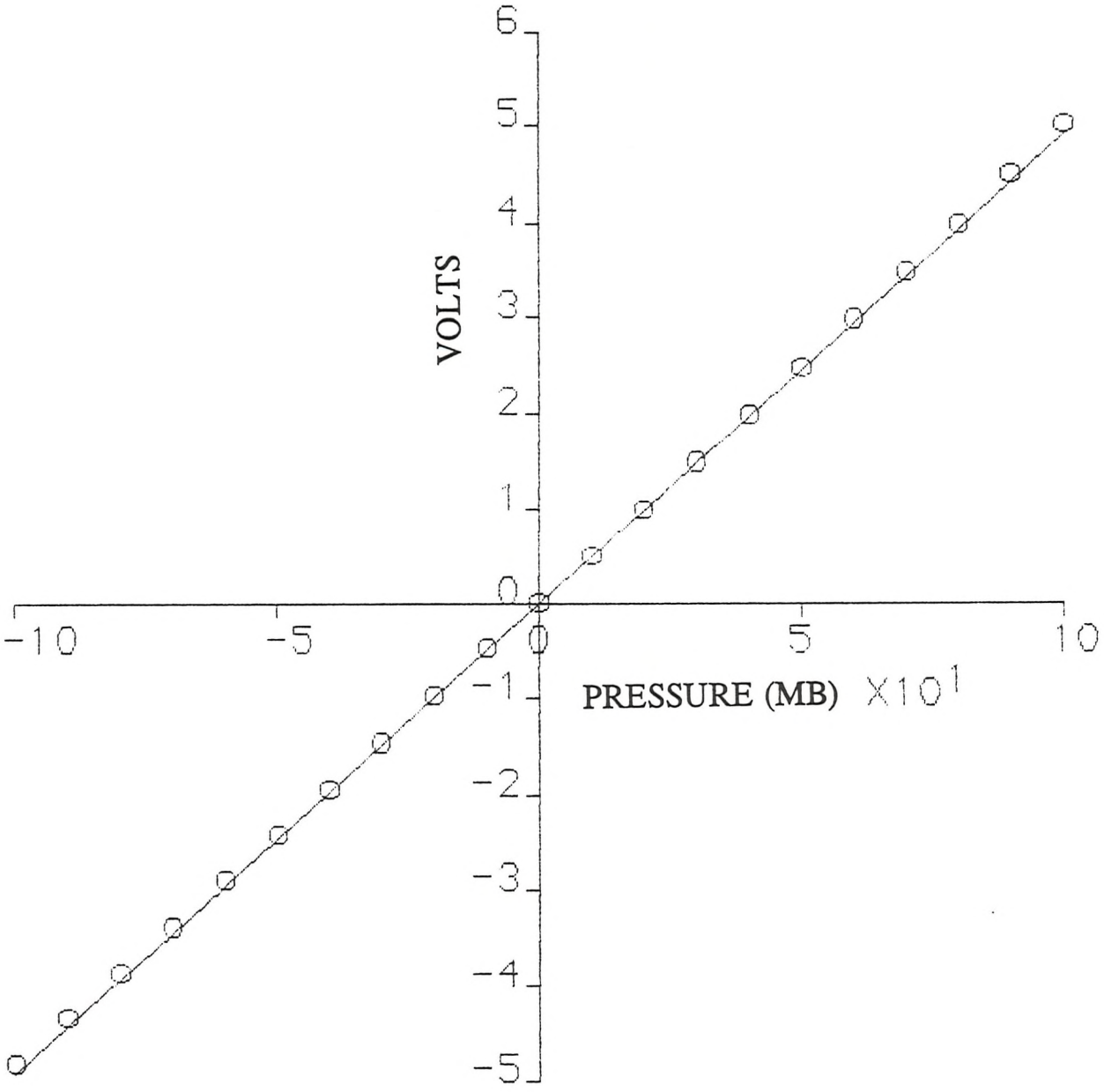

FIG.24 CALIBRATION GRAPH FOR VORTICITY PRESSURE TRANSDUCER

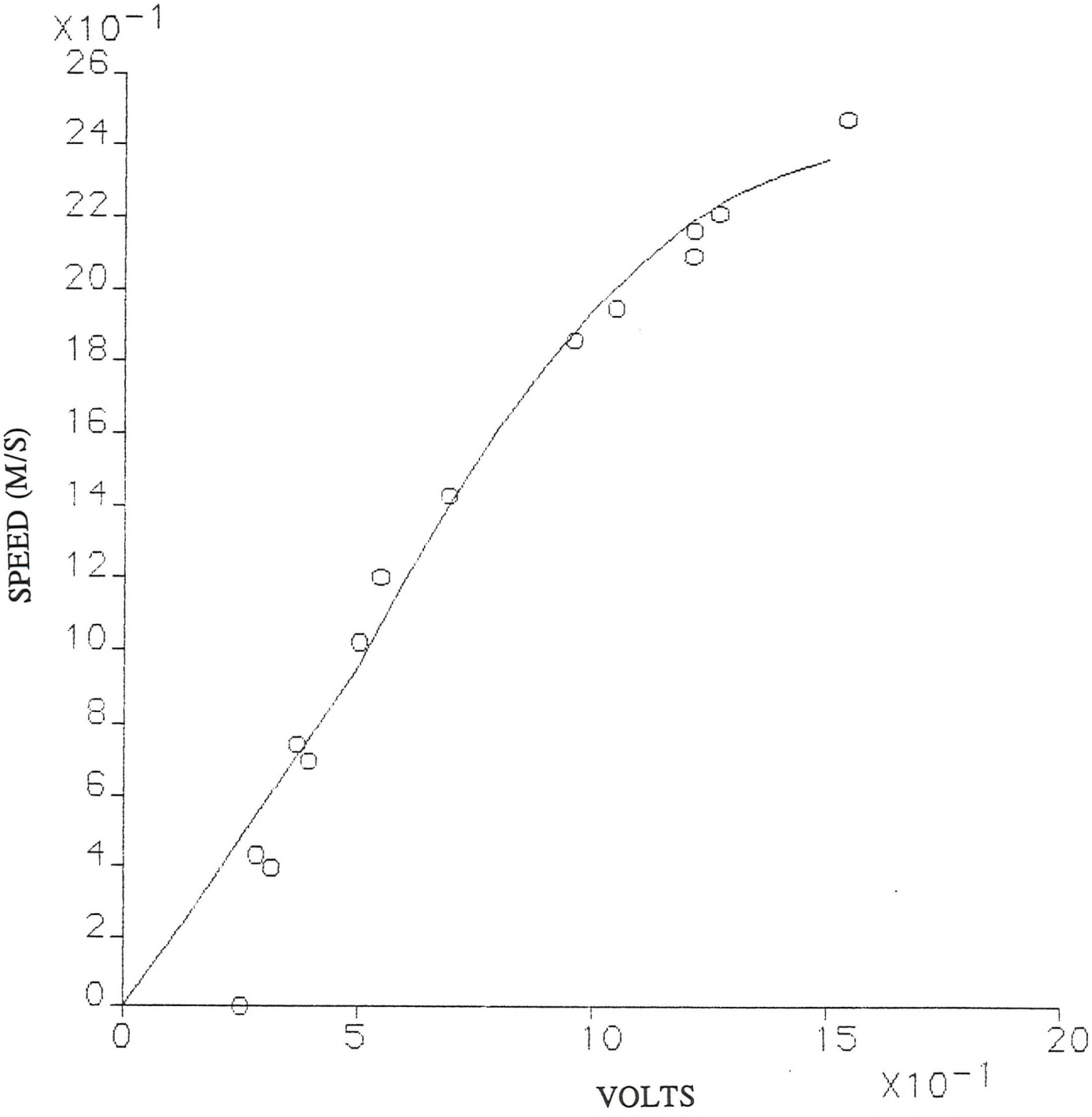

FIG.25 CALIBRATION GRAPH FOR PITOT STATIC TUBE ON PROBE

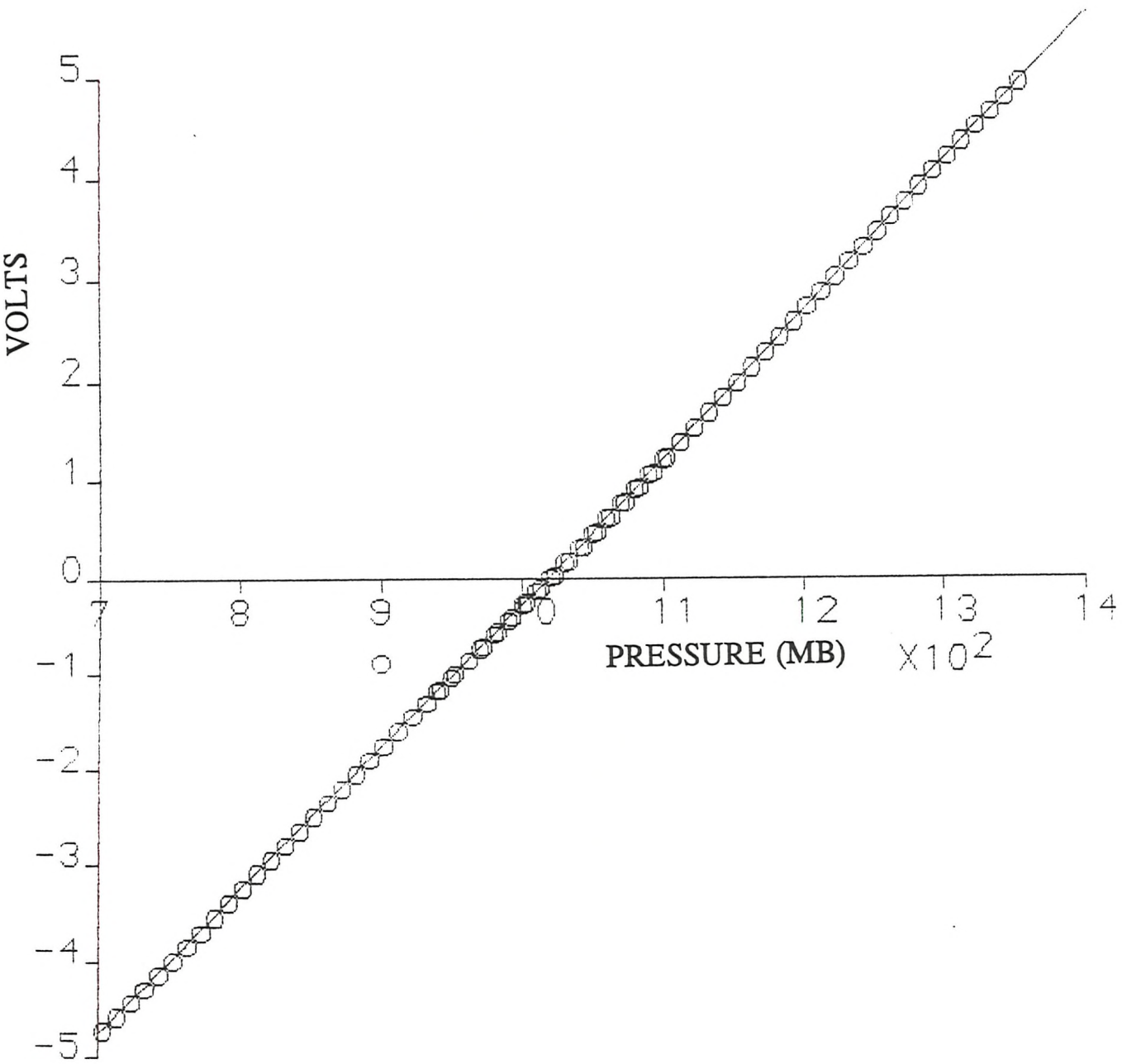

FIG.26 CALIBRATION GRAPH FOR SCANIVALVE TRANSDUCER

5.2.7 1990 Experiments

5.2.7.1 Problems with the model

It was intended that pressure measurements would be taken using a Scanivalve. Unfortunately aluminium was used for the rings; the metal corroded in the stainless steel Circulating Water Channel, blocking the pressure tappings and preventing any valid pressure measurements. Blisters at the rear of the model are clearly visible in Figure 27. Other quality problems were also evident: the strut supporting the model was coarse and the finish of the model was rough. Rough areas of the model can trigger separation and separated flow from the strut supporting the model may cause interference in the flow. Despite these problems it was felt that it was worth continuing and using the experiments as a learning period. Plans were initiated to have the model modified using brass rings and a new strut manufactured that would create less of an obstacle in the flow.

Due to the unavailability of a DEC PDP11 microcomputer a Hewlett Packard Micro was used which produced hard copies of voltages. These voltages were transferred manually to the PRIME 9955 mainframe where voltages were converted to vorticity values and thereafter analysed. Offset values were taken without flow and subtracted from the measurements taken with flow.

5.2.7.2 Vorticity measurements

During 1990 vorticity measurements were taken at five stations aft of the bridge fin (see Figure 18) with the following configurations

a. body at 0 degrees (relative to the channel), appendage at -10 degrees (relative to the model).
b. body at 10 degrees (relative to the channel), appendage at 0 degrees (relative to the model).

A probe was specially manufactured at RAE Pyestock and

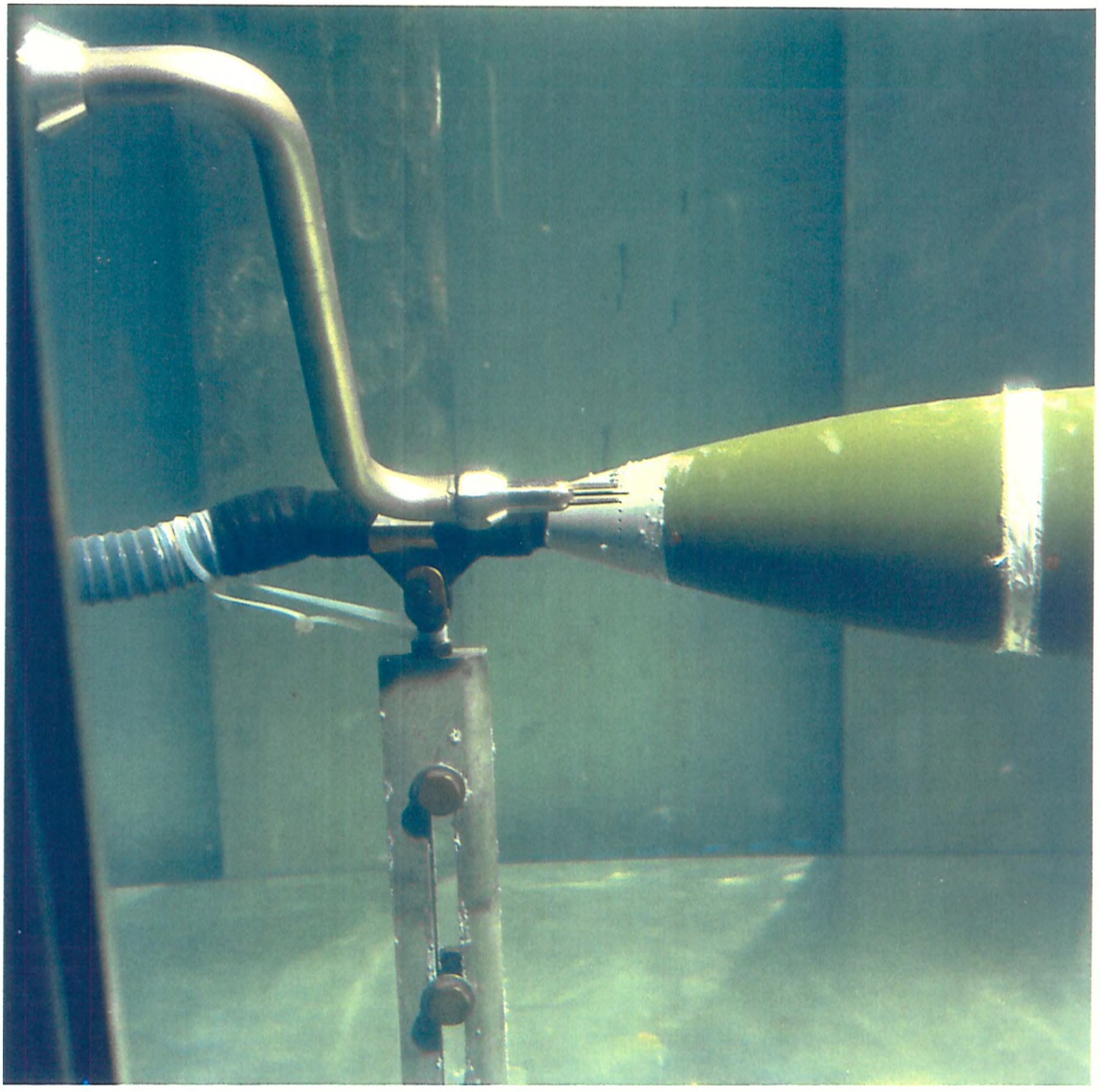

FIG.27 FREESTONE PROBE AT REAR OF MODEL 1990
BLISTERS ARE VISIBLE ON REAR OF MODEL

a quality control inspection showed slight positional inaccuracies in the yaw meters, however these were minimal.

5.2.8 1991 Experiments

5.2.8.1 The modified model

The model used in the 1990 experiments was modified with brass rings and a new strut manufactured to create less of an obstacle in the flow (Figure 28). A brass base plate (Figure 29) was manufactured to allow the model to be used without the appendage and ensure a flush surface at the appendage position.

During 1991 vorticity and pressure measurements were carried out. The DEC PDP11 microcomputer was used with the DATS acquisition and analysis package.

5.2.8.2 Computer Package for Data Acquisition and Analysis

DATS consists of a number of modules which can be used in a computer program with FORTRAN commands such as DO loops and IF statements. Data is recorded in multiplexed digital format. It is particularly useful for time series work as files are created over acquisition periods and the user can acquire time histories of a number of measurements simultaneously. For the purpose of this experiment short acquisition periods were used and averages were taken over the period to give the acquired value. An example of the two DATS 'jobs' used are given in Appendix 1.

Modules PULSE and MOVER were written in-house by DRA Haslar staff.

5.2.8.3 Measurements

The vorticity measurements were taken at $x'=0.575$ and $x'=0.925$ with:

a. Body at 5 degrees (relative to the channel), appendage at 0 degrees (relative to the model).

FIG.28 MODEL DRN 1991 - MODIFIED WITH BRASS RINGS
NOTE RING AT FRONT OF MODEL AND WIRE ON FIN FOR
TURBULENCE STIMULATION

FIG.29 BASE PLATE FOR UNAPPENDED MODEL

b. Body at 10 degrees (relative to the channel), appendage at 0 degrees (relative to the model).
c. Body at 15 degrees (relative to the channel), appendage at 0 degrees (relative to the model).

All measurements were repeated at $x'=0.925$ without an appendage.

Pressure measurements were taken at four stations at the following conditions:
(a) Unappended with body yawed 0 degrees to 17.5 degrees relative to centre line (2.5 degree intervals).
(b) Appended (as (a)).
(c) Body at 0 degrees, appendage at 5 degrees, 10 degrees, 15 degrees and 20 degrees.

A Scanivalve was used to scan round the 36 pressure tappings at each station.

Ascii files were created and transferred from the PDP11 to the Prime 9955 mainframe via magnetic tape. A more refined analysis of the data was carried out using the Prime system.

Chapter 6

Analysis of Results

6.1 1990 Results

6.1.1 The analysis

The horizontal traverses of vorticity were plotted. The traverses tended to have an offset value in the region 5 rad/sec where zero vorticity was expected from theory and practice. This is certainly due to the fact that the probe was not aligned with the local flow direction. Average offset values were calculated and subtracted from the overall data. A typical corrected traverse plot is shown in Figure 30. Figure 31 shows a contour plot of vorticity measurements behind the bridge fin i.e. at $x'=0.33$.

The fin vortex can be seen shedding in Figures 15 and 16. Figure 15 shows a normal exposure, typically 1/200 sec shutter time. The bubbles in the channel distort the picture and to create a clearer photograph a long exposure (typically 1/2 sec) was used for Figure 16. The fin vortex can be seen as it carries downstream in Figures 19 and 20.

The horizontal traverses were integrated using a simple trapezoidal rule to give the circulation density. The circulation density values were then integrated (Equation 6.1) in the vertical direction to give the total circulation in that area of the body.

$$\Gamma=\int_{-\infty}^{\infty}\int_{-\infty}^{\infty}\zeta_x dydz \qquad (6.1)$$

The results are presented in Tables 3 and 4.

Due to the high turbulence in the channel the vortex is moving around. The fixed probe therefore picks up fluctuating vorticity values. The measured strength of the

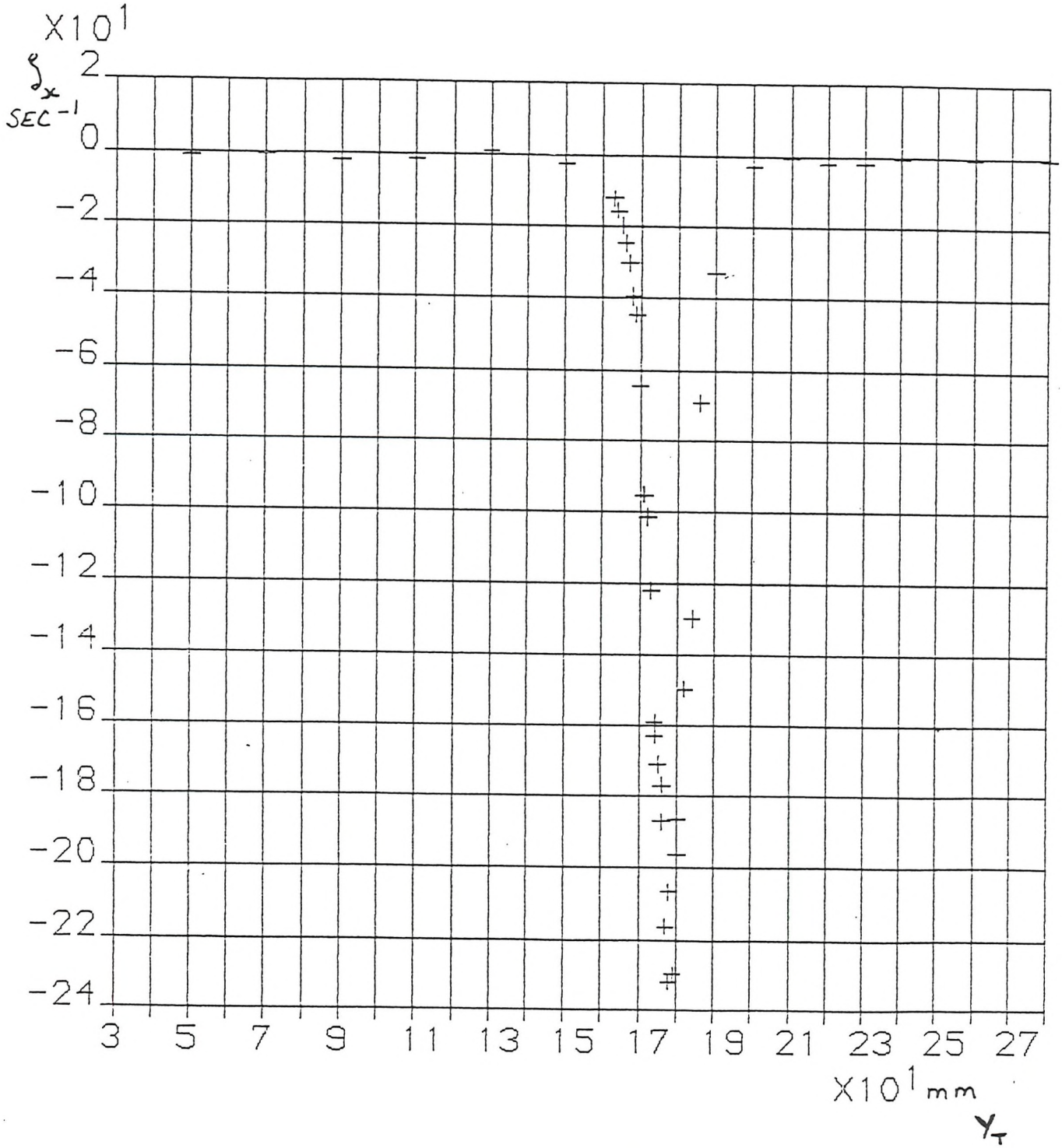

FIG.30 TYPICAL APPENDAGE VORTEX TRAVERSE
BODY INCIDENCE 0°, APPENDAGE INCIDENCE -10°
Z = 143 mm, X' = 0·33

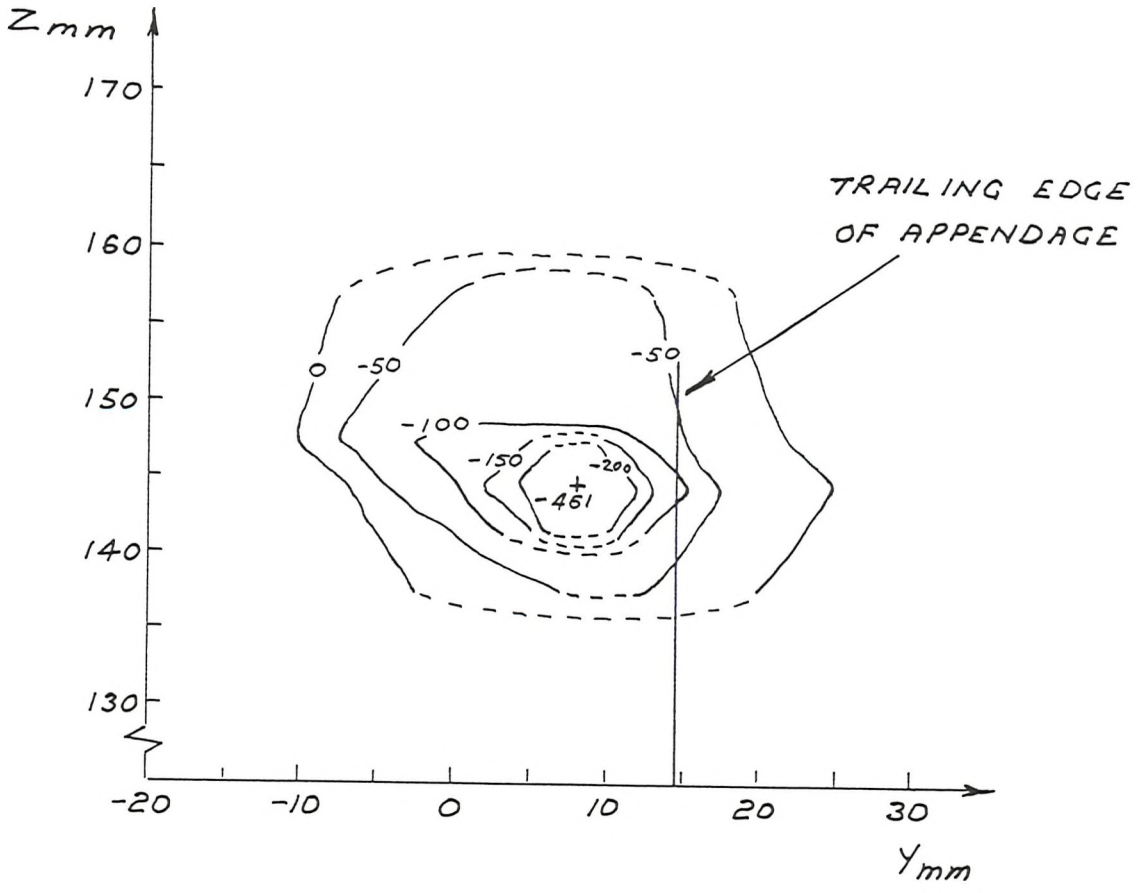

FIG.31 APPENDAGE CIRCULATION CONTOURS

Table 3

APPENDAGE VORTEX CIRCULATION AND PEAK VORTICITY

x′	Body α Degrees	Fin α Degrees	Γ_F	Γ_F/cU	ζ_{MAX}	(y_{max}, z_{max}) mm
0.33	0	-10	-0.067	-0.24	-461	8, 144.5
0.33	10	0	0.070	0.25	515	8, 143.5
0.4	0	-10	-0.059	-0.21	-312	6.5, 147.5
0.4	10	0	0.068	0.24	314	17.5, 146.5
0.575	0	-10	-0.072	-0.257	-289	11.5, 148
0.575	10	0	0.072	0.256	305	47, 147
0.75	0	-10	-0.062	-0.219	-310	17, 139.5
0.75	10	0	0.080	0.284	323	72, 135.5
0.925	0	-10	-0.064	-0.226	-265	19, 129
0.925	10	0	0.063	0.224	227	96.5, 125

Table 4

BODY VORTEX CIRCULATION

x'	Body α Degrees	Fin α Degrees	Γ_D	Γ_X	Γ_D/UD	Γ_X/UD
0.575	10	0	0.001	-0.034	0.005	-0.11
0.75	10	0	0.004	-0.034	0.013	-0.11
0.925	10	0	0.009	-0.072	0.029	-0.25

appendage vortex fluctuates as does the measured peak vorticity. The appendage vortex strength and peak value should be taken as the value measured directly behind the fin.

According to Whicker and Fehlner [25]

$$\frac{dC_L}{d\alpha} = \frac{1.8\pi a_e}{1.8+\sqrt{4+a_e^2}} \qquad (6.2)$$

According to Glauert [24]

$$\Gamma = \frac{L}{\rho U S_1} \qquad (6.3)$$

where

$$S_1 = \frac{\pi}{4} S \qquad (6.4)$$

From equation (6.2) the lift on the fin at -10 degrees was calculated to be -11.5 N, and from equation (6.4) the spanwise location S_1 of the vortex is 0.071 metres. Therefore by equation (6.3) the circulation would be -0.065 m^2/sec. Taking the circulation measured directly behind the fin to be Γ_F=-0.067 m^2/sec which is 4 per cent more than the theoretical estimate. Thus a good agreement gives confidence in the results.

As seen in other papers on this subject (Kaplan [38]) the presence of the fin vortex appears to reduce the upper body vortex strength. Vorticity contour plots, Figures 32 and 33, show body vortex contours at two different stations. These plots are of vorticity values measured at each station with body incidence of 10 degrees and the appendage at 0 degrees to the body. The asymmetry between deck and keel vortices is apparent and the fin vortex can also be seen. The lower body vortex extends into the upper quadrant.

From the results of the lower body vortex there appears to be interference from the strut holding the model. This

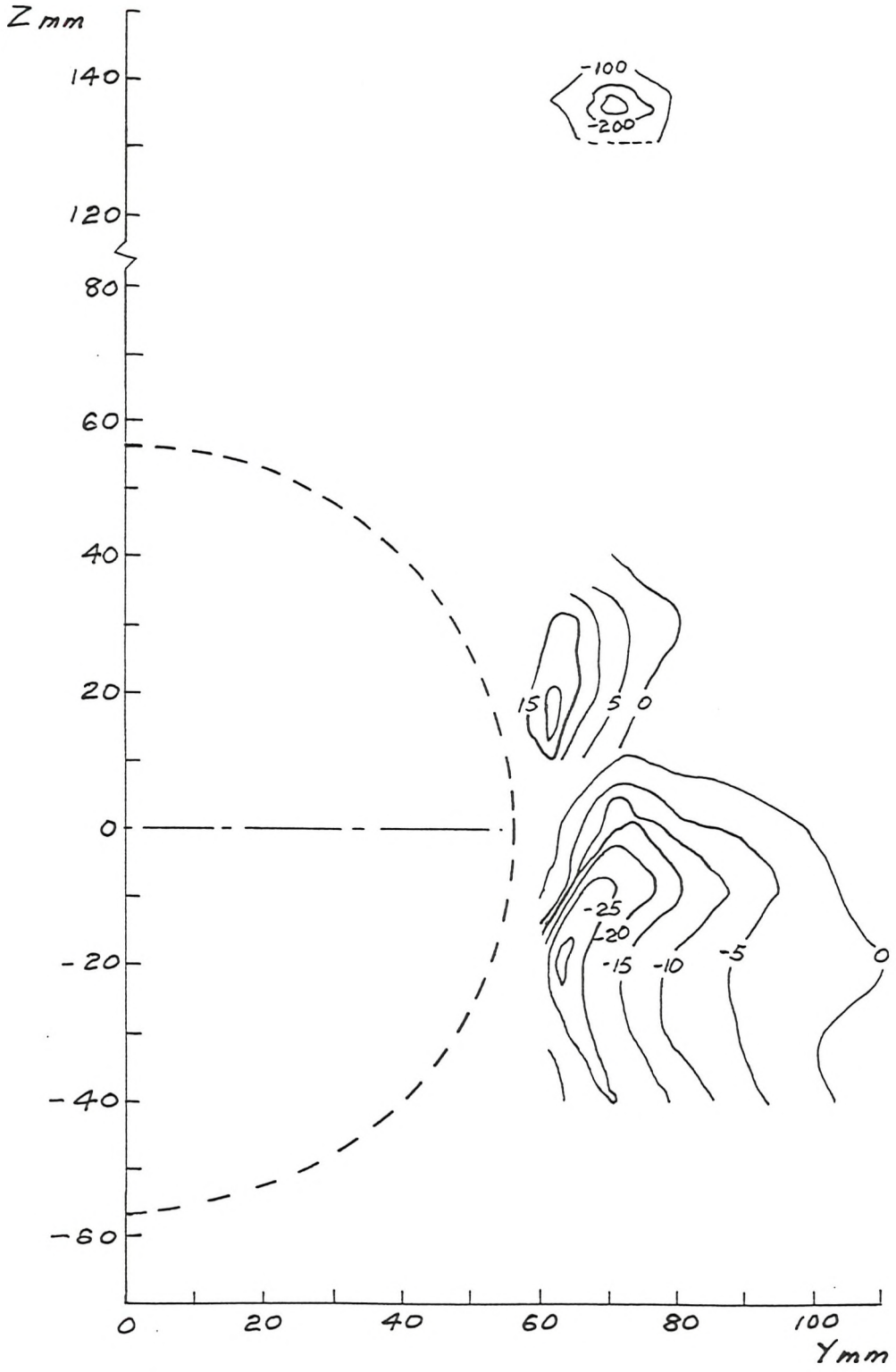

FIG.32 BODY VORTEX CONTOURS, BODY INCIDENCE 10 DEGREES, APPENDAGE INCIDENCE 0 DEGREES, X'=0.75

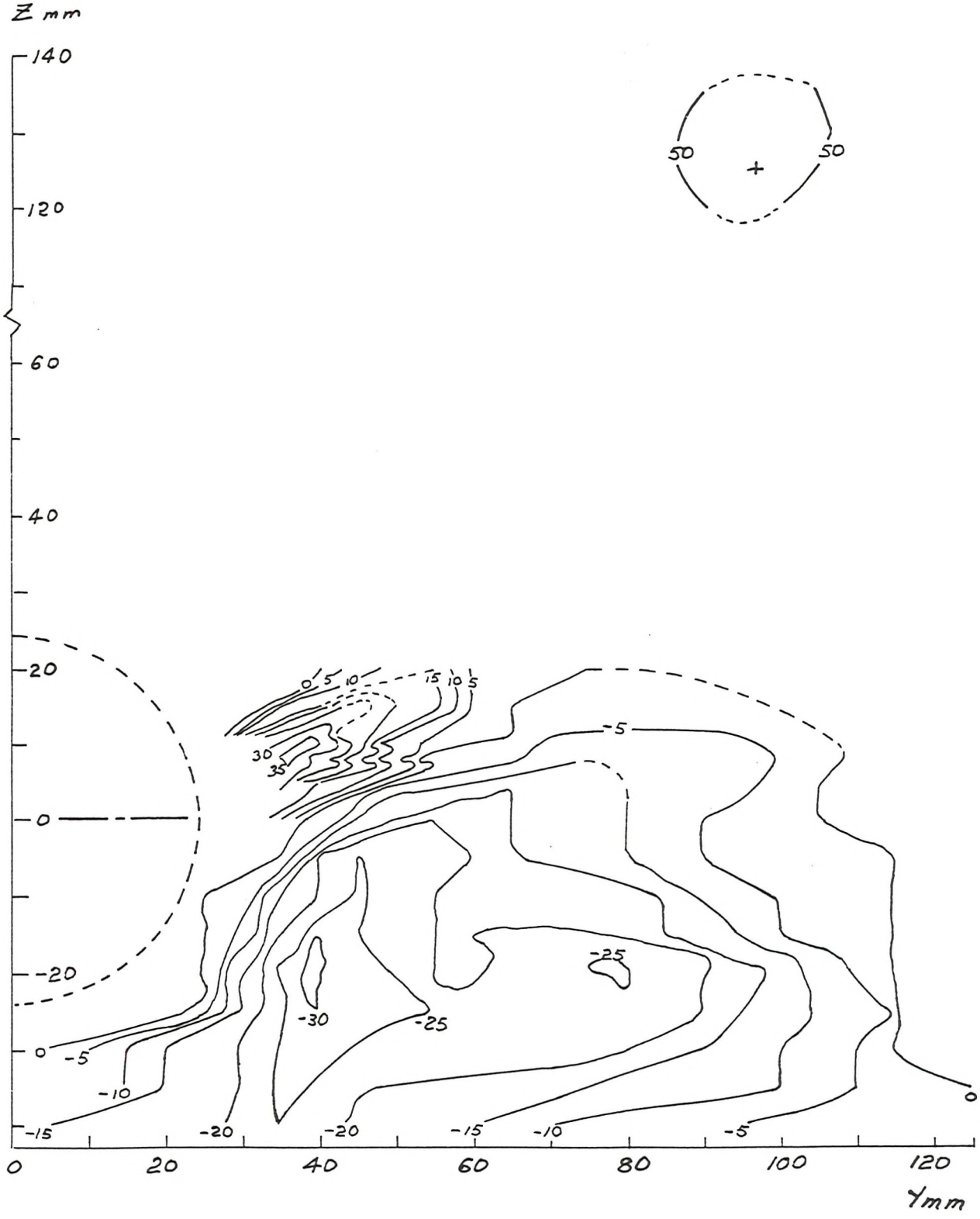

FIG.33 BODY VORTEX CONTOURS, BODY INCIDENCE 10 DEGREES, APPENDAGE INCIDENCE 0 DEGREES, X' =0.925

is clearly evident in the contour plot shown in Figure 33 and also in the traverse plot shown in Figure 34. Looking at the results at $x'=0.575$ for circulation there appears to be a disturbance in the flow pattern probably caused by the presence of the strut. A flow visualisation study was conducted and small vortices were seen to be shedding from the strut but did not appear prominent at the rear of the model.

6.1.2 Accuracy of Data

As in all experimental work there is an element of error involved in obtaining accurate results. This particular experiment had several factors that contributed towards experimental error.

(i) The use of transducers in measuring pressure can be problematic. Air in the tubing can distort results. The transducers were bled regularly with deaerated water during the experiment.

(ii) The use of the Circulating Water Channel as a facility. Due to the size of the facility a 1 metre model was used. This gave a Reynolds number of 0.3×10^6 (calculating R_e with diameter) which is below the critical Reynolds number of 1.0×10^6.

A 1 metre model at incidence will create a blockage in the channel causing slight changes in flow velocity.

Channel walls and floor will also affect the results.

It is difficult to have the probe exactly aligned with the flow. Offset values measured at a distance remote from the vortex centre were subtracted to account for this.

(iii) The model had rough areas which may have triggered separation.

(iv) Separated flow from the strut supporting the model may cause interference in the flow.

(v) Accuracy of the Freestone probe as an instrument to

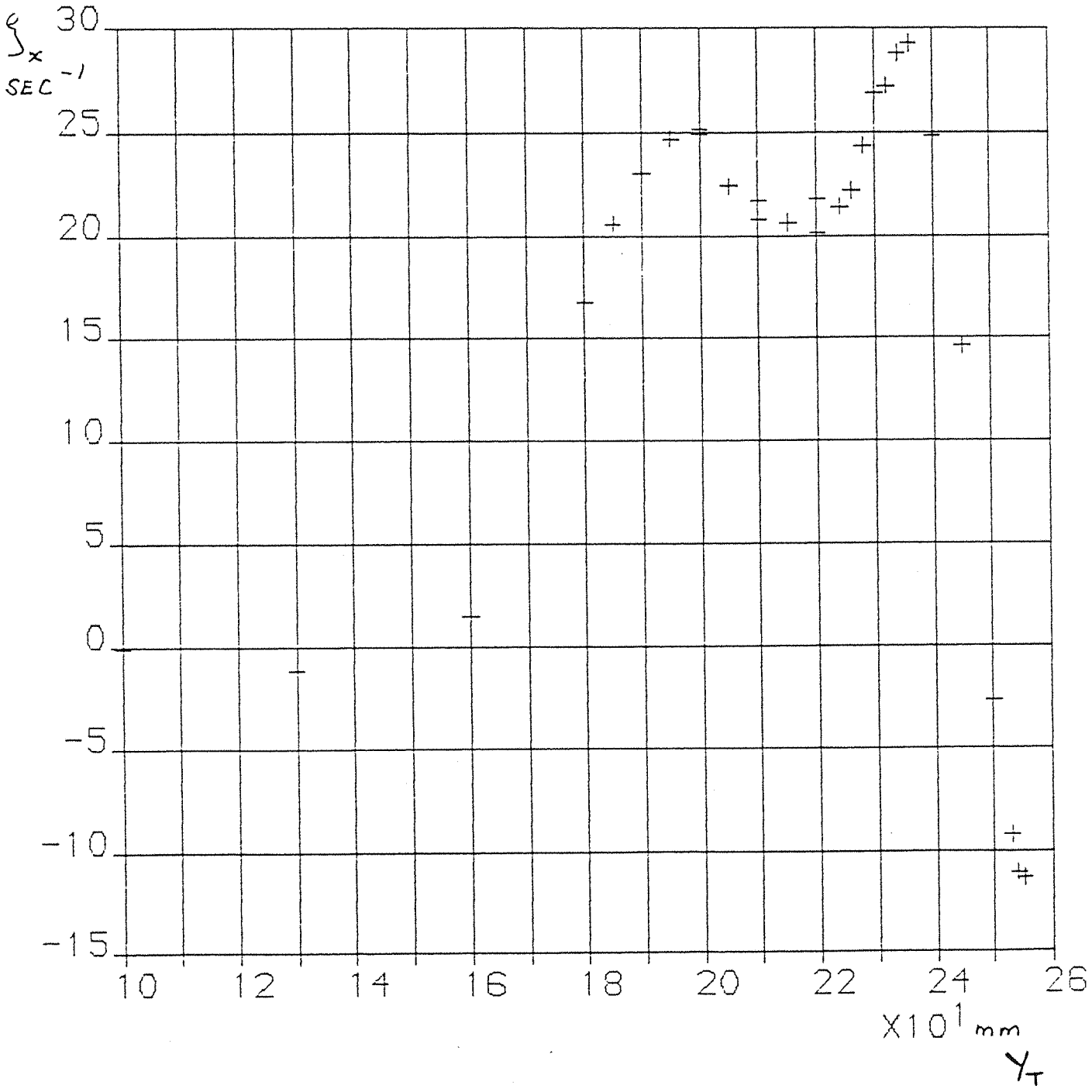

FIG.34 BODY VORTEX TRAVERSE, BODY INCIDENCE 10 DEGREES, APPENDAGE INCIDENCE 0 DEGREES, Z=-20mm, X'=0.925

measure vorticity.
(a) Is K=2.47 the correct calibration factor given the probe was not calibrated?
(b) How important are the positional inaccuracies in the probes manufacture?

On reflection the 1990 vorticity results were more significant than first assumed despite the problems with the model.

6.2 1991 Results

6.2.1 Problems with the probe

The probe used in the 1990 experiments was broken during the setting up of these experiments and a replica probe had to be manufactured. During the analysis of the experiment results it became apparent that 1990 and 1991 results didn't compare and that there were considerable offsets in the 1991 results. A comparison of the appended body results at 10 degrees for $x'=0.925$ in each year give an idea of the magnitude of the offsets in 1991. On consideration these offsets were due to imperfections in the new probe. Uncorrected vorticity plots are shown in Figures 35 to 37. The plots do give a qualitative impression of the flow around the body under various conditions. However errors deter any valid calculations of circulation actually being made. The strut used in the 1990 experiments was replaced by a NACA 0020 brass strut which was always aligned with the flow. It was hoped this would cause less of an obstruction in the flow.

6.2.2 Pressure measurements

Pressure coefficients were calculated from the pressure tappings. Pressure measurements were taken for 0 incidence with no appendage which should ideally be zero. Due to the fact that the reference pressure was taken at $x'=0.4$ and a slight change in depth exists between stations because of a wave on the free surface there will be a discrepancy in

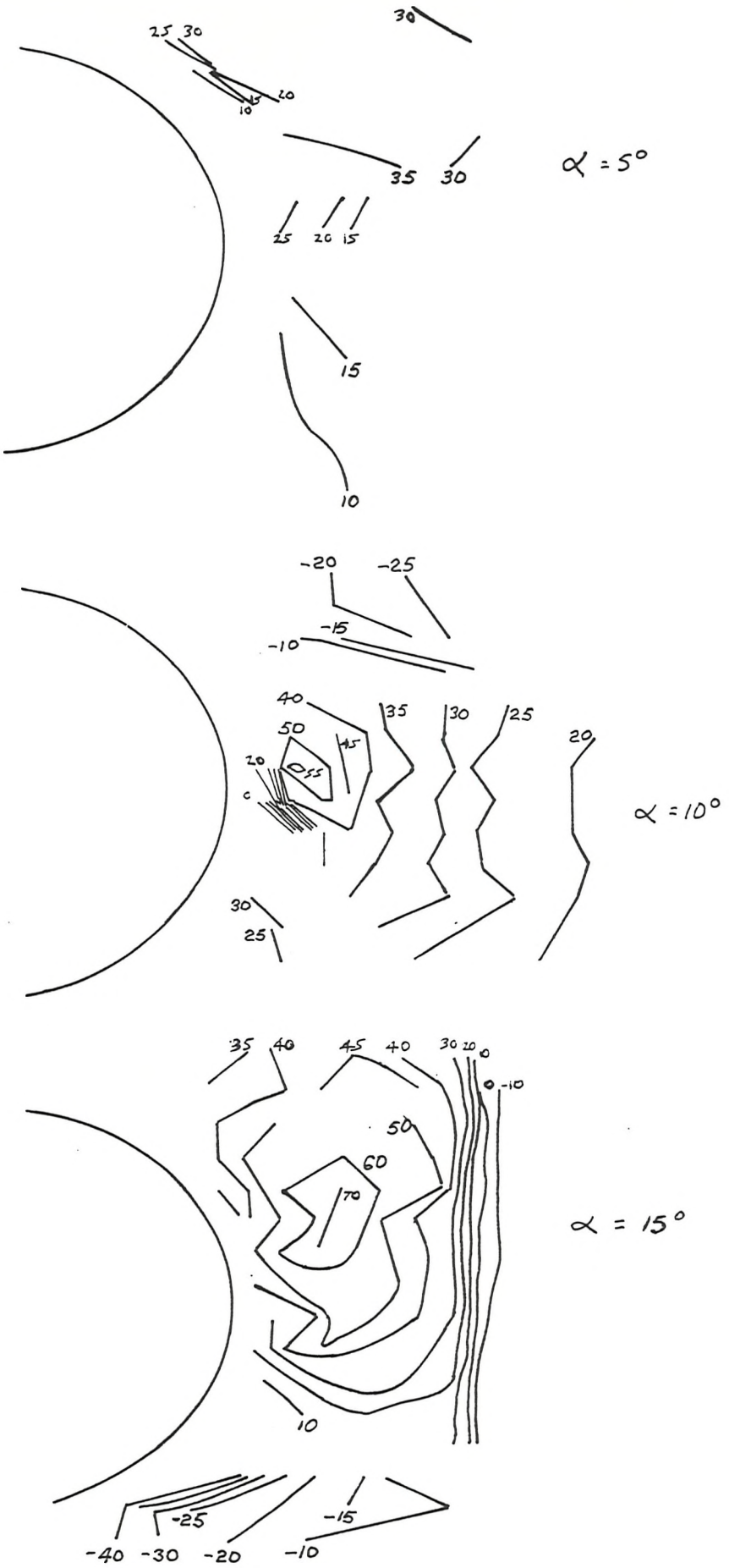

FIG.35 BODY VORTEX CONTOURS,
APPENDAGE 0 DEGREES,X' =0.575

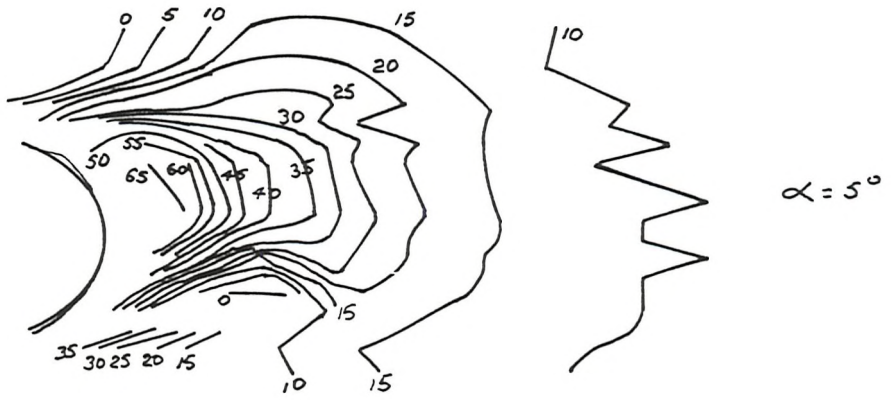

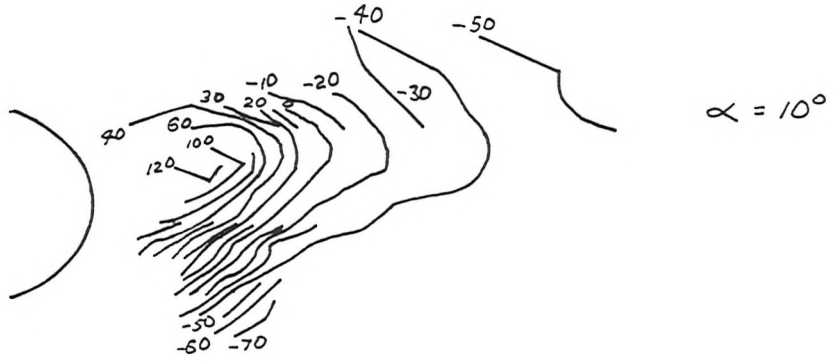

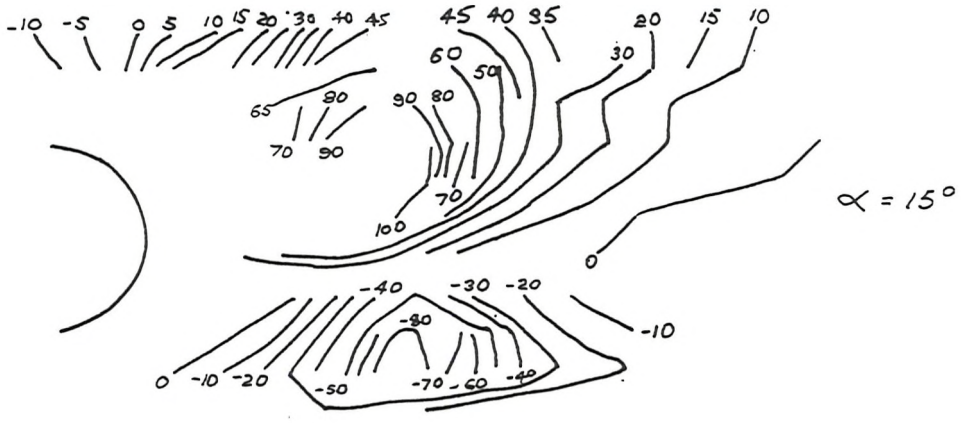

FIG.36 BODY VORTEX CONTOURS, NO APPENDAGE, X'=0.925

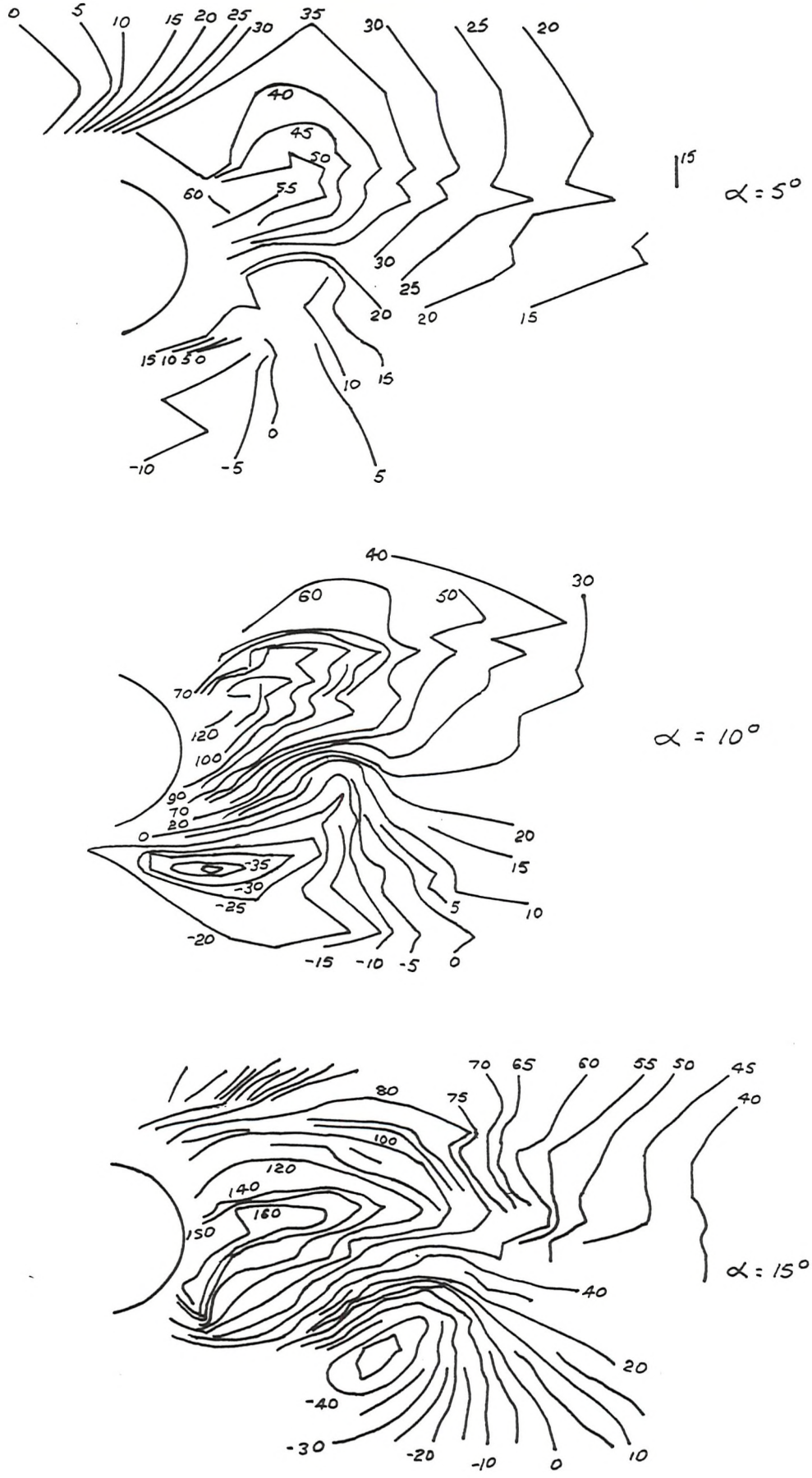

FIG.37 BODY VORTEX CONTOURS,
APPENDAGE 0 DEGREES, X'=0.925

the overall results. The zero incidence results were therefore subtracted from all other results to correct for any wave effect. This should also correct for the fact that the flow was shown to be angled at 8 degrees.

Numerical values for all the pressure coefficients are presented in Appendix 2. Array position 1 is at the top of the model and numbers increment round clockwise looking forward.

Figures 38 to 41 show plots of pressure coefficient for unappended and appended bodies. Note the suction on the top of the body for the unappended case at high angles; this doesn't occur with the presence of the appendage vortex.

Pressure coefficients were integrated to give force per unit length in both the Y and Z plane as given in equations 6.5 and 6.6.

$$F'_Y = \frac{-2\pi R}{36} \sum C_P \sin\theta_P \qquad (6.5)$$

$$F'_Z = \frac{2\pi R}{36} \sum C_P \cos\theta_P \qquad (6.6)$$

Integrated values (Figures 42 and 43) show that the distribution of side force along the body changes with the presence of the appendage.

Figure 44 shows Z forces for the unappended body which ideally should be zero. The offsets due to pitch should have been omitted by subtracting the zero incidence unappended case results. The values are certainly due to the fact that the model is slightly pitched.

Figure 45 shows Z force distribution for the appended case. There is a significant downward force on the model in this case which gets higher as the model is yawed to higher angles. The force reduces along the length of the model partly due to the fact that the surface area reduces but

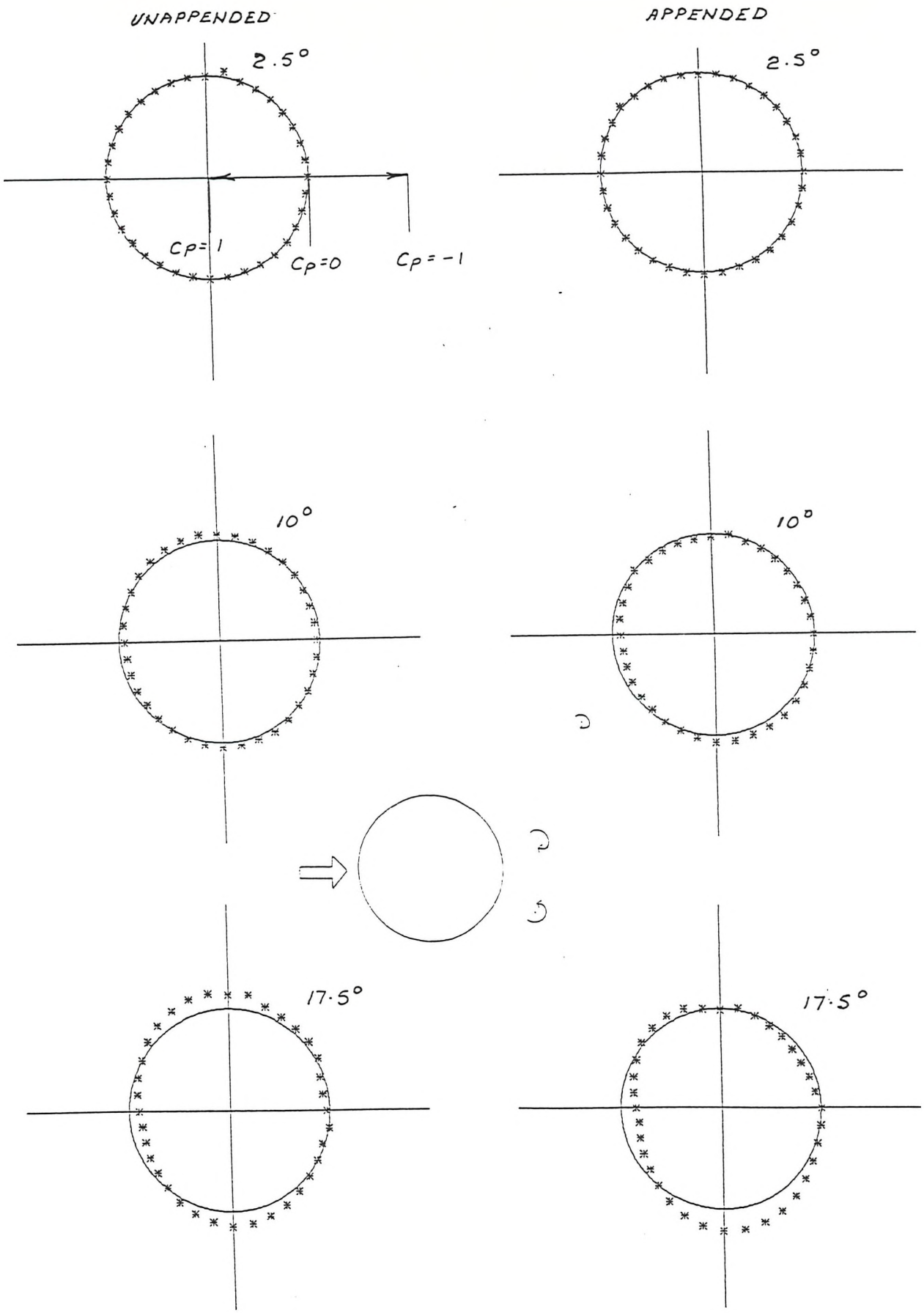

FIG.38 PRESSURE COEFFICIENTS X'=0.4

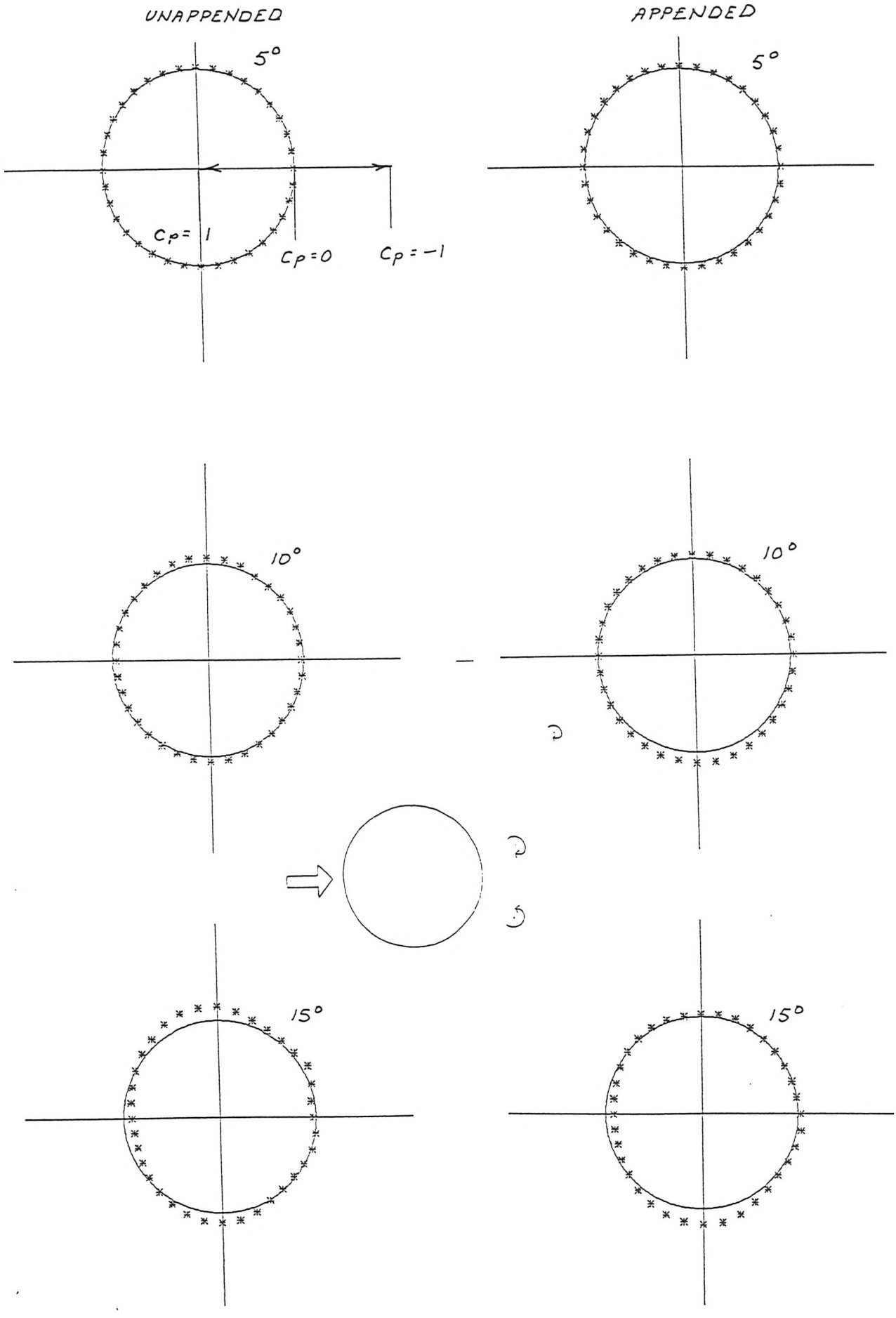

FIG.39 PRESSURE COEFFICIENTS X' =0.575

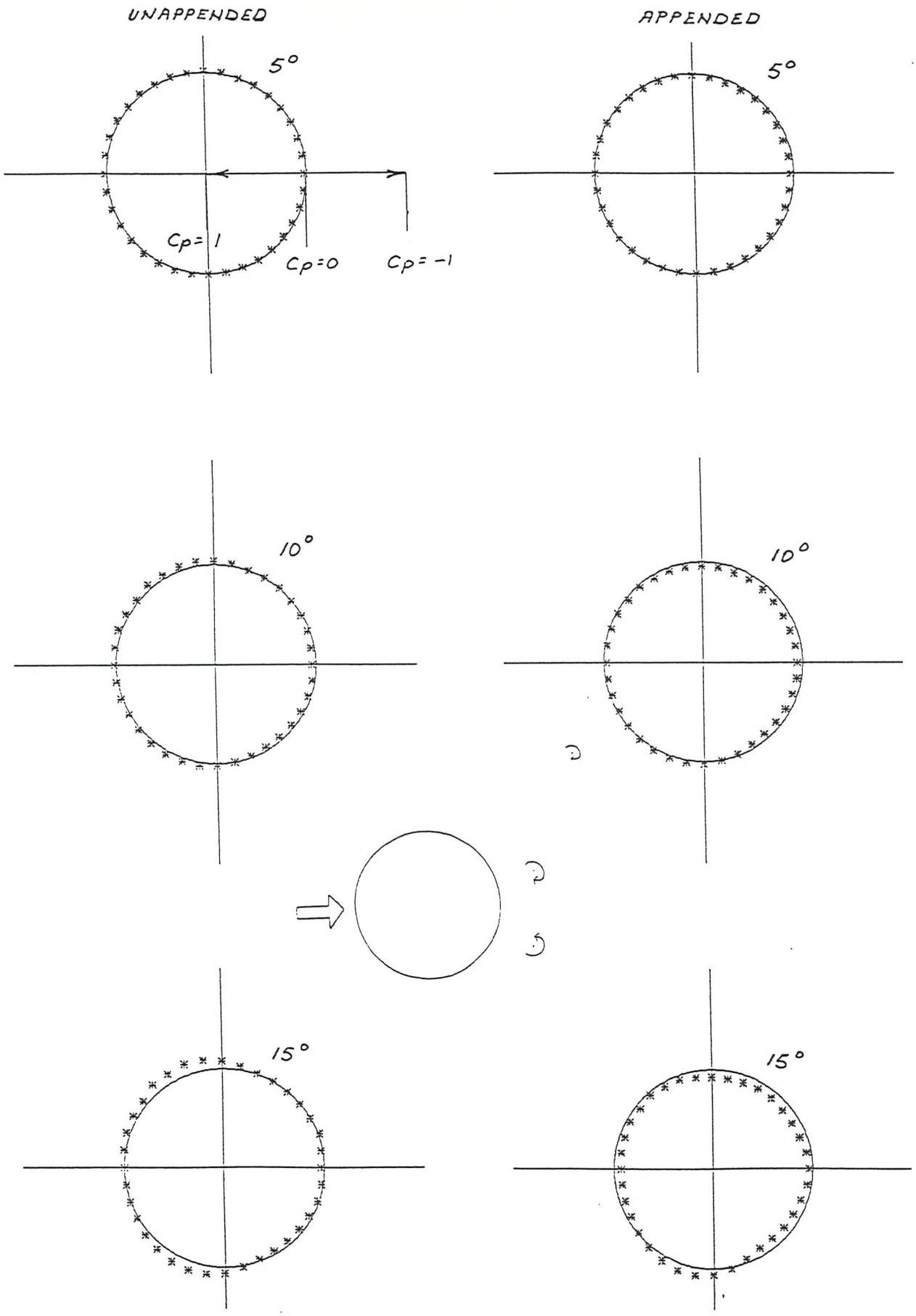

FIG.40 PRESSURE COEFFICIENTS X'=0.75

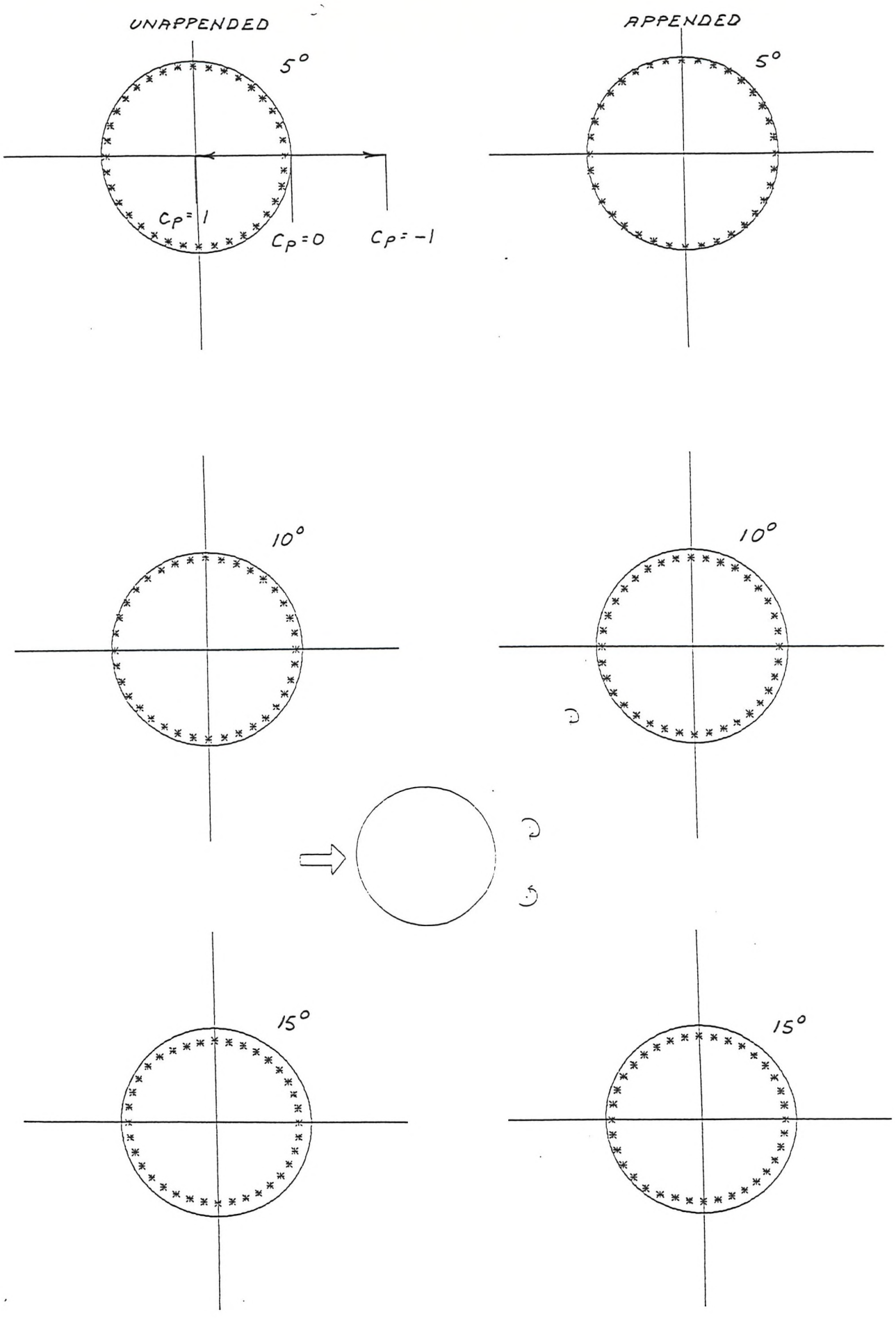

FIG.41 PRESSURE COEFFICIENTS X' =0.925

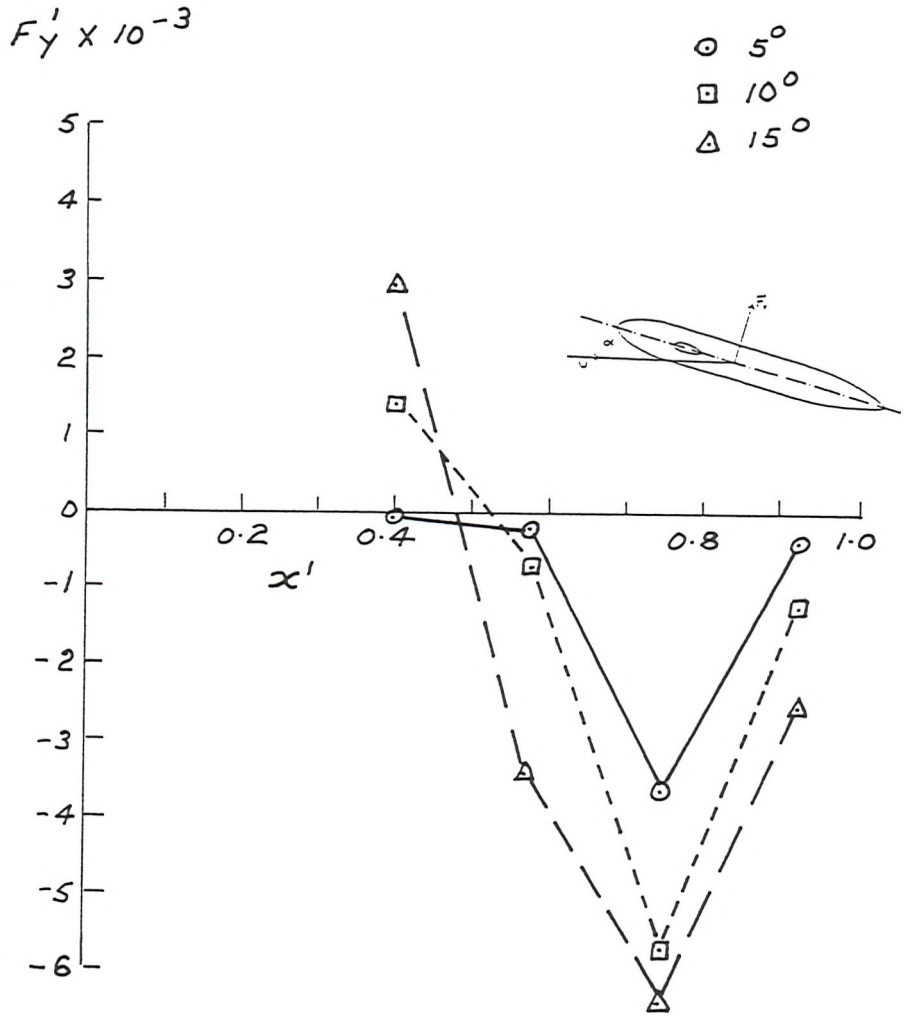

FIG.42 SIDE FORCE DISTRIBUTION FOR UNAPPENDED BODY

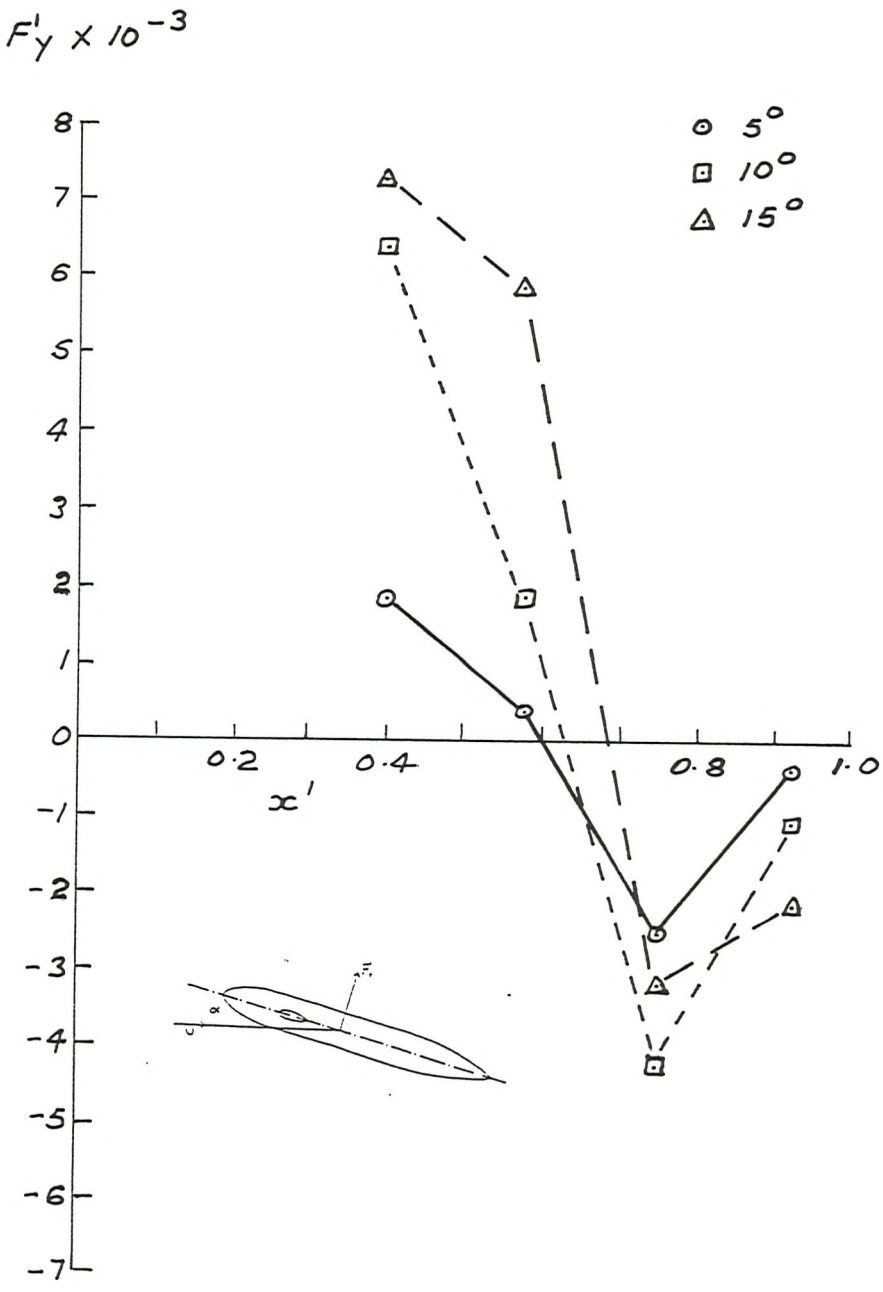

FIG.43 SIDE FORCE DISTRIBUTION FOR APPENDED BODY

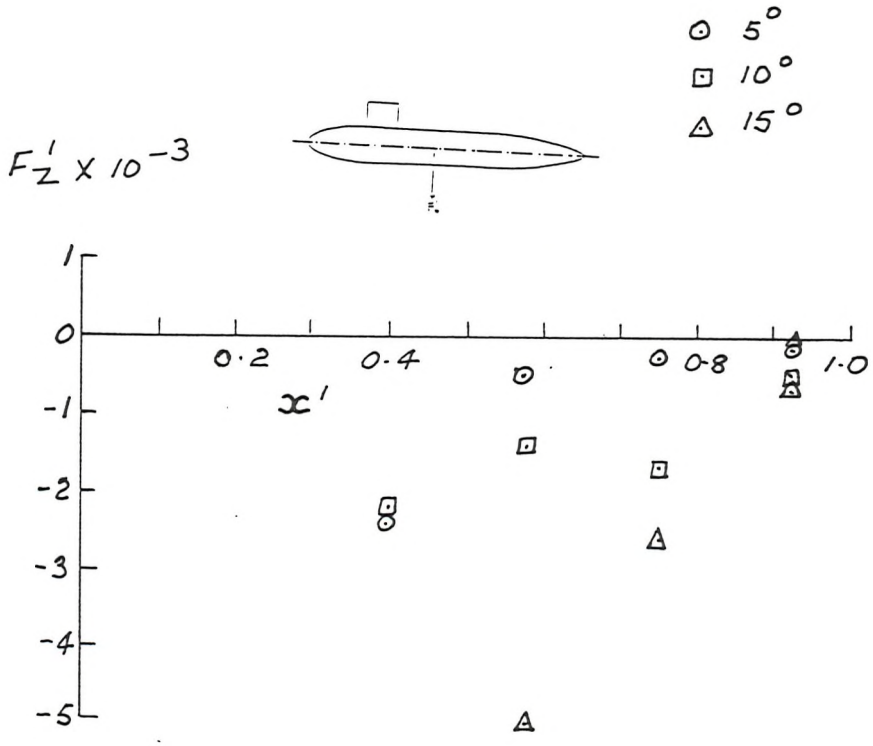

FIG.44 Z FORCE DISTRIBUTION FOR UNAPPENDED BODY

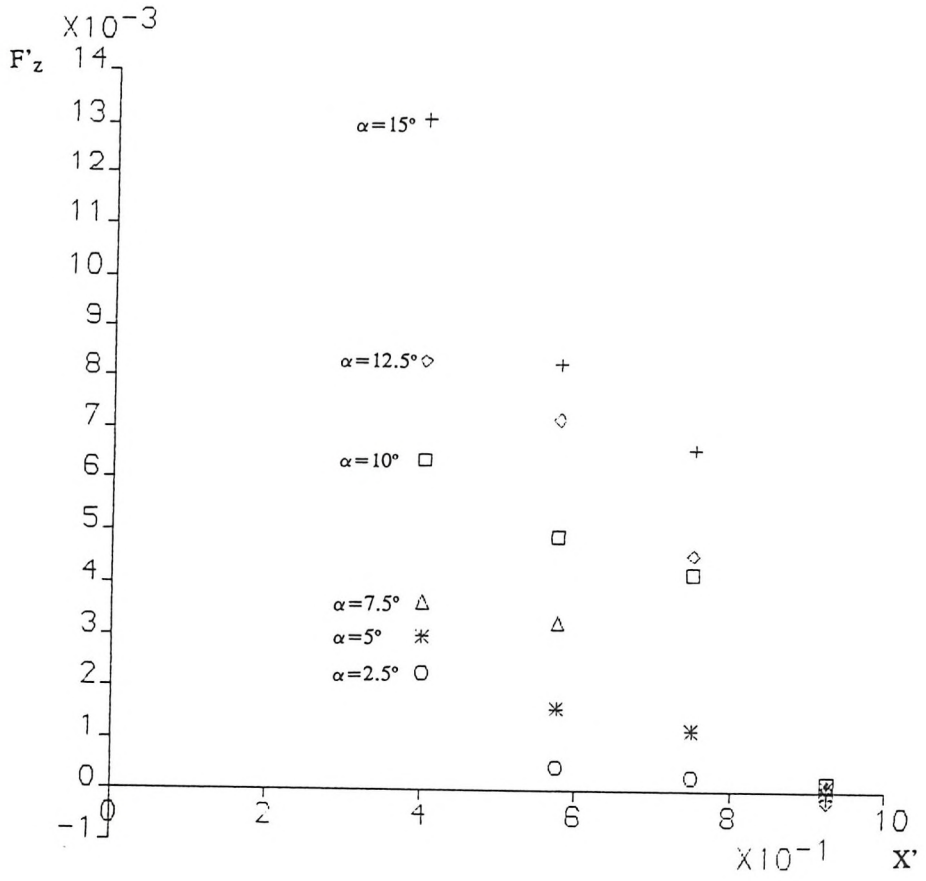

FIG.45 Z FORCE DISTRIBUTION FOR APPENDED BODY

also due to the change in flow pattern.

Figure 46 shows plots of pressure coefficient for an appended body at 0 incidence with the appendage at 20 degrees.

Integrated values are shown in Figures 47 and 48; values are small but variations do exist between station and angle.

There is a less significant effect on the body due to an isolated vortex compared with the change in pressure distribution for a body yawed at a high incidence. However; the presence of the appendage does change the pressure distribution around the body when the body is yawed.

6.3 Discussion of Vortex Results

From the vorticity contour plots an asymmetry between the deck and the keel vortices is apparent i.e. the keel vortex covers a much larger area. The values for circulation in Table 4 confirm this. Vorticity contours for $x'=0.575$ show there appears to be a single vortex certainly shed from the keel side of the body. For $x'=0.925$ there is evidence of two distinct vortices.

Table 4 shows at $x'=0.575$ $\Gamma_D=0.001$ which builds up to 0.009 at $x'=0.925$. Hence there is evidence of a deck vortex at $x'=0.575$.

The SUBSIM model at present assumes no separation until $x'=0.65$ and then two identical sets of vortices are created which as mentioned earlier is not the case in reality. This asymmetry in the circulation around the body then causes an asymmetry in the pressure distribution hence an out-of-plane force.

The change in circulation around the aft end of the body is not caused by the vortex from the tip of the fin but the presence of the fin itself. The fin acts as a

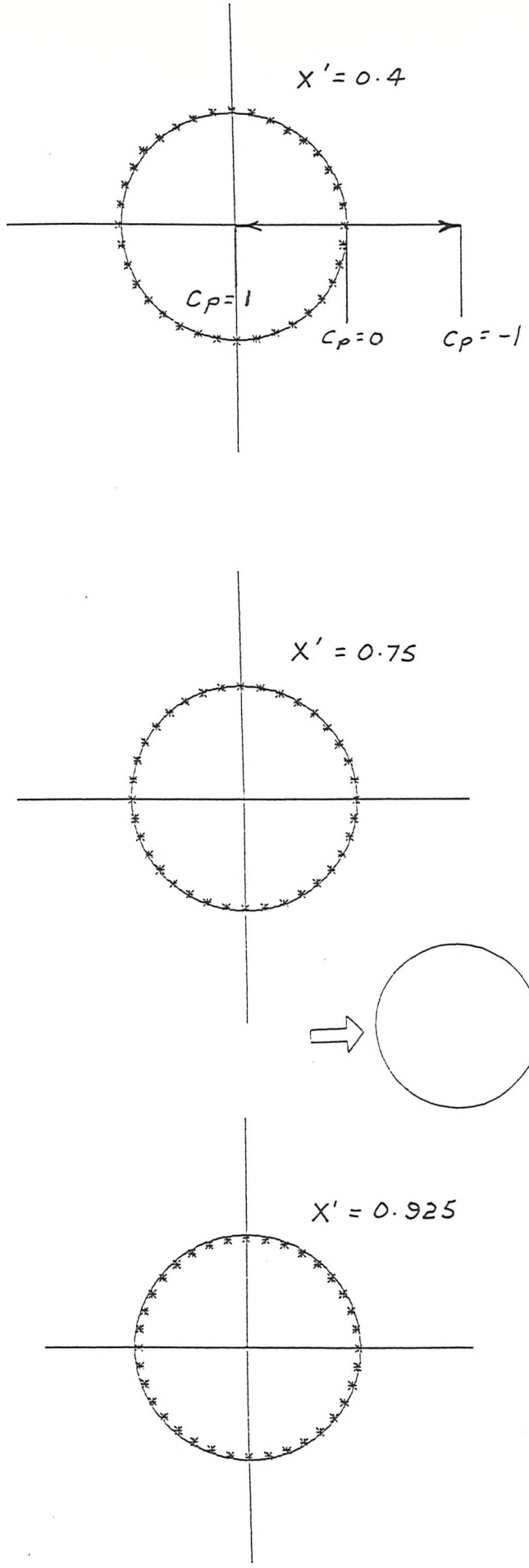

FIG.46 PRESSURE COEFFICIENT, BODY INCIDENCE 0 DEGREES
APPENDAGE 20 DEGREES

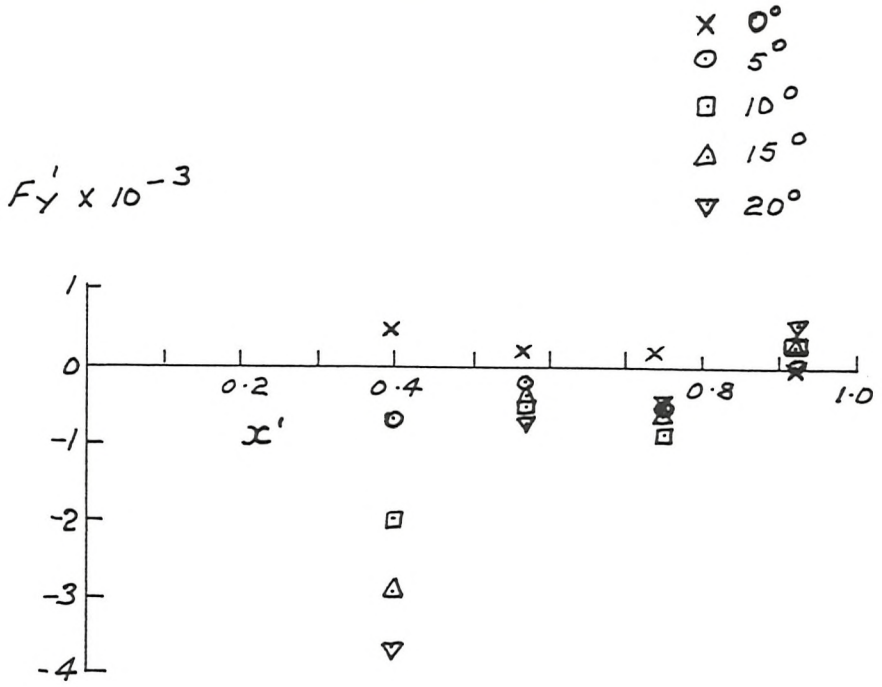

FIG.47 SIDE FORCE DISTRIBUTION FOR VARIOUS ANGLES OF APPENDAGE WITH BODY AT ZERO INCIDENCE

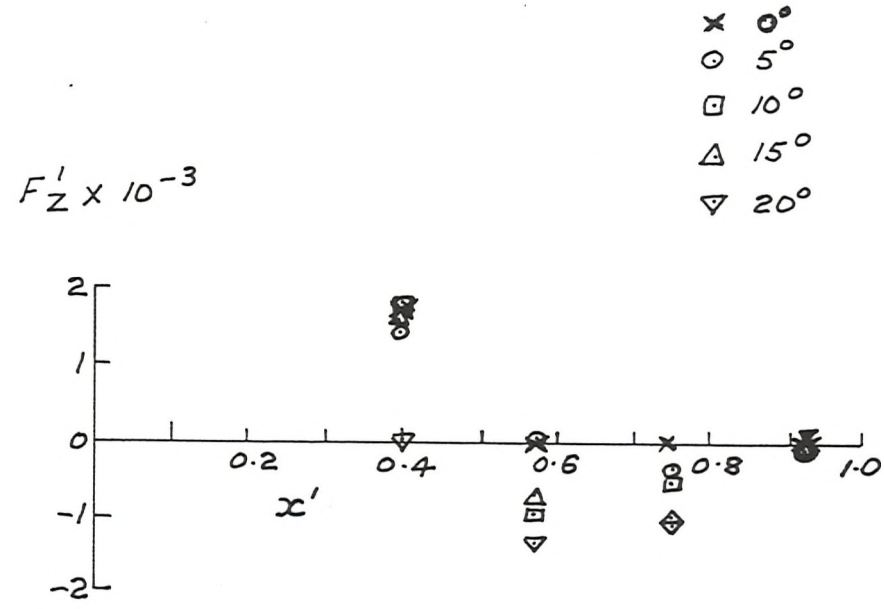

FIG.48 Z FORCE DISTRIBUTION FOR VARIOUS ANGLES OF APPENDAGE WITH BODY AT ZERO INCIDENCE

spoiler and delays the longitudinal point of separation hence the reduced strength of the upper body vortex (Figure 49).

With the fin at 0 degrees aligned to the body and the body yawed at 10 degrees, the circulation from the fin was found to be Γ_F=0.07. Assume that little change will take place over the last part of the stern aft of x'=0.925; add the strength of the deck and keel vortices at x'=0.925 to the strength of the fin vortex. The total circulation at the rear of the body is therefore approximately zero, as predicted by Stokes' theorem. Perhaps this factor could point the way to modelling the reduced strength of the upper body vortex. Taking the whole body as one closed system the circulation will add up to zero as shown in Figure 49.

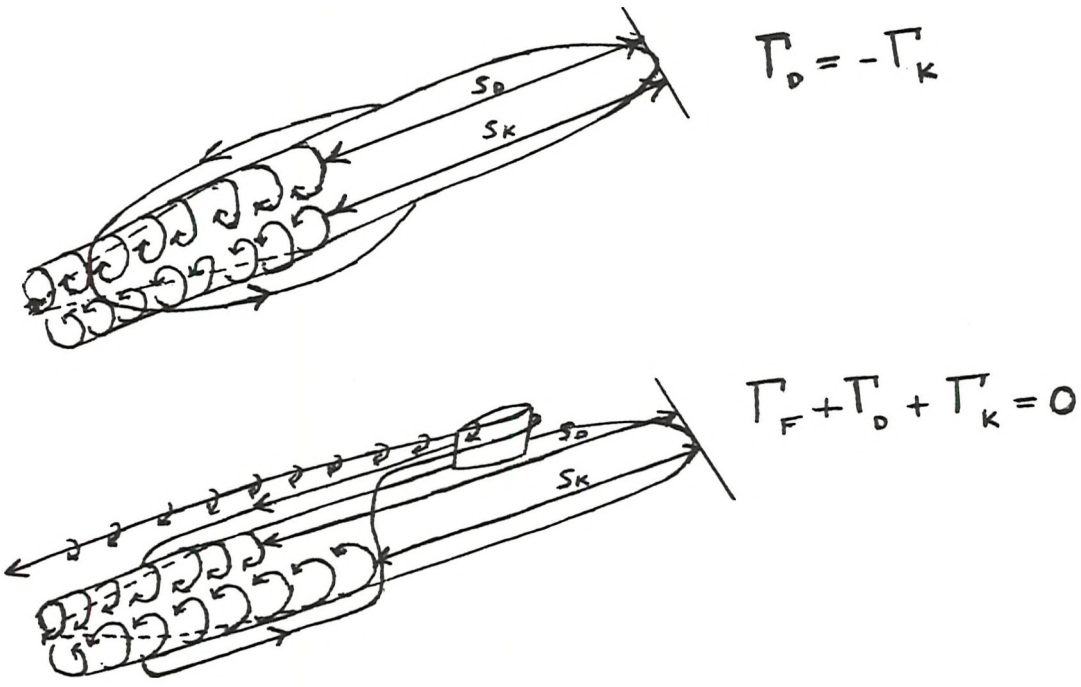

FIG.49 ILLUSTRATION OF VORTEX SEPARATION AND STOKES' THEOREM

Chapter 7

A Computational Approach to the Estimation of Forces on a Body of Revolution in a Vortex Flow Field

7.1 Introduction

This chapter describes a simple computational method to determine the force distribution on an appended body of revolution. A combination of classical theory (Milne-Thomson Circle Theorem, Stokes' Theorem, and Glauert Theory) and empirical formulae derived from experiment results are used to estimate various parameters used in the model. Comparison of results have been made with experiment data.

7.2 Vortex Strength

Using the data from the experiment described in Chapter 5 and the experiment descibed in Ward [37] the following empirical equation was calculated for the circulation of the keel vortex on an unappended body.

$$\Gamma_K=\{-0.018+0.082x'\}.\{0.0069\alpha^2+0.031\alpha\} \qquad (7.1)$$

If $\Gamma_K<0$ then $\Gamma_K=0$.

Assume the strength of the fin vortex remains constant along the length of the body and calculate its strength from Glauert's [24] and Whicker's [25] work.

At the rear of the body the total circulation should equal zero exactly, hence it is possible to calculate the deck vortex strength by the application of Stokes' theorem

$$\Gamma_F+\Gamma_D+\Gamma_K=0 \text{ at } x'=1 \qquad (7.2)$$

It has been found from the experiments, that the deck vortex is reduced in strength when in the presence of an appendage.

A reduction factor is defined by

$$R_F=\Gamma_D/\Gamma_K \qquad (7.3)$$

where Γ_D is the strength of the vortex on the deck side and Γ_K is the strength of the vortex on the keel side or alternatively

$$\Gamma_D=R_F.\Gamma_K \qquad (7.4)$$

using the circulation values from the experiment to arrive at the empirical estimate of R_F.

7.3 Location of Vortices

The 'Foppl curve' is the locus of points where a vortex pair can be at rest with respect to a cylinder in a steady flow.

Von Karman's observations led him to assume that two vortices of equal strength and opposite direction of rotation lie in parallel lines.

It is assumed for the purpose of this simple model that the body vortex position is where the 'Foppl curve' and 'Von Karman lines' intersect. This is very much a stop gap estimate and a more accurate determination of the vortex position should be made in refining this model.

The position of the fin vortex is determined by Glauert taking

$$S_1=\frac{\pi}{4}S \qquad (7.5)$$

where S_1 is the vertical distance of the fin vortex centre from the body surface. Assuming that the vortex is shed from the tail of the fin and travels in a straight path downstream.

Glasson [42] noted that by Kelvin's Theorem the fin vortex would follow a path maintaining the same distance from the body. Examining the experiment results of fin vortex path the vortex does move towards the body but not as much as Kelvin's theorem would suggest. In two dimensions the hull surface would act as a streamline drawing the vortex to the hull, whereas in three dimensions the powerful freestream flow carries the vortex downstream.

7.4 Vortex Core Radii

Grow [43] investigated the trailing vortex system behind a series of model wings in a wind tunnel. The test wings all had a NACA 0012 section and included a set of rectangular planform wings with aspect ratios varying from 2.0 to 6.0. Reynold's number was 0.35×10^6.

McCormick et al [44] found that Grow's measurements could be fitted by the following empirical formula,

$$r_*=\{0.02+0.35C_L\}c \qquad (7.6)$$

In Wardlaw [45] the viscous crossflow plane is simulated by superimposing a large number of point vortices on the potential solution for the flow about a cylinder. Wardlaw stated that the matching between the rotational and irrotational velocity is at the point dV/dr=0. In terms of Reynolds number, and distance along the body, this can be written

$$r_*=3.17\sqrt{\frac{R.x'}{R_e\cos\alpha}} \qquad (7.7)$$

As the vortex core radius is related to circulation it is assumed that the reduction factor above can be used to calculate the core radius of the deck vortex.

7.5 Forces on a Body of Revolution

The body is split into slices and forces are calculated in two dimensions using the Milne-Thomson circle theorem as described in Van Den Pol [11].

In the presence of n vortices and their images the local fluid velocity at a point ζ in the plane is given by

$$w=[-V_s-iW_s]\,[1-\frac{R^2}{\zeta^2}(cos2\alpha'+isin2\alpha')]-\frac{i}{2\pi}\sum_1^n\Gamma[\frac{k_{cn}}{\zeta-\zeta_n}-\frac{k_{cin}}{\zeta-\frac{R^2}{\zeta_n}}] \qquad (7.8)$$

The first term inside the summed bracket represents the contribution of the vortex ; the second term gives the contribution of its image.

k_{cn} and k_{cin} are factors from Lloyd [35] which allow for the effects of the vortex cores. They are

$$k_{cn}=1-\exp[-1.26[\frac{\zeta-\zeta_n}{r_{*n}}]^2] \qquad (7.9)$$

$$k_{cin}=1-\exp[-1.26[\frac{\zeta-\frac{R^2}{\zeta_n}}{r_{*n}}]^2] \qquad (7.10)$$

Using the above method to calculate the local velocity at a point on a cylinder in the presence of vortices. The pressure can be calculated by Bernoulli's equation.

$$P=-\rho\frac{q^2}{2} \qquad (7.11)$$

Then integrate these pressures to give the force per unit length along the body.

7.6 Validation

Comparisons with the experiment results are shown in Figures 50 to 55. Clearly the results are bad as the model requires certain refinements. The problem probably lies in the fact that the body vortices are modelled as both single deck and keel vortices. The method used is also a potential flow solution which obviously does not account for viscous effects. Also a two dimensional solution is given therefore the effects of the freestream flow are not taken into account.

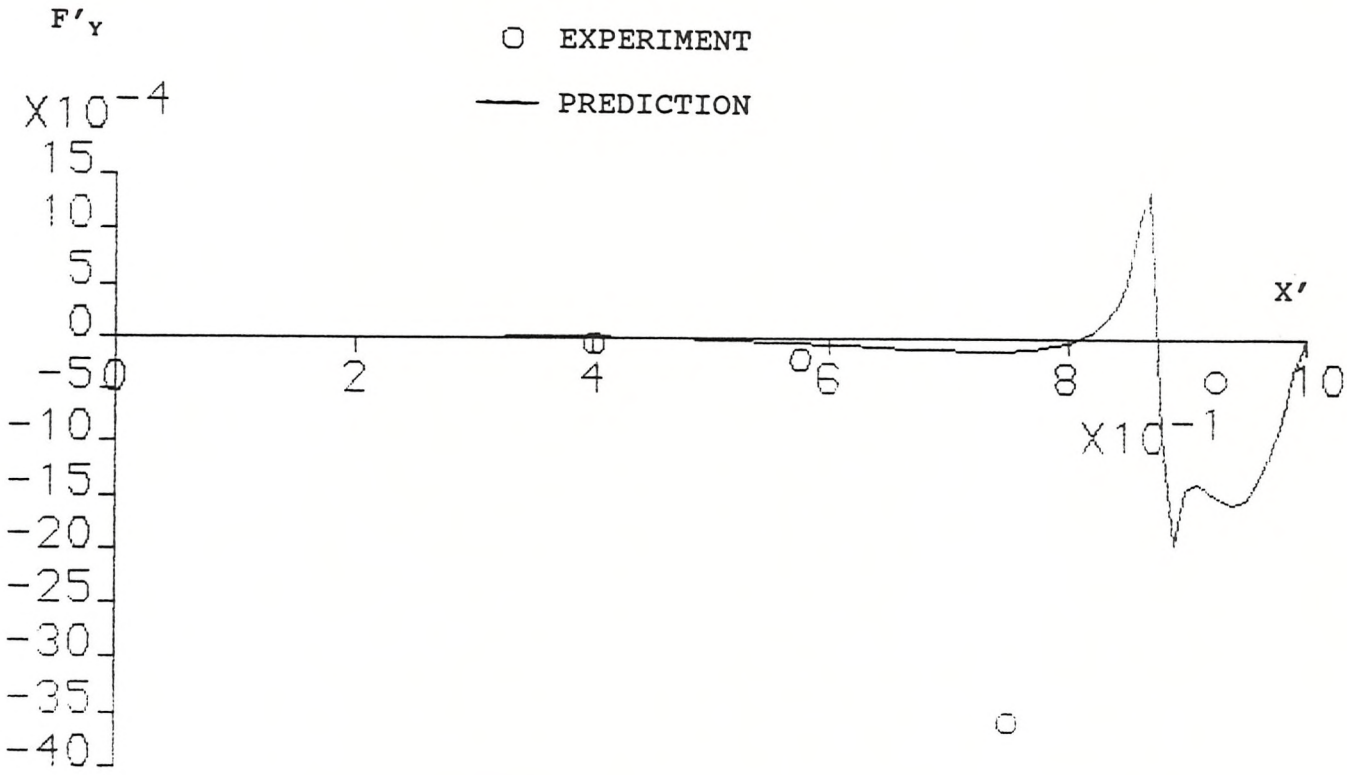

FIG.50 BODY INCIDENCE 5 DEGREES, UNAPPENDED

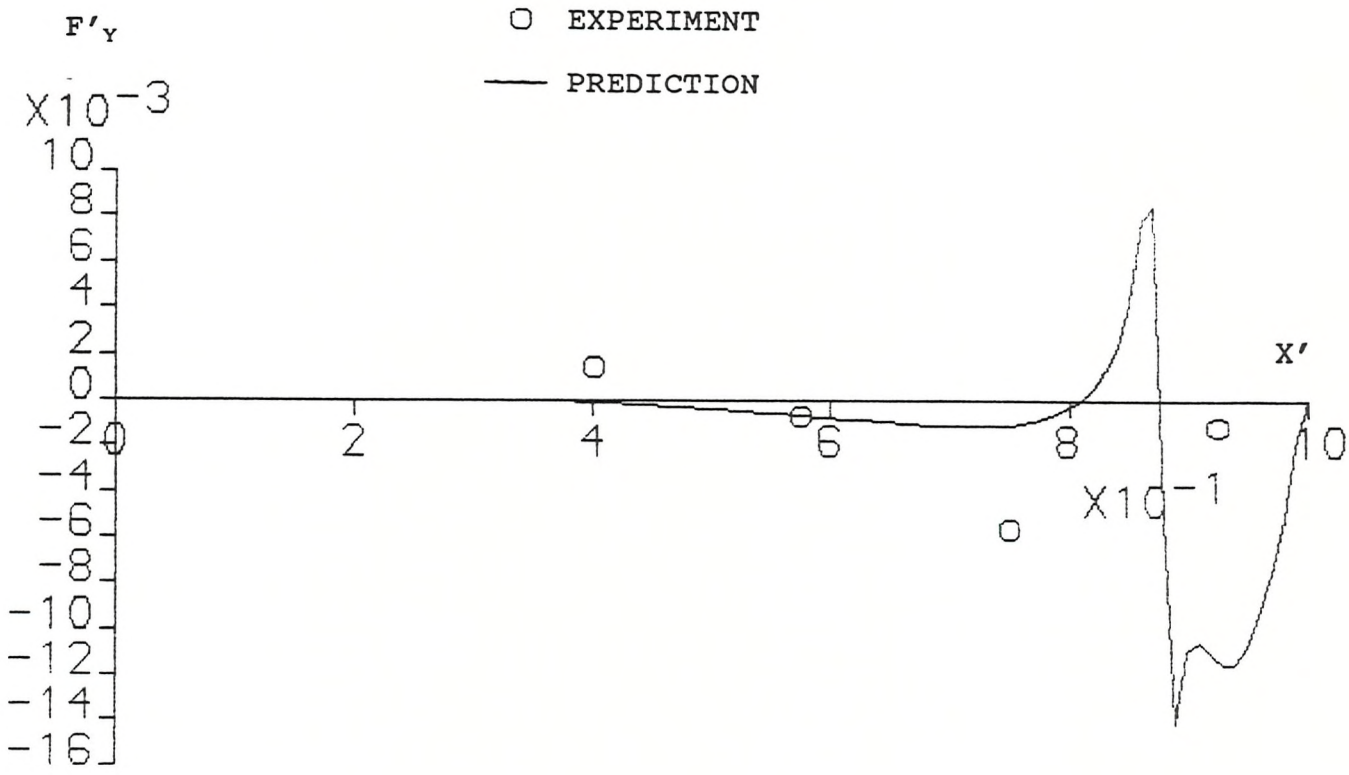

FIG.51 BODY INCIDENCE 10 DEGREES, UNAPPENDED

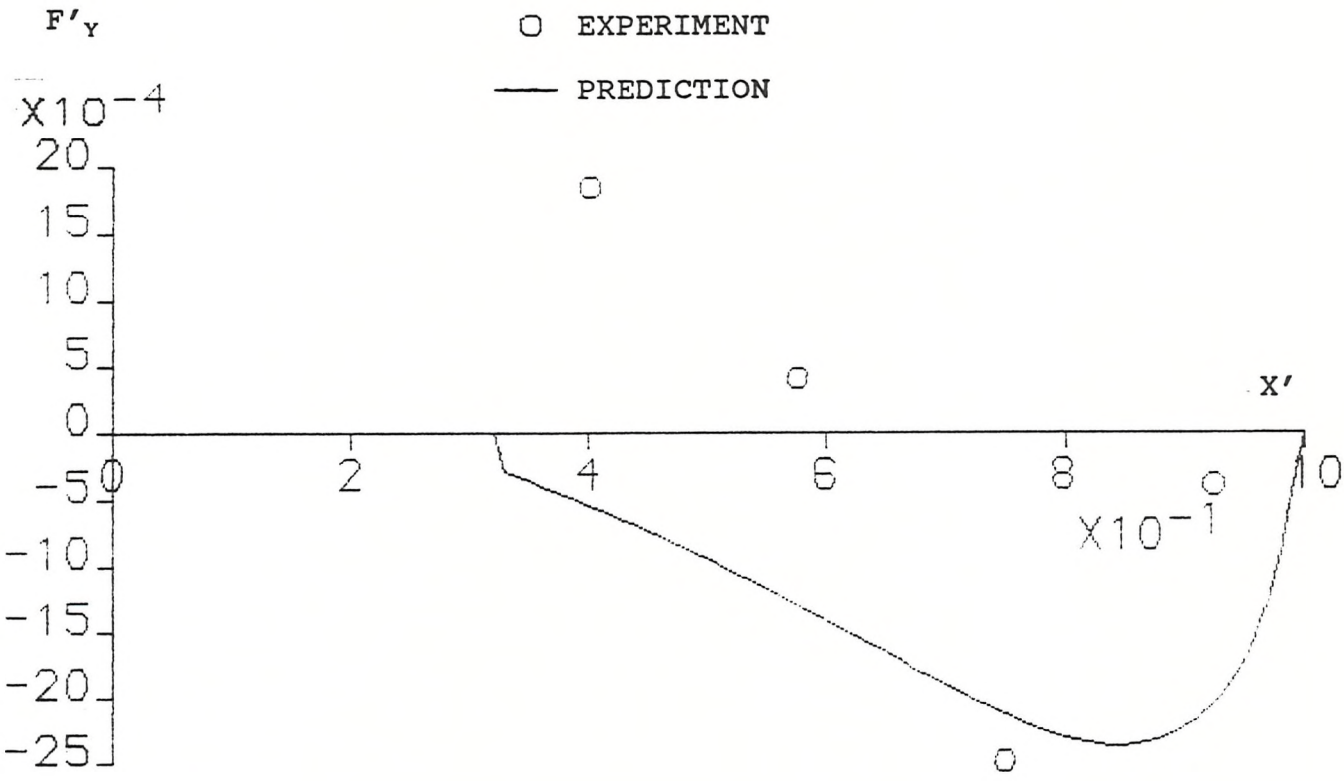

FIG.52 BODY INCIDENCE 5 DEGREES, APPENDAGE 0

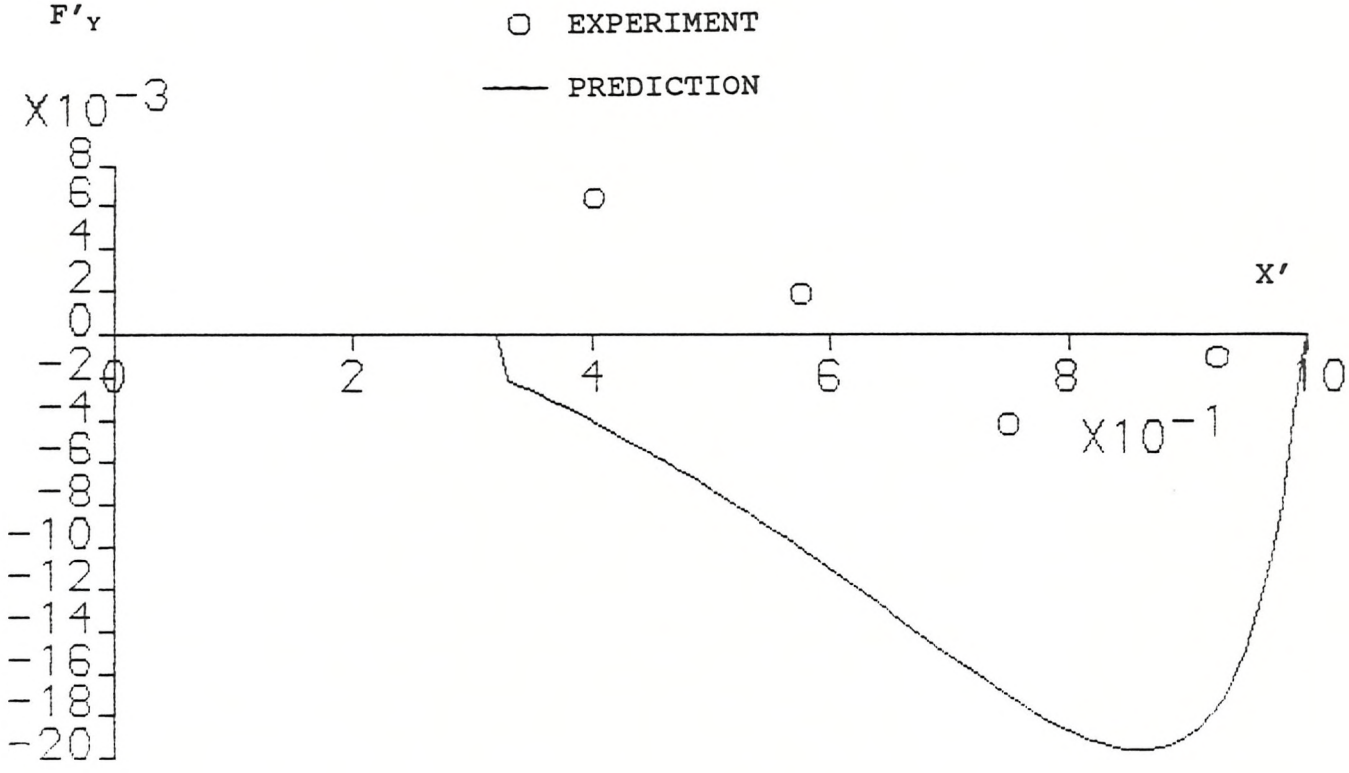

FIG.53 BODY INCIDENCE 10 DEGREES, APPENDAGE 0

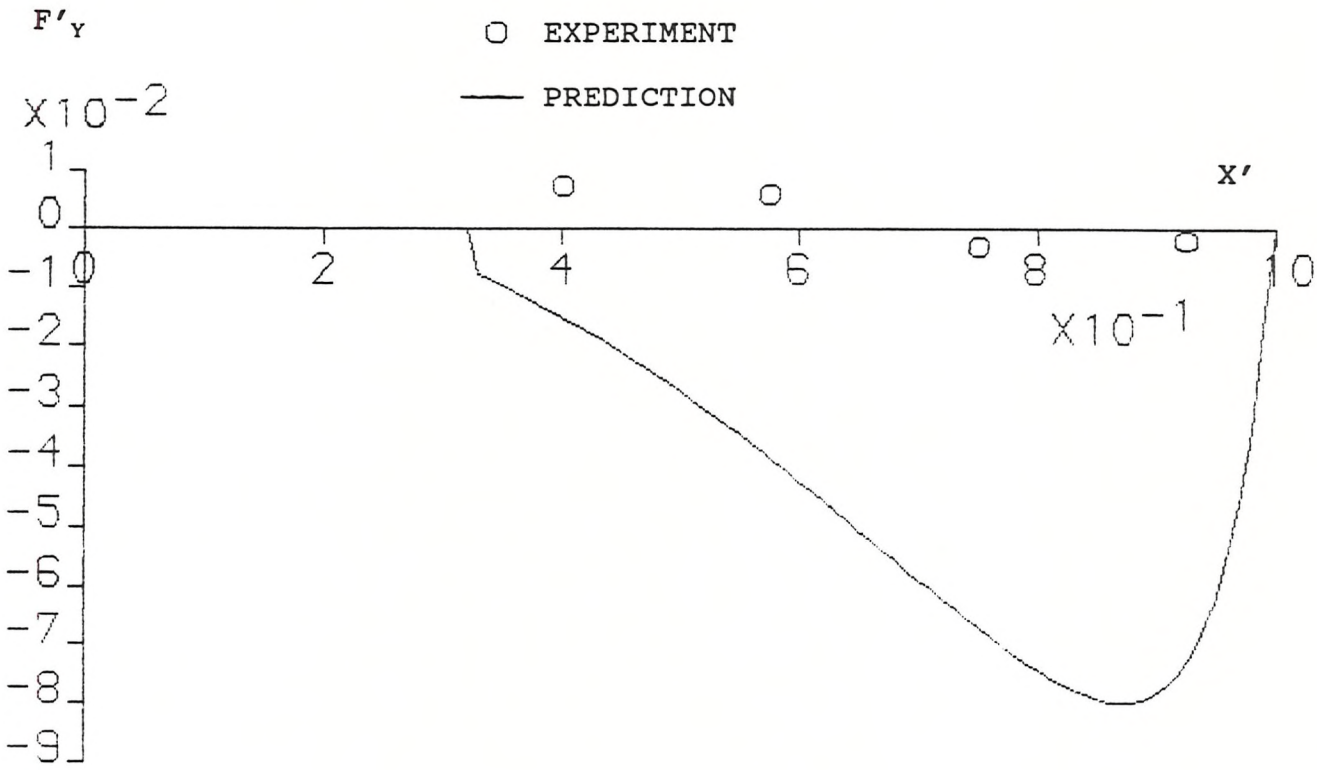

FIG.54 BODY INCIDENCE 15 DEGREES, APPENDAGE 0

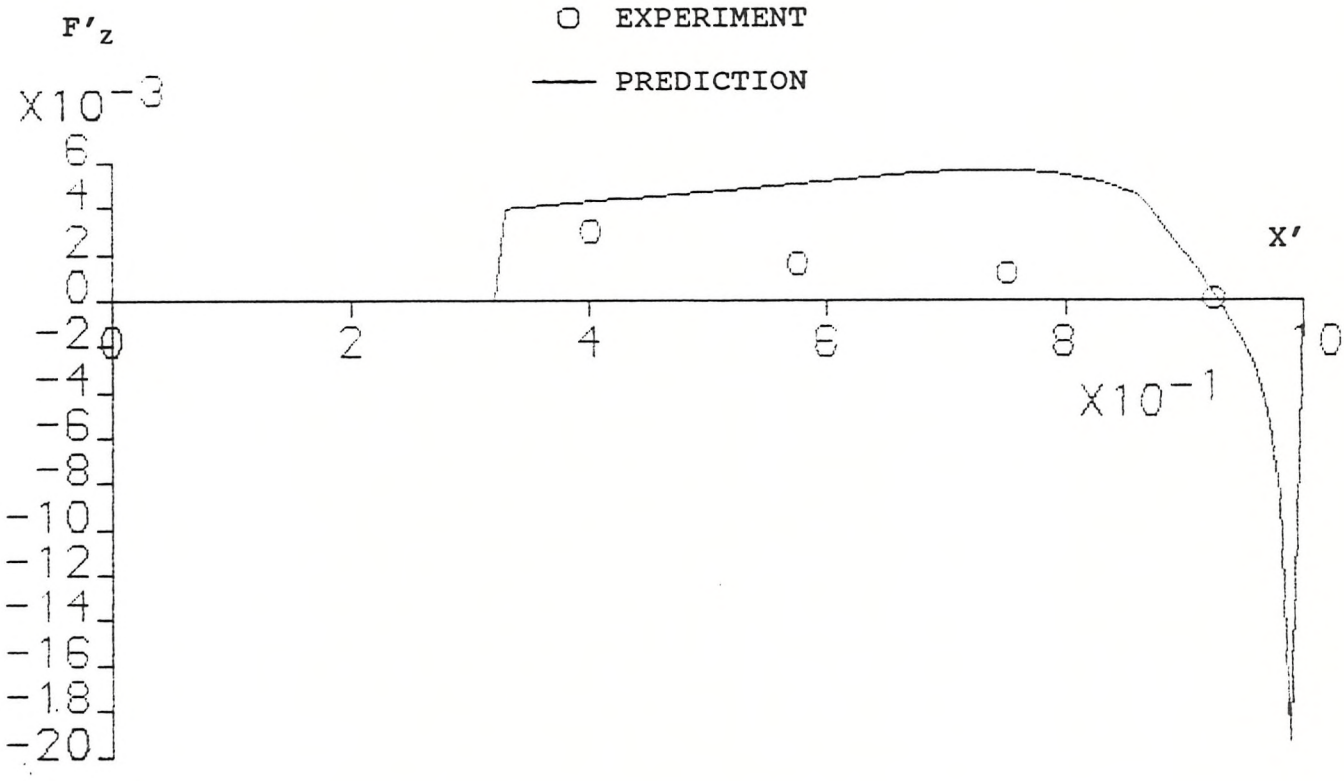

FIG.55 BODY INCIDENCE 5 DEGREES, APPENDAGE 0

Chapter 8

Summary, conclusions and future work

This thesis has made a study into submarine manoeuvring research and in particular the prediction of forces on a turning submarine. A history of the subject is given, and experiment and theoretical methods are described.

Work on the development of a computer model SUBSIM started in the early eighties at DRA Haslar. The idea was to develop a computer model independent of experiment derivative data. The validation of the 1989 version of the model showed predictions to be good however prediction of depth change in the turn remained a problem. This initiated an experiment to examine the flow around an appended body of revolution. The experiments were conducted in two stages during 1990 and 1991 and took thirteen weeks in total to complete.

A 1 metre model was tested over a range of angles with and without an appendage. Vorticity and pressure measurements were taken at four stations along the hull. Results showed that the appendage has a significant effect on both circulation and pressure distribution. The conclusion made is that the vortex shed from the appendage does not itself have a significant effect. It is the appendage that acts as a spoiler and delays the longitudinal point of separation on that side of the model. The body vortex on the appendage side of the model is therefore weaker in strength. This asymmetry in the flow causes an asymmetry in the pressure distribution. In modelling the vortices in a computer model the asymmetry in the flow pattern must be accounted for.

The experiment results do give a visual impression of the flow pattern around an appended body. To investigate this problem further it would be useful to use a larger model in a towing tank to achieve a higher Reynold's number and therefore hopefully acquire more accurate data.

A computational method is described and although comparison with the experiments are poor such an approach with a more refined modelling of circulation could be the way ahead as an extension of this thesis.

It is however unlikely that the prediction of the out-of-plane forces will lie in a basic empirical solution. A submarine body is not a body of revolution but is pear shaped, hence an asymmetry in the flow would exist without any appendages. This makes the accurate modelling of the complex flow patterns extremely difficult. A naval architect would wish to assess a new design in various turning manoeuvres and also under emergency conditions. This would require accurate prediction of forces under different yaw, pitch and roll rates simultaneously, further complicating the problem.

The solution is more likely to lie in a detailed mathematical solution of the flow, taking account of the shape of the body. This would involve the solution of the Navier-Stokes equations and any attempt at predicting a submarine manoeuvre would be extremely computational. It may be more efficient in terms of time to predict derivatives under a variety of static and dynamic conditions for a particular design using computational techniques. These derivatives could then be used in a derivative computer model such as that described by Gertler [15] and Feldman [16].

As far as submarine manoeuvring and future submarine designs are concerned; with the end of the cold war the pace of development will slow down. However the world remains unstable and British involvement in future conflicts is likely and the submarine will play an integral part in any naval fleet of the future.

References

1. E Horton. The Illustrated History of the Submarine. Published by Sidgwick and Jackson. 1974.

2. E S Arentzen, P Mandel. Naval Architectural Aspects of Submarine Design. Tran. Soc. Nav. Archit. Mar. Engin. 1960.

3. M M Munk. The Aerodynamic Forces on Airship Hulls. NACA Report 184. 1924.

4. H Lamb. Hydrodynamics. Cambridge University Press. 1932.

5. T Von Karman. Calculation of Pressure Distribution on Airship Hulls. NACA TM No.574. 1930.

6. J B Spencer. Stability and Control of Submarines. JRNSS. Vol. 23 No. 3. 1967.

7. I Lotz. Calculation of Potential Flow Past Airship Bodies in Yaw. NACA TM No. 675. 1932.

8. A M O Smith, J Pierce. Exact solution of the Neumann Problem, Calculation of Non-circulatory Plane and Axially Symmetric Flows About or Within Arbitrary Boundaries. Douglas Aircraft Company. Report No. E S 26988. 1958.

9. J L Hess, A M O Smith. Calculation of Potential Flow About Arbitrary Bodies. Progress in Aeronautical Sciences 8 (1967) No.1, p 1-139.

10. M Mackay. Prediction of Out-of-plane Forces on Submarine Bodies. RINA Symposium on Naval Submarines. London 1988.

11. E Van Den Pol. An Estimation of the Normal Force and Pitching Moment of 'Tear Drop' Underwater Vehicles. Drukkerij J H Pasmans. S'Gravenhage Holland 1976.

12. M R Mendenhall, S B Spangler, S C Perkins. Vortex Shedding from Circular and Non-circular Bodies at High Angles of Attack. AIAA Paper 79-0026. 1979.

13. S J Tinker. A Discrete Vortex Model of Separated Flow Over Manoeuvring Submersibles. Advances in Underwater Technology, Ocean Science and Offshore Engineering. Volume 15 : Technology Common to Aero and Marine Engineering. 1988.

14. Naval Engineers Journal Vol 104, No 3. May 1992.

15. M Gertler, G R Hagen. Standard Equations of Motion for Submarine Simulation. DTNSRDC Report 2510. 1967.

16. J Feldman. DTNSRDC Revised Standard Submarine Equations of Motion. DTNSRDC/SPD-0393-09. 1979.

17. H J Bohlmann. An Analytic Method for the Prediction of Submarine Manoeuvrability. RINA Symposium on Naval Submarines. London 1991.

18. H J Bohlmann. Calculation of the Hydrodynamic Coefficients of Submarines to Forecast their Motional Behaviour. University of Hamburg, Institute of Shipbuilding. Report No 513. Phd Thesis. December 1990.

19. J N Newman. Marine Hydrodynamics. M.I.T. Press. Cambridge MA/USA.1977.

20. M Mackay, J T Conway. Modelling the Crossflow Body Separation on a Submarine using a Panel Method. RINA Symposium on Naval Submarines. London 1991.

21. A R J M Lloyd. Progress Towards a Rational Method of Predicting Submarine Manoeuvres. RINA Symposium on Naval Submarines. London 1983.

22. A R J M Lloyd. Developments in the Prediction of Submarine Manoeuvres. Undersea Defence Technology. 1988.

23. B Ward. Experiments to Improve Predictions of Submarine Manoeuvres. MCMC Conference. University of Southampton. July 1992.

24. H Glauert. The Elements of Aerofoil and Airscrew Theory. Cambridge University Press. 1947.

25. L F Whicker, L F Fehlner. Freestream Characteristics of a Family of Low Aspect Ratio all Moveable Control Surfaces for Application to Ship Design. DTMB Report 933. December 1958.

26. B Ward, P A Wilson. Forces on a Body of Revolution in a Vortex Flow Field. RINA Written Transactions Part B. 1992.

27. B Ward, P A Wilson. Experiments to Investigate Vortex Separation on an Appended Body of Revolution. MCMC Conference. University of Southampton. July 1992.

28. R K Burcher. Model Testing. J.Mech.Eng.Sci.14:(Suppl.Iss.Paper 9),62-69. 1972.

29. M Gertler. Some Recent Advances in Dynamic Stability and Control of Submerged Vehicles. J.Mech.Eng.Sci. 14:(Suppl.Iss.Paper 3),14-19. 1972.

30. T B Booth, R E D Bishop. Planar Motion Mechanism. AEW. 1973.

31. P J Lamont. Pressure Around an Inclined Ogive Cylinder with Laminar, Transitional, or Turbulent Separation. AIAA 80-1556R. 1982.

32. Jones-Bell. Spheroid. ARC RM 858. 1922.

33. S F Hoerner. Fluid Dynamic Drag. Published by the Author. 1965.

34. S J Tinker, A R Bowman, T B Booth. Identifying Submersible Dynamics from Free Model Experiments. RINA 1979.

35. A R J M Lloyd, I F Campbell. Experiments to Investigate Vortices Shed from a Submarine-like Body of Revolution. 59th Meeting of the AGARD Fluid Dynamics Panel Symposium, Monterey, California, USA. Aerodynamic and Related Hydrodynamic Studies Using Water Facilities. AGARD-CCP 413. October 1986.

36. A R J M Lloyd. Experiments to Investigate the Vorticity Shed by a Body of Revolution in Curved Flow. International Conference on Technology Common to Aero and Marine Engineering. Society for Underwater Technology. January 1988.

37. B Ward, A R J M Lloyd. Analysis of Experiments to Measure Vortices in Curved Flow. ARE TM(UHU)88305. June 1988.

38. J Kaplan. Velocity Measurements about a Body of Revolution with and without a Fin at Angles of Attack. MSc Thesis. 1982. MIT.

39. J S Reed. Measurement of Forces and Moments on, and Velocity about a Body of Revolution with an Appended Fin at Angles of Attack. MSc Thesis. 1987. MIT.

40. M M Freestone. Vorticity Measurement by a Pressure Probe. The Aeronautical Journal of the Royal Aeronautical Society. January 1988.

41. C J Drummond. Vortex Metering of Vortices from Submerged Bodies. M Eng Final Year Project. University of Liverpool. 1988.

42. D P Glasson. Unsteady Hydrodynamics of a Body of Revolution with Fairwater and Rudder. MIT Report 74-7. March 1974.

43. T L Grow. The Effect of Wing Geometry and Lower Surface Boundary Layer on the Rolled Up Vortex. MS Thesis. Pennsylvania State University. 1967.

44. B W McCormick, J L Tangler, H E Sherrieb. Structure of Trailing Vortices. Journal of Aircraft. Vol 5 No 3. May-June 1968.

45. A B Wardlaw. Multivortex Model of Asymmetric Shedding on Slender Bodies at High Angle of Attack. AIAA 13th Aerospace Science Meeting. Pasadena, California. January 20-22 1975.

Appendix 1

DATS programs used to acquire and analyse data during the 1991 stage of the experiment are presented in this section.

```
PROGRAM PTAP
! AUTHOR : BRIAN WARD
! DATE : NOVEMBER 1990
! THIS PROGRAM ACQUIRES DATA USING DATS
! 36 PRESSURE TAPPINGS AROUND A BODY OF REVOLUTION ARE READ IN TURN
!
! INPUT
!
/READ('RUN NUMBER ',IRUN)
/READ('STATION ',IS)
/READ('ANGLE OF INCIDENCE ',ANG)
!
! WRITE INFORMATION TO SCREEN AND DUMP ONTO HARD COPY
!
/SCNPRT(1)
/WRITE('RUN NUMBER ',IRUN)
/WRITE('STATION ',IS)
/WRITE('ANGLE OF INCIDENCE ',ANG)
/WRITE(' ')
/SCNPRT(0)
!
! CALCULATE REFERENCE PRESSURE
!
! HOMECK FINDS REFERENCE POINT
!
! TIME DELAY LOOP TO ALLOW SCANIVALVE TO SETTLE DOWN
!
DO 1 N=1,1001
1 CONTINUE
/ACQUIR(10,80,1,1,1,1,0,'CONSX')
/DEMUX
/DSAVE3(IRUN,1,1,'OFF','ACQ')
/ARITH
/STAT(1,OMEAN,OSD,OSK,OKT,OMAX,OMIN)
/KILL(1,'DATA.ACQ')
!
! RUN DATA
!
/SCNPRT(1)
/WRITE('REFERENCE PRESSURE = ',OMEAN)
/SCNPRT(0)
/WRITE('REFERENCE PRESSURE CALCULATED, RETURN TO CONTINUE',*)
111 CONTINUE
! INITIALISE SCANIVALVE - MOVE TO FIRST PRESSURE TAPPING
/PULSE
!
! CHANNEL 1 PRESSURE AT STATION N - REFERENCE PRESSURE
!
/SCNPRT(1)
/WRITE(' ')
/WRITE('PRESSURE    PRESSURE    PRESSURE    STD')
/WRITE('TAPPING     DIFF        COEFF       DEV')
/WRITE('            Pa      ')
/SCNPRT(0)
DO 10 NSTAT=1,36
KRUN=(IRUN-1)*36+NSTAT
! TIME DELAY LOOP TO ALLOW PRESSURE TRANSDUCER AND SCANIVALVE
!    TO SETTLE DOWN BETWEEN EACH STEP
DO 5 N=1,1000
5 CONTINUE
/ACQUIR(10,80,1,1,1,1,0,'CONSX')
/DEMUX
/DSAVE3(KRUN,1,1,'PRS','ACQ')
```

```
PROGRAM PTAP


!
! DYNAMIC PRESSURE
!
DP=3125
!
! FILE 2 = FILE 1 - REFERENCE PRESSURE
!
/ARITH(1,2,6,OMEAN)
!
! FILE 3 = FILE 2 / DP
!
/ARITH(2,3,8,DP)
!
/STAT(2,PMEAN,PSD,PSKEW,PKURT,PMAX,PMIN)
/STAT(3,CMEAN,CSD,CSKEW,CKURT,CMAX,CMIN)
!
! OUTPUT
!
/SCNPRT(1)
/WRITE(NSTAT,PMEAN,CMEAN,CSD)
/SCNPRT(0)
/KILL('DATA.ACQ',1,2,3)
!
! SCANIVALVE STEP
!
/PULSE
! RETURN TO REFERENCE POINT
/HOMECK
10 CONTINUE
/READ('DO YOU WISH TO REPEAT RUN 1 = Y, 2 = N',I2)
IF ((I2.EQ.1) GOTO 111
END
```

```
PROGRAM TRAV
! AUTHOR : BRIAN WARD
! DATE : JANUARY 1991
! THIS PROGRAM ACQUIRES DATA USING DATS
! AREAS ARE MAPPED OUT AND MAXIMUM VORTICITY IS FOUND
REAL X
/READ('INPUT RUN NO. ',IRUN)
/READ('INPUT LAST COUNT ',LASTC)
/READ('Y POSITION : ',Y)
/READ('XMIN : ',XMIN)
/READ('XMAX : ',XMAX)
! OFFSETS CALCULATED WITHOUT FLOW
! TO BE CHANGED EACH TIME FLOW IS STOPPED
XOFF=94.83
VOFF=62.82
/OUTPUT('RUN NO. ',IRUN)
ICOUNT=0
/READ('XSTEP : ',XSTEP)
/WRITE(' I       X        Y        VORT        PDIFF        VEL        VOL')
DO 10 X=XMIN,XMAX,XSTEP
ICOUNT=ICOUNT+1
! 'MOVER' CONTROLS TRAVERSE RIG
IF (ICOUNT.NE.0) THEN
  /MOVER('Y',XSTEP)
ENDIF
/KILL(1,2,'DATA.ACQ')
IX=LASTC+ICOUNT
! ACQUIRE DATA
/ACQUIR(10,80,1,1,1,1,0,'CONS2')
/DSAVE3(IX,1,1,'BVV')
/DEMUX
/STAT(2,PDIFFX)
/STAT(1,VOLX)
PDIFF=PDIFFX-XOFF
VOL=VOLX-VOFF
IF (VOL.LT.0.5) THEN
 VEL1=1.912*VOL
ELSE
 VEL1=-1.136*VOL*VOL+3.672*VOL-0.596
ENDIF
IF (VEL1.LT.0.000001) VEL1=0.000001
! CALCULATE VORTICITY
VORT=0.3239*PDIFF/VEL1
/WRITE(ICOUNT,X,Y,VORT,PDIFF,VEL1,VOL)
! OUTPUT TO AN ASCII FILE CALLED OUTPUT.LST)
/OUTPUT(ICOUNT,X,Y,VORT,PDIFF,VEL1,VOL)
10 CONTINUE
/WRITE('LAST COUNT = ',IX)
END
```

Appendix 2

Numerical values for all the pressure coefficients are presented in this section. Array position 1 is at the top of the model and numbers increment round clockwise looking forward.

X'=0.4

RUN19D
APPENDAGE = 0, BODY ANGLE = 0
CP(1...36)= 4.070000E-02 -1.600000E-02 1.100000E-02
1.800000E-02 1.400000E-02 9.000000E-03 9.000000E-03
4.000001E-03 2.999999E-03 5.999997E-03 8.000001E-03
1.000002E-03 -9.999946E-04 0.000000 1.000002E-03
9.999983E-04 4.000001E-03 9.999983E-04 -1.999997E-03
-9.999983E-04 9.999983E-04 0.000000 0.000000
6.000005E-03 9.999983E-04 2.000000E-03 6.999999E-03
1.000000E-02 1.100000E-02 9.999998E-03 1.200000E-02
2.100000E-02 2.100000E-02 1.800000E-02 1.900000E-02
2.500000E-02
Y"= 5.173815E-04 Z"= 1.755437E-03
RUN20D
APPENDAGE = 0, BODY ANGLE = 0
CP(1...36)= 3.269999E-02 -2.000000E-02 5.999997E-03
1.500000E-02 1.000000E-02 1.200000E-02 6.999999E-03
4.000001E-03 9.999983E-04 0.000000 2.000004E-03
1.000002E-03 -9.999946E-04 -9.999983E-04 -9.999983E-04
9.999983E-04 0.000000 9.999983E-04 -4.999999E-03
-2.000000E-03 -2.000000E-03 -4.999999E-03 1.999997E-03
2.000004E-03 -1.000002E-03 -2.000000E-03 5.000000E-03
4.000001E-03 2.999999E-03 9.000000E-03 6.999999E-03
-1.600000E-02 1.700000E-02 1.900000E-02 2.200000E-02
2.600000E-02
Y"= 1.018381E-04 Z"= 1.468951E-03
RUN21D
APPENDAGE = 0, BODY ANGLE = 10
CP(1...36)= 3.070000E-02 -6.999999E-03 1.900000E-02
1.600000E-02 2.400000E-02 2.700000E-02 2.800000E-02
2.430000E-02 1.800000E-02 9.999998E-03 2.000004E-03
-2.999999E-03 -2.600000E-02 -4.600001E-02 -6.200000E-02
-6.600000E-02 -6.400000E-02 -7.400002E-02 -7.200000E-02
-4.100000E-02 -1.600000E-02 -9.999983E-04 2.800000E-02
4.700000E-02 5.800000E-02 7.699999E-02 8.999999E-02
8.100000E-02 6.400000E-02 5.599999E-02 4.300000E-02
1.000000E-03 3.000000E-02 3.500000E-02 3.600000E-02
4.200000E-02
Y"= 6.383203E-03 Z"= 6.372112E-03
RUN22D
APPENDAGE = 0, BODY ANGLE = 12.5
CP(1...36)= 2.170000E-02 -1.800000E-02 2.200000E-02
2.900000E-02 2.500000E-02 2.900000E-02 3.300000E-02
3.600000E-02 3.699999E-02 1.100000E-02 6.999999E-03
2.000004E-03 -2.299999E-02 -5.400000E-02 -7.400002E-02
-9.100001E-02 -9.700000E-02 -0.107000 -0.109000
-8.800000E-02 -5.800001E-02 -2.600000E-02 9.999998E-03
4.200000E-02 6.200000E-02 8.699998E-02 0.103000
9.299999E-02 7.099999E-02 5.800000E-02 3.500000E-02
-4.999999E-03 3.000000E-03 7.999999E-03 1.900000E-02
3.200000E-02
Y"= 5.667523E-03 Z"= 8.329013E-03
RUN23D
APPENDAGE = 0, BODY ANGLE = 2.5
CP(1...36)= 2.070000E-02 1.000002E-03 0.000000
6.000001E-03 2.000000E-03 1.000000E-03 9.999983E-04
-6.999999E-03 -9.000000E-03 -1.100000E-02 -1.100000E-02
-1.700000E-02 -2.000000E-02 -2.200000E-02 -2.900000E-02
-2.400000E-02 -1.300000E-02 -1.600000E-02 -2.100000E-02
-1.400000E-02 -1.000000E-02 -9.000000E-03 -6.000005E-03
-2.999999E-03 -6.999999E-03 -2.000000E-03 4.000000E-03
9.999983E-04 -1.000002E-03 -9.999983E-04 1.999997E-03
-2.100000E-02 5.000000E-03 6.700000E-03 6.999999E-03

```
    1.400000E-02
 Y"=    1.034089E-03  Z"=    2.262524E-03
RUN24D
APPENDAGE = 0, BODY ANGLE = 7.5
 CP(1...36)=    2.770000E-02   4.999995E-03   1.399999E-02
    1.300000E-02   1.500000E-02   1.800000E-02   1.700000E-02
    1.100000E-02   8.000001E-03   2.999999E-03  -1.999997E-03
   -1.300000E-02  -2.299999E-02  -3.400000E-02  -3.100000E-02
   -3.200000E-02  -2.200000E-02  -3.200000E-02  -2.600000E-02
   -1.500000E-02  -1.000002E-03   9.000000E-03   2.600000E-02
    3.400000E-02   3.999999E-02   5.000000E-02   5.900000E-02
    5.200000E-02   4.200000E-02   3.399999E-02   3.200000E-02
    6.000000E-03   3.000000E-02   2.600000E-02   3.600000E-02
    3.500000E-02
 Y"=    4.690230E-03  Z"=    3.631558E-03
RUN25D
APPENDAGE = 0, BODY ANGLE = 5
 CP(1...36)=    2.270000E-02  -1.800000E-02  -5.000003E-03
   -3.000000E-03  -2.000000E-03   0.000000      -4.000001E-03
   -9.000000E-03  -1.000000E-02  -1.300000E-02  -1.700000E-02
   -2.000000E-02  -3.599999E-02  -4.200000E-02  -4.100000E-02
   -3.400000E-02  -2.900000E-02  -3.800001E-02  -3.900000E-02
   -3.200000E-02  -1.800000E-02  -1.800000E-02  -8.000001E-03
   -2.999999E-03  -5.000003E-03   6.000001E-03   1.070000E-02
    4.999999E-03   1.999997E-03  -3.999997E-03  -2.000000E-03
   -2.700000E-02   2.000000E-03   2.000000E-03   4.000000E-03
    5.999999E-03
 Y"=    1.858040E-03  Z"=    2.976486E-03
RUN26D
APPENDAGE = 0, BODY ANGLE = 15
 CP(1...36)=    2.770000E-02   8.000001E-03   2.300000E-02
    4.000000E-02   3.500000E-02   4.400000E-02   4.700000E-02
    4.600000E-02   3.040000E-02  -4.000001E-03  -5.999997E-03
   -1.499999E-02  -5.400000E-02  -7.900001E-02  -0.116000
   -0.134000      -0.152000      -0.170000      -0.171000
   -0.140000      -9.700002E-02  -5.600000E-02  -5.000003E-03
    4.000000E-02   6.999999E-02   0.102000       0.126000
    0.114000       9.199999E-02   6.899999E-02   4.099999E-02
   -1.600000E-02  -7.000001E-03  -7.000000E-03   7.699999E-03
    3.000000E-02
 Y"=    7.309289E-03  Z"=    1.309612E-02
RUN27D
APPENDAGE = 0, BODY ANGLE = 17.5
 CP(1...36)=    1.170000E-02  -1.800000E-02   3.999997E-03
    3.300000E-02   4.899999E-02   6.600000E-02   7.499999E-02
    6.100000E-02   4.300000E-02  -6.999999E-03  -9.999998E-03
   -2.000000E-02  -5.199999E-02  -8.800001E-02  -0.140000
   -0.181000      -0.205000      -0.225000      -0.223000
   -0.191000      -0.134000      -7.000001E-02  -2.000004E-03
    5.800000E-02   9.699999E-02   0.133000       0.166000
    0.148000       0.115000       7.399999E-02   3.000000E-02
   -2.900000E-02  -5.500001E-02  -7.000001E-02  -5.800001E-02
   -1.000000E-02
 Y"=    7.860359E-03  Z"=    1.369060E-02
RUN2E
APPENDAGE = 10, BODY ANGLE = 0
 CP(1...36)=    2.070000E-02   1.700000E-02   2.300000E-02
    1.800000E-02   1.000000E-02   1.200000E-02   1.100000E-02
    4.999999E-03   2.999999E-03   4.999999E-03   5.000003E-03
    2.000004E-03  -5.999997E-03  -9.999983E-04  -6.000001E-03
   -6.000001E-03  -3.999997E-03  -9.000000E-03  -7.999998E-03
   -3.999997E-03  -7.000003E-03  -7.999998E-03  -8.000001E-03
   -1.199999E-02  -1.600000E-02  -1.300000E-02  -1.000000E-02
```

```
   -1.300000E-02  -1.500000E-02  -1.800000E-02  -9.000000E-03
   -3.100000E-02  -7.000001E-03  -9.999992E-04   9.999998E-03
    1.500000E-02
 Y"=   -1.976781E-03  Z"=    1.750523E-03
RUN3E
APPENDAGE = 20, BODY ANGLE = 0
 CP(1...36)=   -2.830000E-02  -1.900000E-02   7.999998E-03
    2.500000E-02   2.300000E-02   2.000000E-02   2.200000E-02
    1.700000E-02   1.600000E-02   1.800000E-02   1.800000E-02
    1.300000E-02   6.000001E-03   6.999999E-03   4.999999E-03
    2.000000E-03   1.000002E-03  -3.999997E-03  -6.999999E-03
   -2.999999E-03  -7.000003E-03  -1.400000E-02  -8.000001E-03
   -1.199999E-02  -1.700000E-02  -1.400000E-02  -1.800000E-02
   -2.200000E-02  -1.900000E-02  -2.000000E-02  -1.800000E-02
   -3.100000E-02  -7.000001E-03  -1.999999E-03  -1.100000E-02
   -1.700000E-02
 Y"=   -3.666252E-03  Z"=    2.885126E-06
RUN4E
APPENDAGE = 5, BODY ANGLE = 0
 CP(1...36)=    2.570000E-02  -8.000001E-03   1.200000E-02
    9.000000E-03   9.000000E-03   1.100000E-02   9.000000E-03
    2.999999E-03   0.000000       1.999997E-03   1.000002E-03
    2.000004E-03  -2.999999E-03  -2.000000E-03  -2.999999E-03
   -4.999999E-03  -2.000000E-03  -3.000002E-03   0.000000
   -2.999999E-03  -5.000003E-03  -6.999999E-03  -2.999999E-03
   -4.999995E-03  -9.000003E-03  -4.000001E-03  -1.000000E-03
   -8.000001E-03  -1.000002E-03  -6.000001E-03   1.999997E-03
   -2.100000E-02   9.000000E-03   1.400000E-02   1.900000E-02
    1.600000E-02
 Y"=   -6.335936E-04  Z"=    1.450231E-03
RUN5E
APPENDAGE = 15, BODY ANGLE = 0
 CP(1...36)=    8.699998E-03   8.999996E-03   3.200000E-02
    3.700000E-02   2.000000E-02   2.400000E-02   2.200000E-02
    1.500000E-02   1.600000E-02   1.600000E-02   1.300000E-02
    1.200000E-02   5.000003E-03   6.999999E-03   4.000001E-03
    2.000000E-03   0.000000       9.999983E-04   0.000000
    0.000000      -5.000003E-03  -1.400000E-02  -6.999999E-03
   -1.100000E-02  -1.300000E-02  -1.200000E-02  -1.200000E-02
   -1.600000E-02  -1.000001E-02  -9.000000E-03  -5.000003E-03
   -1.800000E-02   1.000000E-03   7.999999E-03   8.079998E-03
    5.600000E-03
 Y"=   -2.887454E-03  Z"=    1.680441E-03
RUN7E
NO APPENDAGE, BODY ANGLE = 10
 CP(1...36)=   -5.130000E-02  -5.100001E-02  -3.600001E-02
   -2.000000E-02  -1.000000E-02   1.000000E-03   2.060000E-02
    3.200000E-02   3.399999E-02   2.600000E-02   2.200000E-02
    1.900000E-02   4.000001E-03  -4.999999E-03  -2.900000E-02
   -4.000000E-02  -3.500000E-02  -4.700000E-02  -5.200000E-02
   -3.600000E-02  -2.100000E-02   0.000000       2.200000E-02
    3.760000E-02   4.300000E-02   5.700000E-02   6.699999E-02
    5.300000E-02   3.219999E-02   1.900000E-02   1.999997E-03
   -2.400000E-02  -4.000001E-02  -5.500000E-02  -6.400001E-02
   -6.800000E-02
 Y"=    1.465564E-03  Z"=   -2.179478E-03
RUN8E
NO APPENDAGE, BODY ANGLE = 5
 CP(1...36)=   -3.500001E-03  -4.050001E-02  -1.766000E-02
   -1.177000E-02  -2.800000E-03   9.199999E-03   1.700000E-02
    1.930000E-02   2.460000E-02   2.870000E-02   3.110000E-02
    2.900000E-02   2.100000E-02   1.600000E-02   1.100000E-02
    1.000000E-02   1.800000E-02   1.800000E-02   9.000001E-03
```

```
    1.000000E-02   1.640000E-02   1.760000E-02   2.540000E-02
    2.820000E-02   2.230000E-02   1.370000E-02   1.310000E-02
    1.910000E-02   2.400000E-02   2.130000E-02   1.350000E-02
    2.400000E-03   3.200000E-03   5.999999E-04  -1.600001E-03
   -2.000000E-03
 Y"=   -5.284388E-05  Z"=   -2.408728E-03
RUN10E
NO APPENDAGE, BODY ANGLE = 7.5
 CP(1...36)=   -2.030000E-02  -8.200000E-02  -2.600000E-02
   -1.470000E-02  -5.000000E-03   1.070000E-02   2.030000E-02
    2.600000E-02   3.179999E-02   3.550000E-02   3.399999E-02
    2.900000E-02   1.800000E-02   1.100000E-02   8.000001E-03
    1.300000E-02   1.800000E-02   1.100000E-02   1.600000E-02
    2.900000E-02   4.000000E-02   4.700000E-02   6.299999E-02
    7.099999E-02   7.099999E-02   7.099999E-02   7.299998E-02
    7.099999E-02   6.400000E-02   5.700000E-02   4.499999E-02
    2.700000E-02   1.600000E-02   7.999999E-03   7.989999E-03
    4.799999E-03
 Y"=    4.521543E-03  Z"=   -4.090171E-03
RUN11E
NO APPENDAGE, BODY ANGLE = 2.5
 CP(1...36)=    4.699999E-03  -5.500001E-02   9.999983E-04
    6.699998E-03   7.999999E-03   1.200000E-02   1.100000E-02
    1.200000E-02   1.100000E-02   9.000000E-03   1.100000E-02
    9.000003E-03   3.000002E-03  -7.000003E-03  -6.999999E-03
   -9.999983E-04   9.000000E-03   6.000001E-03   1.000002E-03
    8.000001E-03   1.200000E-02   1.200000E-02   1.300000E-02
    1.800000E-02   1.100000E-02   1.670000E-02   1.600000E-02
    1.300000E-02   1.200000E-02   1.200000E-02   3.999997E-03
    1.000000E-03   4.000001E-03   6.000000E-03   1.999999E-03
   -1.000000E-03
 Y"=    6.137234E-04  Z"=   -8.243788E-04
RUN12E
NO APPENDAGE, BODY ANGLE = 12.5
 CP(1...36)=   -7.530001E-02  -0.103000      -5.000000E-02
   -3.100000E-02  -2.000000E-02  -3.000000E-03   1.300000E-02
    3.100000E-02   4.200000E-02   3.299999E-02   2.100000E-02
    2.500000E-02   1.300000E-02  -3.999997E-03  -2.600000E-02
   -4.300000E-02  -5.000000E-02  -6.500001E-02  -7.400000E-02
   -5.600000E-02  -3.200001E-02  -9.000000E-03   2.100000E-02
    4.500000E-02   5.800000E-02   6.899999E-02   8.299999E-02
    6.600000E-02   4.700000E-02   2.400000E-02  -4.000001E-03
   -3.600000E-02  -6.400001E-02  -7.799999E-02  -9.800002E-02
   -9.800000E-02
 Y"=    1.721920E-03  Z"=   -3.821753E-03
RUN13E
NO APPENDAGE, BODY ANGLE = 17.5
 CP(1...36)=   -0.129300      -0.145000      -7.900001E-02
   -5.300000E-02  -4.400001E-02  -4.400000E-02  -3.000000E-02
    3.399999E-02   5.599999E-02   2.900000E-02  -8.000001E-03
    2.300000E-02   1.000002E-03  -1.900000E-02  -5.100001E-02
   -8.800000E-02  -0.114000      -0.139000      -0.151000
   -0.116000      -8.500001E-02  -4.500001E-02   9.999998E-03
    4.900000E-02   7.599999E-02   0.106000       0.118000
    9.700000E-02   7.099999E-02   3.500000E-02   9.999983E-04
   -5.700000E-02  -9.900001E-02  -0.126000      -0.155000
   -0.156000
 Y"=    4.304287E-03  Z"=   -3.591450E-03
```

X'=0.575

X'=0.575
RUN13C
NO APPENDAGE, BODY ANGLE = 5
CP(1...36)= -2.000000E-02 -1.900000E-02 -1.600000E-02
-7.960001E-03 -2.300000E-03 4.999999E-03 9.000000E-03
7.000001E-03 7.999998E-03 5.999997E-03 3.999997E-03
3.000002E-03 4.000001E-03 9.999946E-04 -8.999996E-03
-9.000003E-03 -9.000003E-03 -1.400000E-02 -1.200000E-02
-1.100000E-02 -9.000000E-03 -5.000003E-03 2.000004E-03
1.999997E-03 1.999997E-03 9.000003E-03 1.100000E-02
4.000001E-03 4.000001E-03 0.000000 -4.000001E-03
-6.000000E-03 -9.000001E-03 -1.500000E-02 -1.600000E-02
-1.700000E-02
Y"= -2.020649E-04 Z"= -5.273549E-04
RUN14C
NO APPENDAGE, BODY ANGLE = 10
CP(1...36)= -5.900000E-02 -5.400000E-02 -3.500000E-02
-6.000000E-03 9.999999E-04 -9.000001E-03 -2.000000E-03
1.200000E-02 2.320000E-02 1.900000E-02 3.999997E-03
1.500000E-02 7.999998E-03 1.100000E-02 -4.999995E-03
-1.600000E-02 -3.600000E-02 -5.000000E-02 -5.500000E-02
-4.400000E-02 -2.900000E-02 -2.000000E-02 -4.999995E-03
1.400000E-02 2.200000E-02 3.600000E-02 4.200000E-02
3.800000E-02 2.900000E-02 1.500000E-02 6.000000E-03
-2.000000E-03 -2.500000E-02 -4.700001E-02 -6.100000E-02
-6.800000E-02
Y"= 7.014021E-04 Z"= -1.411806E-03
RUN15C
NO APPENDAGE, BODY ANGLE = 7.5
CP(1...36)= -4.100000E-02 -4.000000E-02 -2.900000E-02
-2.300000E-02 -1.900000E-02 -3.000000E-03 1.100000E-02
1.400000E-02 1.200000E-02 5.999997E-03 4.999999E-03
1.200000E-02 -1.000002E-03 -3.000006E-03 -8.000001E-03
-1.300000E-02 -2.800000E-02 -3.400000E-02 -3.500000E-02
-2.900000E-02 -2.300000E-02 -1.100000E-02 -6.999999E-03
0.000000 1.200000E-02 2.300000E-02 1.900000E-02
9.000003E-03 1.000002E-03 -6.999999E-03 -1.800000E-02
-2.700000E-02 -2.300000E-02 -3.600001E-02 -4.600000E-02
-4.700001E-02
Y"= -4.937763E-04 Z"= -1.538332E-03
RUN16C
NO APPENDAGE, BODY ANGLE = 2.5
CP(1...36)= -2.100000E-02 -1.900000E-02 -1.720000E-02
-1.000000E-02 -1.400000E-02 -1.200000E-02 -9.000000E-03
-9.000000E-03 -1.000000E-02 -1.200000E-02 -1.300000E-02
-9.999998E-03 -1.400000E-02 -1.500000E-02 -1.600000E-02
-1.500000E-02 -2.000000E-02 -1.800000E-02 -1.800000E-02
-1.500000E-02 -1.400000E-02 -1.500000E-02 -1.100000E-02
-9.000003E-03 -1.100000E-02 -8.999996E-03 -9.000003E-03
-1.500000E-02 -1.700000E-02 -1.500000E-02 -1.700000E-02
-1.500000E-02 -1.400000E-02 -1.600000E-02 -1.800000E-02
-1.900000E-02
Y"= -1.109508E-04 Z"= -1.239188E-04
RUN17C
NO APPENDAGE, BODY ANGLE = 12.5
CP(1...36)= -0.102000 -8.000000E-02 -4.900000E-02
-3.000000E-02 -2.300000E-02 -2.300000E-02 -3.000000E-02
6.000001E-03 3.200000E-02 2.300000E-02 -6.999999E-03
5.000003E-03 4.999999E-03 8.999996E-03 -1.999997E-03
-2.300000E-02 -5.400000E-02 -7.000001E-02 -7.700001E-02
-7.000001E-02 -5.500000E-02 -3.900000E-02 -1.500000E-02
1.400000E-02 3.869999E-02 4.100000E-02 4.600000E-02
4.400000E-02 3.100000E-02 9.000000E-03 -6.999999E-03

X'=0.575

-2.600000E-02 -5.200000E-02 -7.900001E-02 -9.200001E-02
-9.900001E-02
Y"= 8.906400E-04 Z"= -2.963543E-03
RUN18C
NO APPENDAGE, BODY ANGLE = 15
CP(1...36)= -0.141000 -0.101000 -5.800001E-02
-3.400000E-02 -2.900000E-02 -3.300001E-02 -7.100001E-02
-2.100000E-02 3.299999E-02 3.000000E-02 -6.000001E-03
-1.300000E-02 4.000001E-03 1.500000E-02 1.200000E-02
-9.000003E-03 -5.900001E-02 -9.400000E-02 -0.102000
-9.700000E-02 -7.700001E-02 -4.400001E-02 -1.400000E-02
2.200000E-02 5.800000E-02 8.400001E-02 9.400000E-02
8.700000E-02 6.700000E-02 3.900000E-02 2.000000E-03
-3.800001E-02 -7.200001E-02 -0.111000 -0.137000
-0.142000
Y"= 3.347143E-03 Z"= -4.931972E-03
RUN2D
APPENDAGE = 0, BODY ANGLE = 17.5
CP(1...36)= -8.400001E-03 -2.300000E-02 -2.500000E-02
-1.900000E-02 -1.200000E-02 9.999992E-04 1.700000E-02
1.800000E-02 -3.000002E-03 -4.000001E-02 -8.100002E-02
-6.100000E-02 -4.000001E-02 -3.300000E-02 -5.300000E-02
-9.800002E-02 -0.170000 -0.215000 -0.219000
-0.201000 -0.161000 -0.105000 -4.600000E-02
1.800000E-02 6.299999E-02 0.111000 0.128000
0.133000 0.112000 7.900000E-02 3.400000E-02
5.999999E-03 -2.900000E-02 -4.600000E-02 -3.100000E-02
-1.600000E-02
Y"= 9.153109E-03 Z"= 1.155415E-02
RUN3D
APPENDAGE = 0, BODY ANGLE = 15
CP(1...36)= -2.300000E-02 -3.400000E-02 -3.500000E-02
-1.700000E-02 -6.000000E-03 9.999992E-04 6.000000E-03
3.000000E-03 9.999983E-04 -2.500000E-02 -4.700000E-02
-3.400000E-02 -3.100000E-02 -2.100001E-02 -4.700000E-02
-7.900001E-02 -0.126000 -0.162000 -0.162000
-0.146000 -0.122000 -8.600001E-02 -4.300001E-02
4.000001E-03 3.399999E-02 6.999999E-02 8.000000E-02
8.499999E-02 7.200000E-02 5.700000E-02 2.500000E-02
2.000000E-03 -1.800000E-02 -2.700000E-02 -3.100000E-02
-1.900000E-02
Y"= 5.897094E-03 Z"= 8.274004E-03
RUN4D
APPENDAGE = 0, BODY ANGLE = 12.5
CP(1...36)= -2.500000E-02 -2.900000E-02 -1.900000E-02
-9.999992E-04 4.000000E-03 7.799999E-03 1.000000E-02
1.200000E-02 -2.000000E-03 -2.200000E-02 -3.300000E-02
-2.600000E-02 -2.600000E-02 -3.000001E-02 -5.400000E-02
-8.700001E-02 -0.117000 -0.126000 -0.134000
-0.119000 -9.800002E-02 -7.300001E-02 -4.100000E-02
-1.200000E-02 1.600000E-02 3.800000E-02 5.100000E-02
4.899999E-02 3.500000E-02 2.300000E-02 3.000000E-03
-8.000001E-03 -2.500000E-02 -3.400000E-02 -2.900000E-02
-3.300000E-02
Y"= 3.015613E-03 Z"= 7.198679E-03
RUN5D
APPENDAGE = 0, BODY ANGLE = 2.5
CP(1...36)= -2.600000E-02 -3.100000E-02 -2.800000E-02
-3.000000E-02 -3.200001E-02 -2.800000E-02 -2.700000E-02
-2.700000E-02 -2.900000E-02 -3.000000E-02 -3.400000E-02
-2.999999E-02 -3.500000E-02 -3.400000E-02 -3.900000E-02
-3.600001E-02 -3.900000E-02 -3.600000E-02 -3.800000E-02
-3.300001E-02 -3.000000E-02 -3.400000E-02 -2.899999E-02

X'=0.575

-3.000000E-02 -3.000001E-02 -2.299999E-02 -2.500001E-02
-2.900000E-02 -2.700000E-02 -2.500000E-02 -2.700000E-02
-2.800000E-02 -3.000000E-02 -3.100000E-02 -3.600001E-02
-3.700000E-02
Y"= 3.896395E-04 Z"= 4.535620E-04
RUN7D
APPENDAGE = 0, BODY ANGLE = 7.5
CP(1...36)= -2.700000E-02 -2.100000E-02 -2.300000E-02
-2.200000E-02 -2.500000E-02 -1.600000E-02 -1.200000E-02
-1.500000E-02 1.870000E-02 -2.700000E-02 -2.700000E-02
-2.500000E-02 -3.200001E-02 -3.800001E-02 -5.099999E-02
-5.899999E-02 -6.700000E-02 -7.300000E-02 -7.000001E-02
-6.800000E-02 -5.400000E-02 -4.600000E-02 -3.599999E-02
-2.300000E-02 -1.600000E-02 -2.999999E-03 -1.000002E-03
-1.999997E-03 -8.000001E-03 -1.200000E-02 -1.700000E-02
-2.100000E-02 -2.500000E-02 -3.000000E-02 -3.100000E-02
-3.200001E-02
Y"= 8.486754E-04 Z"= 3.259992E-03
RUN8D
APPENDAGE = 0, BODY ANGLE = 10
CP(1...36)= -4.300000E-02 -4.700000E-02 -3.600001E-02
-2.800000E-02 -3.400000E-02 -2.300000E-02 -1.800000E-02
-2.000000E-02 -2.500000E-02 -3.200001E-02 -3.400000E-02
-3.699999E-02 -4.200000E-02 -5.100001E-02 -6.700000E-02
-8.600001E-02 -0.104000 -0.117000 -0.114000
-0.101000 -9.300001E-02 -7.400002E-02 -5.400000E-02
-3.200001E-02 -1.900000E-02 -3.999993E-03 5.000003E-03
5.000003E-03 0.000000 -6.999999E-03 -2.400000E-02
-3.400001E-02 -3.600001E-02 -4.400001E-02 -4.500001E-02
-4.500000E-02
Y"= 1.886989E-03 Z"= 4.920334E-03
RUN10D
APPENDAGE = 0, BODY ANGLE = 5
CP(1...36)= -2.300000E-02 -2.400000E-02 -1.900000E-02
-2.300000E-02 -1.700000E-02 -1.800000E-02 -1.600000E-02
-2.000000E-02 -2.300000E-02 -2.000000E-02 -3.100000E-02
-2.299999E-02 -3.000000E-02 -3.000001E-02 -3.699999E-02
-3.600001E-02 -4.400001E-02 -4.400000E-02 -4.700000E-02
-4.000001E-02 -3.700001E-02 -3.600001E-02 -3.100000E-02
-2.400000E-02 -2.200000E-02 -1.499999E-02 -1.400000E-02
-1.700000E-02 -1.600000E-02 -1.900000E-02 -2.100000E-02
-2.200000E-02 -2.300000E-02 -2.500000E-02 -2.800000E-02
-2.900000E-02
Y"= 4.075989E-04 Z"= 1.591647E-03
RUN11D
APPENDAGE = 0, BODY ANGLE = 0
CP(1...36)= -2.200000E-02 -2.500000E-02 -2.900000E-02
-3.200001E-02 -2.700000E-02 -2.600000E-02 -2.400000E-02
-2.600000E-02 -2.900000E-02 -2.400000E-02 -2.900000E-02
-2.400000E-02 -3.100000E-02 -2.800000E-02 -3.400000E-02
-2.900000E-02 -3.000000E-02 -2.500000E-02 -2.700000E-02
-2.400000E-02 -2.700000E-02 -2.800000E-02 -2.299999E-02
-2.500001E-02 -2.700000E-02 -2.299999E-02 -2.200000E-02
-2.400000E-02 -2.599999E-02 -2.400000E-02 -2.700000E-02
-2.800000E-02 -2.500000E-02 -3.100000E-02 -3.000000E-02
-2.400000E-02
Y"= 2.692980E-04 Z"= 3.154373E-05
RUN12D
APPENDAGE = 5, BODY ANGLE = 0
CP(1...36)= -2.900000E-02 -2.300000E-02 -2.200000E-02
-2.200000E-02 -2.400000E-02 -1.900000E-02 -1.900000E-02
-1.900000E-02 -2.300000E-02 -1.800000E-02 -2.100000E-02
-2.100000E-02 -2.400000E-02 -2.500000E-02 -2.700000E-02

X'=0.575

-2.100000E-02 -2.600000E-02 -2.600000E-02 -2.600000E-02
-2.100000E-02 -2.400000E-02 -2.500000E-02 -2.000000E-02
-2.100000E-02 -2.700000E-02 -2.099999E-02 -2.300000E-02
-2.599999E-02 -2.200000E-02 -2.100001E-02 -2.700000E-02
-2.700000E-02 -2.100000E-02 -2.600000E-02 -2.300000E-02
-2.200000E-02
Y"= -2.142658E-04 Z"= 7.067509E-05
RUN15D
APPENDAGE = 10, BODY ANGLE = 0
CP(1...36)= -2.100000E-02 -2.400000E-02 -1.900000E-02
-1.500000E-02 -1.600000E-02 -1.700000E-02 -1.400000E-02
-1.300000E-02 -1.600000E-02 -1.700000E-02 -2.000000E-02
-1.800000E-02 -1.900000E-02 -1.700000E-02 -1.800000E-02
-1.300000E-02 -2.000000E-02 -1.800000E-02 -1.700000E-02
-1.700000E-02 -1.800000E-02 -2.100001E-02 -1.500000E-02
-2.100000E-02 -2.000000E-02 -1.899999E-02 -1.500000E-02
-2.100000E-02 -1.500000E-02 -1.700000E-02 -2.100000E-02
-2.000000E-02 -1.600000E-02 -1.900000E-02 -9.700002E-02
-2.200000E-02
Y"= -4.867758E-04 Z"= -8.904532E-04
RUN16D
APPENDAGE = 15, BODY ANGLE = 0
CP(1...36)= -3.100000E-02 -3.000000E-02 -2.700000E-02
-1.800000E-02 -1.900000E-02 -2.100000E-02 -2.300000E-02
-2.000000E-02 -1.700000E-02 -1.400000E-02 -1.900000E-02
-1.700000E-02 -2.200000E-02 -1.900000E-02 -1.900000E-02
-1.900000E-02 -2.500000E-02 -2.300000E-02 -1.600000E-02
-1.700000E-02 -2.100000E-02 -1.900000E-02 -1.700000E-02
-2.300000E-02 -2.200000E-02 -2.500000E-02 -2.000000E-02
-2.400000E-02 -2.000000E-02 -1.900000E-02 -2.400000E-02
-2.100000E-02 -2.300000E-02 -2.600000E-02 -3.200001E-02
-3.800000E-02
Y"= -3.318519E-04 Z"= -7.058671E-04
RUN17D
APPENDAGE = 20, BODY ANGLE = 0
CP(1...36)= -3.900000E-02 -4.200000E-02 -3.300000E-02
-2.300000E-02 -1.700000E-02 -1.300000E-02 -1.800000E-02
-1.300000E-02 -1.300000E-02 -1.100000E-02 -1.500000E-02
-1.100000E-02 -1.600000E-02 -1.600000E-02 -1.600000E-02
-1.100000E-02 -1.700000E-02 -1.400000E-02 -1.600000E-02
-1.700000E-02 -1.100000E-02 -2.200000E-02 -1.600000E-02
-2.400000E-02 -2.100001E-02 -2.400000E-02 -2.000000E-02
-2.300000E-02 -2.000000E-02 -2.000000E-02 -2.200000E-02
-1.900000E-02 -1.700000E-02 -2.500000E-02 -3.100000E-02
-4.000001E-02
Y"= -7.097787E-04 Z"= -1.275207E-03

X'=0.75

X'=0.75
RUN8B
APPENDAGE = 5, BODY ANGLE = 0
CP(1...36)= 0.000000 3.000006E-03 1.400000E-02
9.000003E-03 8.000001E-03 8.999996E-03 1.000001E-02
1.099999E-02 1.000001E-02 1.099999E-02 1.200001E-02
7.999986E-03 6.000012E-03 4.999995E-03 9.999990E-03
5.999997E-03 4.000008E-03 8.000001E-03 6.000012E-03
4.000008E-03 5.000010E-03 5.999997E-03 8.000001E-03
1.099999E-02 1.199999E-02 9.999990E-03 6.999999E-03
5.999997E-03 0.000000 0.000000 -5.999997E-03
2.000004E-03 1.000002E-03 -1.000002E-03 0.000000
0.000000
Y"= -5.335114E-04 Z"= -3.421246E-04
RUN9B
APPENDAGE = 5, BODY ANGLE = 0
CP(1...36)= -8.000001E-03 -3.000006E-03 4.000008E-03
2.000004E-03 0.000000 0.000000 1.000002E-03
6.999999E-03 1.000002E-03 8.999988E-03 2.000004E-03
1.999989E-03 3.000006E-03 -3.000006E-03 0.000000
2.000004E-03 3.000006E-03 1.000002E-03 3.000006E-03
3.000021E-03 3.000021E-03 2.000004E-03 6.999999E-03
1.099999E-02 1.099999E-02 6.999999E-03 3.999993E-03
-1.000002E-03 -1.000002E-03 1.000002E-03 -8.000001E-03
1.000002E-03 -1.999997E-03 -1.000002E-03 -9.999946E-04
0.000000
Y"= 5.491831E-06 Z"= -4.594168E-04
RUN10B
APPENDAGE = 20, BODY ANGLE = 0
CP(1...36)= -1.000002E-03 -1.000002E-03 4.000008E-03
9.000003E-03 8.999996E-03 2.100000E-02 1.800000E-02
9.999990E-03 3.999993E-03 9.999990E-03 1.400001E-02
1.400000E-02 1.300001E-02 9.000003E-03 1.600000E-02
1.400000E-02 9.000003E-03 1.500000E-02 1.600000E-02
1.800001E-02 1.800001E-02 1.500000E-02 1.300000E-02
1.500000E-02 1.600000E-02 1.300000E-02 1.099999E-02
3.000006E-03 3.999993E-03 0.000000 -2.000004E-03
5.000003E-03 4.000001E-03 5.000003E-03 2.999999E-03
1.999997E-03
Y"= -4.490580E-04 Z"= -1.050562E-03
RUN11B
APPENDAGE = 15, BODY ANGLE = 0
CP(1...36)= 5.000003E-03 9.000003E-03 1.500000E-02
1.500000E-02 1.400000E-02 2.300000E-02 1.600000E-02
1.600000E-02 1.700000E-02 2.299999E-02 2.100001E-02
2.200000E-02 1.800001E-02 1.500000E-02 2.000000E-02
2.100000E-02 1.600000E-02 2.200000E-02 1.900001E-02
1.700000E-02 1.800001E-02 1.800001E-02 1.899999E-02
1.600000E-02 2.200000E-02 1.600000E-02 1.500000E-02
1.500000E-02 1.199999E-02 6.999999E-03 2.999999E-03
1.300000E-02 1.000001E-02 5.000003E-03 2.999999E-03
2.999999E-03
Y"= -6.179088E-04 Z"= -9.585237E-04
RUN12B
APPENDAGE = 10, BODY ANGLE = 0
CP(1...36)= 6.000005E-03 1.100001E-02 1.700000E-02
1.600000E-02 1.600000E-02 2.400000E-02 1.600000E-02
2.200000E-02 1.700000E-02 2.499999E-02 1.800001E-02
1.699999E-02 2.000001E-02 1.700000E-02 2.000000E-02
1.500000E-02 1.600000E-02 1.500000E-02 1.800001E-02
1.700000E-02 1.900001E-02 1.500000E-02 1.699999E-02
1.500000E-02 1.699999E-02 1.500000E-02 1.400000E-02
1.000001E-02 8.000001E-03 3.000006E-03 -1.000002E-03

X'=0.75

1.300000E-02 1.000001E-02 1.300000E-02 1.200000E-02
1.100000E-02
Y"= -8.129181E-04 Z"= -4.750579E-04
RUN13B
APPENDAGE = 0, BODY ANGLE = 0
CP(1...36)= 1.100000E-02 8.000001E-03 1.400000E-02
1.000001E-02 5.999997E-03 1.300000E-02 1.000001E-02
9.999990E-03 1.000001E-02 1.199999E-02 9.000003E-03
7.999986E-03 1.200001E-02 6.999999E-03 8.000001E-03
4.000008E-03 5.000010E-03 9.000003E-03 1.200001E-02
1.000001E-02 1.100001E-02 1.600000E-02 1.300000E-02
1.300000E-02 1.799999E-02 1.699999E-02 1.500000E-02
1.300000E-02 9.999990E-03 1.000001E-02 0.000000
9.999998E-03 1.000001E-02 8.000001E-03 8.000001E-03
1.500000E-02
Y"= 2.600808E-04 Z"= -7.358125E-05
RUN14B
APPENDAGE = 0, BODY ANGLE = 0
CP(1...36)= 1.200000E-02 1.400000E-02 2.200000E-02
1.600000E-02 1.100000E-02 1.800000E-02 1.800000E-02
1.699999E-02 1.799999E-02 2.000000E-02 2.000001E-02
1.899999E-02 1.300001E-02 9.999990E-03 1.600000E-02
1.600000E-02 1.400000E-02 1.900001E-02 2.100000E-02
2.100001E-02 2.200001E-02 2.200000E-02 2.599999E-02
2.900000E-02 3.000000E-02 2.499999E-02 2.400000E-02
2.400000E-02 2.599999E-02 2.000001E-02 1.199999E-02
2.200000E-02 1.700000E-02 1.700000E-02 2.000000E-02
2.700000E-02
Y"= 6.889149E-04 Z"= -2.532753E-04
RUN15B
APPENDAGE = 0, BODY ANGLE = 10
CP(1...36)= 4.500000E-02 4.500000E-02 5.500000E-02
5.600000E-02 5.369999E-02 6.100000E-02 6.400000E-02
6.899999E-02 6.000000E-02 5.499999E-02 4.900001E-02
5.300000E-02 5.100001E-02 5.300000E-02 5.500000E-02
4.200000E-02 1.400000E-02 -5.999997E-03 -2.199998E-02
-2.800000E-02 -2.899998E-02 -2.300000E-02 -1.199999E-02
3.000006E-03 1.400000E-02 2.100000E-02 2.400000E-02
2.600001E-02 2.000000E-02 2.100000E-02 1.700000E-02
3.500000E-02 2.800000E-02 3.800000E-02 3.900000E-02
4.499999E-02
Y"= -4.183445E-03 Z"= 4.206144E-03
RUN16B
APPENDAGE = 0, BODY ANGLE = 5
CP(1...36)= 1.400000E-02 2.300000E-02 3.400000E-02
3.400000E-02 2.200000E-02 3.200000E-02 3.200000E-02
4.000000E-02 3.500000E-02 3.800000E-02 3.400001E-02
3.199999E-02 3.100000E-02 2.800000E-02 3.000000E-02
2.100000E-02 1.300001E-02 8.000001E-03 5.000010E-03
3.000021E-03 2.000004E-03 -2.000004E-03 4.999995E-03
3.000006E-03 8.000001E-03 6.999999E-03 6.999999E-03
4.999995E-03 1.999989E-03 3.000006E-03 2.999999E-03
2.000000E-02 1.700000E-02 1.800000E-02 1.800000E-02
1.700000E-02
Y"= -2.698527E-03 Z"= 1.145296E-03
RUN17B
APPENDAGE = 0, BODY ANGLE = 5
CP(1...36)= 2.000000E-02 2.400000E-02 3.300000E-02
3.900000E-02 2.800000E-02 3.700000E-02 3.700000E-02
3.900000E-02 3.700000E-02 3.999999E-02 3.800001E-02
3.699999E-02 3.600001E-02 3.000000E-02 3.100000E-02
2.400000E-02 1.800001E-02 1.300001E-02 1.000001E-02
9.000003E-03 8.000001E-03 5.999997E-03 5.999997E-03

X'=0.75

```
    8.000001E-03   1.300000E-02   8.000001E-03   1.400000E-02
    1.100001E-02   4.999995E-03   9.000003E-03   9.999998E-03
    2.500000E-02   2.200000E-02   2.500000E-02   2.500000E-02
    2.500000E-02
 Y"=   -2.480468E-03  Z"=    1.181158E-03
RUN19B
APPENDAGE = 0, BODY ANGLE = 7.5
 CP(1...36)=   -5.300000E-02  -1.000002E-03   3.200001E-02
    3.400000E-02   3.500000E-02   3.000000E-02   4.000008E-03
    7.399999E-02   0.117000       9.499998E-02   5.500001E-02
    4.499999E-02   5.800001E-02   6.500000E-02   6.500000E-02
    5.600000E-02   2.500001E-02  -7.999986E-03   2.000004E-03
    1.400001E-02   2.500001E-02   5.200000E-02   8.399999E-02
    0.107000       0.144000       0.168000       0.175000
    0.165000       0.152000       0.120000       5.599999E-02
    2.300000E-02  -1.600000E-02  -4.200000E-02  -5.300000E-02
   -7.100001E-02
 Y"=    4.238297E-03  Z"=   -5.382187E-03
RUN20B
APPENDAGE = 0, BODY ANGLE = 2.5
 CP(1...36)=    1.400000E-02   1.400000E-02   2.500000E-02
    2.400000E-02   1.300000E-02   2.300000E-02   2.300000E-02
    2.400000E-02   2.300000E-02   2.400000E-02   2.300001E-02
    2.100000E-02   2.200001E-02   1.500000E-02   1.899999E-02
    1.199999E-02   1.100001E-02   1.200001E-02   1.300001E-02
    1.200001E-02   1.100001E-02   1.200001E-02   1.099999E-02
    1.199999E-02   1.500000E-02   1.099999E-02   9.999990E-03
    5.999997E-03   2.999991E-03   5.000010E-03   9.999946E-04
    1.700000E-02   1.200000E-02   9.999998E-03   9.999998E-03
    1.899999E-02
 Y"=   -1.250444E-03  Z"=    2.615520E-04
RUN21B
APPENDAGE = 0, BODY ANGLE = 12.5
 CP(1...36)=    4.600000E-02   5.000000E-02   5.400000E-02
    4.600000E-02   5.199999E-02   6.200000E-02   6.299999E-02
    6.200000E-02   4.700000E-02   3.800000E-02   3.400001E-02
    5.699999E-02   5.800001E-02   6.100000E-02   6.699999E-02
    5.800000E-02   2.400000E-02  -1.500000E-02  -4.200000E-02
   -5.100000E-02  -6.299999E-02  -4.899999E-02  -2.700001E-02
   -2.000004E-03   1.600000E-02   2.700000E-02   3.600000E-02
    3.900000E-02   2.599999E-02   2.400000E-02   1.700000E-02
    3.200000E-02   1.500000E-02   2.900000E-02   2.600000E-02
    4.499999E-02
 Y"=   -4.158602E-03  Z"=    4.564901E-03
RUN22B
APPENDAGE = 0, BODY ANGLE = 12.5
 CP(1...36)=    4.400000E-02   5.600000E-02   5.400000E-02
    5.100000E-02   5.359999E-02   6.799999E-02   6.999999E-02
    6.400000E-02   4.900000E-02   4.200000E-02   3.500000E-02
    5.499999E-02   6.400000E-02   6.799999E-02   7.399999E-02
    6.200000E-02   3.000000E-02  -1.400000E-02  -3.599998E-02
   -5.300000E-02  -5.599999E-02  -4.400000E-02  -2.100000E-02
    0.000000       2.400000E-02   3.299999E-02   3.899999E-02
    3.900000E-02   3.500000E-02   2.600001E-02   1.899999E-02
    3.500000E-02   2.200000E-02   3.100000E-02   3.399999E-02
    4.600000E-02
 Y"=   -4.087880E-03  Z"=    4.454385E-03
RUN23B
APPENDAGE = 0, BODY ANGLE = 15
 CP(1...36)=    7.699999E-02   7.900000E-02   7.799999E-02
    7.300000E-02   6.999999E-02   8.199999E-02   7.799999E-02
    7.099999E-02   4.800000E-02   3.800000E-02   4.300001E-02
    6.699999E-02   7.600000E-02   7.599999E-02   8.399999E-02
```

X'=0.75

```
    7.300000E-02   3.100000E-02  -1.799999E-02  -5.899999E-02
   -7.699999E-02  -7.600000E-02  -5.500001E-02  -2.200001E-02
    8.000001E-03   4.300000E-02   5.700000E-02   7.099999E-02
    7.200000E-02   6.299999E-02   5.400001E-02   3.999999E-02
    5.150000E-02   2.900000E-02   4.099999E-02   4.499999E-02
    6.499998E-02
 Y"=   -3.165551E-03  Z"=    6.625243E-03
RUN24B
APPENDAGE = 0, BODY ANGLE = 17.5
 CP(1...36)=    9.299999E-02   9.799999E-02   0.101000
    9.500000E-02   8.800000E-02   9.099999E-02   9.099999E-02
    7.200000E-02   4.300000E-02   2.100000E-02   4.500001E-02
    6.999999E-02   8.000000E-02   8.399999E-02   8.999999E-02
    7.900000E-02   3.900000E-02  -2.300000E-02  -9.500000E-02
   -0.104000      -9.399998E-02  -6.799999E-02  -2.200001E-02
    1.899999E-02   6.699999E-02   9.099999E-02   0.111000
    0.115000       8.999999E-02   7.300000E-02   5.300000E-02
    5.599999E-02   2.800000E-02   4.000000E-02   5.000000E-02
    7.200000E-02
 Y"=   -1.852744E-03  Z"=    8.239293E-03
RUN25B
APPENDAGE = 0, BODY ANGLE = 17.5
 CP(1...36)=    9.899999E-02   9.899999E-02   0.104000
    9.700000E-02   8.600000E-02   9.199999E-02   8.999999E-02
    7.799999E-02   3.900000E-02   2.400000E-02   4.700001E-02
    7.299998E-02   8.200000E-02   9.299999E-02   9.400000E-02
    8.600000E-02   2.800001E-02  -2.699998E-02  -8.699998E-02
   -0.112000      -9.799999E-02  -6.299999E-02  -2.100000E-02
    2.400000E-02   6.899999E-02   9.699999E-02   0.116000
    0.114000       9.799999E-02   8.000000E-02   5.499999E-02
    5.999999E-02   2.800000E-02   4.300000E-02   4.499999E-02
    8.099999E-02
 Y"=   -1.699177E-03  Z"=    8.377541E-03
RUN3C
NO APPENDAGE, BODY ANGLE = 5
 CP(1...36)=   -1.099999E-02  -1.600000E-02  -2.000004E-03
   -6.999992E-03  -2.999999E-03   8.000001E-03   1.000001E-02
    1.899999E-02   1.899999E-02   2.000000E-02   1.500000E-02
    1.199999E-02   1.900001E-02   1.500000E-02   1.300000E-02
    4.999995E-03   3.000006E-03  -1.999989E-03  -6.999999E-03
   -1.600000E-02  -1.999998E-02  -2.100000E-02  -2.300000E-02
   -2.000000E-02  -1.500002E-02  -2.300000E-02  -2.300000E-02
   -2.500001E-02  -2.400000E-02  -2.700000E-02  -2.500001E-02
   -8.999996E-03  -2.000000E-02  -1.199999E-02  -1.200000E-02
   -7.000007E-03
 Y"=   -3.571661E-03  Z"=   -2.370846E-04
RUN4C
NO APPENDAGE, BODY ANGLE = 10
 CP(1...36)=   -3.100000E-02  -2.200000E-02  -1.000002E-03
   -9.999946E-04  -2.000004E-03   6.999999E-03   9.000003E-03
    2.100000E-02   3.800000E-02   4.600000E-02   2.800000E-02
    2.999999E-02   3.400001E-02   3.200000E-02   3.700000E-02
    3.100000E-02   1.900001E-02  -9.999871E-04  -1.899999E-02
   -3.299999E-02  -3.900000E-02  -4.400000E-02  -3.500000E-02
   -2.499999E-02  -1.400000E-02  -1.699999E-02  -1.400000E-02
   -1.600000E-02  -2.300002E-02  -3.300001E-02  -3.300001E-02
   -2.300000E-02  -4.700000E-02  -3.800000E-02  -4.400001E-02
   -4.100000E-02
 Y"=   -5.695164E-03  Z"=   -1.684239E-03
RUN5C
NO APPENDAGE, BODY ANGLE = 7.5
 CP(1...36)=   -1.500000E-02  -6.999999E-03   0.000000
    0.000000       4.999995E-03   1.500000E-02   1.800000E-02
```

X'=0.75

```
    2.900000E-02   3.300000E-02   3.800000E-02   3.000001E-02
    2.899999E-02   2.900001E-02   2.800000E-02   3.200000E-02
    2.700000E-02   1.200001E-02   4.000008E-03  -4.999995E-03
   -1.499999E-02  -2.199998E-02  -2.500001E-02  -2.300000E-02
   -2.200000E-02  -1.300001E-02  -1.899999E-02  -1.500002E-02
   -1.699999E-02  -1.900001E-02  -2.599999E-02  -2.600001E-02
   -1.199999E-02  -2.299999E-02  -1.600000E-02  -1.900000E-02
   -1.800000E-02
 Y"=   -4.846396E-03  Z"=   -8.383035E-04
RUN6C
NO APPENDAGE, BODY ANGLE = 2.5
 CP(1...36)=   -9.000003E-03  -3.000006E-03  -1.000002E-03
    0.000000       0.000000       8.999996E-03   8.000001E-03
    8.000001E-03   9.000003E-03   1.199999E-02   8.000001E-03
    6.999999E-03   8.000001E-03   9.000003E-03   8.000001E-03
   -1.000002E-03   0.000000       0.000000      -1.999989E-03
   -3.999978E-03  -9.000003E-03  -1.199999E-02  -9.000003E-03
   -8.999988E-03  -3.000006E-03  -1.300001E-02  -1.300001E-02
   -1.400000E-02  -1.200001E-02  -1.599999E-02  -1.000001E-02
    1.000002E-03  -6.999999E-03  -2.999999E-03  -9.999946E-04
   -1.999997E-03
 Y"=   -1.772691E-03  Z"=    5.175732E-05
RUN7C
NO APPENDAGE, BODY ANGLE = 12.5
 CP(1...36)=   -5.599999E-02  -3.100000E-02  -6.999999E-03
   -6.999992E-03  -2.999999E-03   5.000003E-03  -8.000001E-03
   -1.000002E-03   2.300000E-02   4.099999E-02   2.100001E-02
    1.899999E-02   3.200001E-02   3.399999E-02   3.399999E-02
    3.000000E-02   1.700000E-02  -8.999988E-03  -3.999999E-02
   -6.099999E-02  -6.599998E-02  -6.299999E-02  -5.300000E-02
   -3.800000E-02  -1.899999E-02  -1.699999E-02  -9.000003E-03
   -1.199999E-02  -2.200000E-02  -3.899999E-02  -4.700001E-02
   -4.099999E-02  -6.700000E-02  -6.500000E-02  -7.799999E-02
   -7.000002E-02
 Y"=   -5.973536E-03  Z"=   -2.209317E-03
RUN8C
NO APPENDAGE, BODY ANGLE = 15
 CP(1...36)=   -7.600000E-02  -3.700000E-02  -1.099999E-02
   -2.999999E-03   5.999997E-03   5.999997E-03   2.000004E-03
   -1.800001E-02   1.500000E-02   3.599999E-02   1.500000E-02
    1.599999E-02   3.500000E-02   3.900000E-02   4.000000E-02
    3.400000E-02   1.800001E-02  -1.500000E-02  -6.299999E-02
   -8.600000E-02  -9.299999E-02  -8.800000E-02  -6.600001E-02
   -4.300000E-02  -1.600000E-02  -5.999997E-03   2.000004E-03
    1.000002E-03  -1.500000E-02  -3.399999E-02  -4.600000E-02
   -4.899999E-02  -9.400001E-02  -9.700000E-02  -0.112000
   -0.102000
 Y"=   -6.313855E-03  Z"=   -2.599228E-03
RUN9C
NO APPENDAGE, BODY ANGLE = 17.5
 CP(1...36)=   -9.599999E-02  -3.399999E-02  -6.999999E-03
    0.000000       1.600000E-02   1.500000E-02   9.000003E-03
   -2.800000E-02   1.000001E-02   2.999999E-02   3.000006E-03
    1.500000E-02   3.100000E-02   3.900000E-02   4.099999E-02
    3.100000E-02   2.000001E-02  -3.299999E-02  -9.500000E-02
   -0.124000      -0.133000      -0.113000      -7.800001E-02
   -4.400001E-02  -9.999990E-03   9.000003E-03   2.200000E-02
    2.600001E-02   5.999997E-03  -3.300001E-02  -5.700000E-02
   -7.099999E-02  -0.130000      -0.140000      -0.157000
   -0.142000
 Y"=   -6.628814E-03  Z"=   -2.709488E-03
RUN10C
NO APPENDAGE, BODY ANGLE = 17.5
```

X'=0.75

```
CP(1...36)=   -8.800000E-02  -2.800000E-02   0.000000
   6.000005E-03   2.300000E-02   1.800000E-02   1.900000E-02
  -1.500000E-02   1.300000E-02   3.500000E-02   1.700000E-02
   2.899999E-02   4.200000E-02   4.499999E-02   4.899999E-02
   4.300000E-02   3.200001E-02  -2.199998E-02  -7.100001E-02
  -0.101000      -0.111000      -9.500000E-02  -6.400001E-02
  -3.100000E-02   3.999993E-03   2.200000E-02   3.399999E-02
   3.500000E-02   2.000000E-02  -1.799999E-02  -3.900000E-02
  -5.200000E-02  -0.113000      -0.125000      -0.138000
  -0.126000
Y"=   -5.937773E-03  Z"=   -3.097919E-03
```

X'=0.925

X'=0.925
RUN4
NO APPENDAGE, BODY ANGLE = 10
CP(1...36)= 4.700002E-02 6.399998E-02 6.299999E-02
6.599998E-02 6.700000E-02 6.500000E-02 6.700000E-02
7.099998E-02 6.599998E-02 6.900001E-02 6.999999E-02
7.299998E-02 7.400000E-02 6.999999E-02 6.900001E-02
7.200000E-02 7.299998E-02 7.100001E-02 6.500000E-02
7.400000E-02 7.399997E-02 7.299998E-02 6.900001E-02
6.099999E-02 4.400000E-02 3.900000E-02 3.500000E-02
3.000000E-02 2.800000E-02 2.699998E-02 3.099999E-02
3.899997E-02 4.300001E-02 5.599999E-02 6.000000E-02
6.299999E-02
Y"= -1.208125E-03 Z"= -5.600512E-04
RUN5
NO APPENDAGE, BODY ANGLE = 10
CP(1...36)= 5.300000E-02 5.300000E-02 5.100000E-02
5.100000E-02 5.300000E-02 5.600002E-02 5.000001E-02
5.599999E-02 5.199999E-02 5.300000E-02 5.599999E-02
6.299999E-02 5.800000E-02 5.999997E-02 5.800000E-02
5.800000E-02 6.200001E-02 6.299999E-02 5.700001E-02
6.200001E-02 6.599998E-02 6.400001E-02 5.599999E-02
4.800001E-02 3.299999E-02 3.200001E-02 2.200001E-02
1.699999E-02 9.999990E-03 1.899999E-02 1.799998E-02
2.699998E-02 3.500003E-02 4.299998E-02 5.100000E-02
5.300000E-02
Y"= -1.123333E-03 Z"= -5.382552E-04
RUN6
NO APPENDAGE, BODY ANGLE = 18
CP(1...36)= 0.123000 0.125000 0.127000
0.122000 0.120000 0.118000 0.116000
0.120000 0.126000 0.129000 0.120000
0.112000 0.113000 0.113000 0.119000
0.122000 0.123000 0.121000 0.116000
0.118000 0.110000 8.300000E-02 6.200001E-02
5.100000E-02 5.000001E-02 5.200002E-02 5.200002E-02
4.999998E-02 4.600000E-02 3.799999E-02 2.899998E-02
3.199998E-02 5.100003E-02 9.099999E-02 0.117000
0.122000
Y"= -3.042583E-03 Z"= 1.855373E-05
RUN7
NO APPENDAGE, BODY ANGLE = 15
CP(1...36)= 0.126000 0.129000 0.126000
0.126000 0.124000 0.121000 0.117000
0.128000 0.125000 0.131000 0.123000
0.131000 0.132000 0.133000 0.140000
0.143000 0.146000 0.147000 0.142000
0.146000 0.142000 0.126000 0.109000
9.299999E-02 8.100000E-02 8.100000E-02 7.700002E-02
7.699999E-02 6.799999E-02 7.099998E-02 6.599998E-02
7.499999E-02 9.400001E-02 0.122000 0.140000
0.141000
Y"= -1.904115E-03 Z"= -5.914859E-04
RUN8
NO APPENDAGE, BODY ANGLE = 15
CP(1...36)= , 0.128000 0.131000 0.132000
0.130000 0.127000 0.125000 0.124000
0.127000 0.133000 0.132000 0.126000
0.119000 0.118000 0.119000 0.125000
0.126000 0.132000 0.132000 0.124000
0.131000 0.130000 0.107000 9.099999E-02
7.600000E-02 6.600001E-02 6.700000E-02 6.200001E-02
6.299999E-02 5.700001E-02 5.499998E-02 5.399999E-02

X'=0.925

```
    6.099999E-02   7.800001E-02   0.107000       0.125000
    0.128000
 Y"=   -2.467775E-03  Z"=   -8.130068E-05
RUN9
NO APPENDAGE, BODY ANGLE = 5
 CP(1...36)=    5.600002E-02   5.800000E-02   5.100000E-02
    5.599999E-02   5.800000E-02   5.700001E-02   5.500001E-02
    6.099999E-02   6.500000E-02   6.299999E-02   6.500000E-02
    5.399999E-02   5.500001E-02   5.299997E-02   5.100000E-02
    5.300000E-02   6.200001E-02   6.400001E-02   6.000000E-02
    6.000000E-02   5.800000E-02   5.599999E-02   5.599999E-02
    5.100000E-02   4.200000E-02   3.999999E-02   4.200000E-02
    5.100000E-02   5.500001E-02   4.899999E-02   4.599997E-02
    4.799998E-02   5.400002E-02   5.800000E-02   5.499998E-02
    5.400002E-02
 Y"=   -3.964896E-04  Z"=   -4.374277E-05
RUN10
NO APPENDAGE, BODY ANGLE = 5
 CP(1...36)=    5.300000E-02   5.399999E-02   6.000000E-02
    5.599999E-02   5.399999E-02   5.800000E-02   5.800003E-02
    5.399999E-02   6.299999E-02   5.800000E-02   5.500001E-02
    5.399999E-02   5.399999E-02   5.999997E-02   5.800000E-02
    6.300002E-02   6.200001E-02   6.600001E-02   6.200001E-02
    6.000000E-02   6.500000E-02   6.099999E-02   6.200001E-02
    5.500001E-02   5.100000E-02   5.599999E-02   5.300000E-02
    5.599999E-02   4.899999E-02   4.999998E-02   5.100000E-02
    5.100000E-02   5.900002E-02   7.200000E-02   6.000000E-02
    5.900002E-02
 Y"=   -9.990601E-05  Z"=   -1.403044E-04
RUN11
NO APPENDAGE, BODY ANGLE = 7.5
 CP(1...36)=   -9.000003E-03  -1.300001E-02  -2.000001E-02
   -1.700000E-02  -1.600000E-02  -1.499999E-02  -1.400000E-02
   -1.200002E-02  -1.200002E-02  -1.499999E-02  -1.400000E-02
   -9.000003E-03  -9.999990E-03  -1.000002E-02  -1.199999E-02
   -9.000003E-03  -8.000016E-03  -7.999986E-03  -1.500002E-02
   -9.000003E-03  -2.000004E-03  -9.000003E-03  -9.999990E-03
   -1.899999E-02  -2.900000E-02  -3.000000E-02  -3.599998E-02
   -3.500001E-02  -3.700000E-02  -3.600001E-02  -3.400001E-02
   -2.500001E-02  -2.399999E-02  -1.800001E-02  -1.300001E-02
   -1.300000E-02
 Y"=   -6.575804E-04  Z"=   -2.825827E-04
RUN12
NO APPENDAGE, BODY ANGLE = 7.5
 CP(1...36)=   -5.999982E-03  -9.000003E-03  -8.000016E-03
   -9.000003E-03  -8.000016E-03  -9.000003E-03  -1.099998E-02
   -6.999999E-03  -4.000008E-03  -6.999999E-03  -6.999999E-03
   -1.000017E-03  -2.999991E-03  -2.000004E-03  -4.000008E-03
   -2.999991E-03   0.000000      -2.999991E-03  -7.999986E-03
   -2.999991E-03   0.000000      -2.000004E-03  -9.999990E-03
   -1.199999E-02  -2.000001E-02  -2.700000E-02  -3.399999E-02
   -3.500001E-02  -3.600000E-02  -3.200001E-02  -3.100002E-02
   -2.300002E-02  -1.699999E-02  -1.000002E-02  -9.000003E-03
   -1.100001E-02
 Y"=   -8.159219E-04  Z"=   -3.056592E-04
RUN13
NO APPENDAGE, BODY ANGLE = 2.5
 CP(1...36)=    1.100001E-02   1.199999E-02   7.999986E-03
    1.100001E-02   1.100001E-02   1.100001E-02   9.000003E-03
    9.999990E-03   1.199999E-02   9.999990E-03   8.000016E-03
    1.199999E-02   1.100001E-02   9.999990E-03   7.999986E-03
    1.100001E-02   1.199999E-02   9.000003E-03   9.000003E-03
    8.000016E-03   1.499999E-02   9.999990E-03   1.199999E-02
```

X'=0.925

9.999990E-03 9.000003E-03 4.999995E-03 6.999999E-03
9.000003E-03 9.000003E-03 9.999990E-03 1.199999E-02
1.499999E-02 1.000002E-02 1.299998E-02 1.099998E-02
1.300001E-02
Y"= -1.301146E-05 Z"= 5.089062E-05
RUN14
NO APPENDAGE, BODY ANGLE = 2.5
CP(1...36)= 1.300001E-02 1.400000E-02 1.199999E-02
1.299998E-02 1.299998E-02 1.500002E-02 1.000002E-02
1.499999E-02 1.999998E-02 1.100001E-02 1.400000E-02
1.299998E-02 1.300001E-02 1.199999E-02 1.199999E-02
1.400000E-02 1.899999E-02 1.600000E-02 1.100001E-02
1.700002E-02 1.999998E-02 1.400000E-02 1.500002E-02
1.199999E-02 9.999990E-03 1.400000E-02 1.200002E-02
1.400000E-02 1.400000E-02 1.799998E-02 1.899999E-02
1.600000E-02 1.600000E-02 1.499999E-02 1.499999E-02
1.600000E-02
Y"= 4.854198E-05 Z"= 1.011364E-06
RUN15
NO APPENDAGE, BODY ANGLE = 12.5
CP(1...36)= 5.400002E-02 5.599999E-02 5.800000E-02
5.899999E-02 5.500001E-02 5.400002E-02 5.300000E-02
6.000000E-02 5.499998E-02 5.800000E-02 5.500001E-02
5.499998E-02 5.300000E-02 5.399999E-02 5.800000E-02
6.000000E-02 6.099999E-02 5.800000E-02 5.500001E-02
6.000000E-02 6.399998E-02 5.399999E-02 4.200000E-02
2.900001E-02 1.699999E-02 1.000002E-02 3.000021E-03
2.999991E-03 -4.000008E-03 -2.000004E-03 -4.000008E-03
4.999995E-03 1.800001E-02 4.099998E-02 4.999998E-02
5.400002E-02
Y"= -1.884390E-03 Z"= -3.652533E-04
RUN16
NO APPENDAGE, BODY ANGLE = 17.5
CP(1...36)= 0.138000 0.136000 0.136000
0.134000 0.132000 0.129000 0.127000
0.131000 0.135000 0.138000 0.130000
0.128000 0.126000 0.123000 0.129000
0.133000 0.135000 0.132000 0.128000
0.130000 0.124000 9.500000E-02 6.700000E-02
6.000000E-02 5.300000E-02 6.100002E-02 5.700001E-02
6.099999E-02 5.000001E-02 4.999998E-02 3.899997E-02
4.799998E-02 6.600001E-02 0.105000 0.131000
0.135000
Y"= -3.113032E-03 Z"= 1.005161E-04
RUN1A
APPENDAGE = 0, BODY ANGLE = 0
CP(1...36)= 4.000002E-02 4.099998E-02 3.799999E-02
2.800000E-02 3.799999E-02 3.900000E-02 3.600001E-02
3.700000E-02 3.799999E-02 3.700000E-02 3.700000E-02
3.700000E-02 4.100001E-02 3.999999E-02 4.200000E-02
3.900000E-02 3.799999E-02 3.800002E-02 3.099999E-02
3.700000E-02 3.999999E-02 3.599998E-02 3.900000E-02
3.700000E-02 3.700000E-02 3.900000E-02 3.700000E-02
3.899997E-02 3.500000E-02 3.599998E-02 3.599998E-02
3.500000E-02 3.400001E-02 3.599998E-02 3.599998E-02
3.700000E-02
Y"= -4.904437E-05 Z"= -6.012868E-05
RUN3A
APPENDAGE = 0, BODY ANGLE = 10
CP(1...36)= 9.000000E-02 8.600000E-02 8.699998E-02
7.499999E-02 8.800000E-02 8.600000E-02 8.000001E-02
8.299997E-02 8.800000E-02 9.000000E-02 9.200001E-02
9.199998E-02 9.299999E-02 9.299999E-02 9.099999E-02

X'=0.925

```
    9.300002E-02   9.299999E-02   9.000000E-02   8.600000E-02
    9.100002E-02   9.099999E-02   7.499999E-02   6.400001E-02
    5.300000E-02   4.400000E-02   4.500002E-02   4.700002E-02
    5.800000E-02   6.200001E-02   7.200000E-02   8.199999E-02
    8.499998E-02   8.800000E-02   8.499998E-02   8.999997E-02
    8.800000E-02
 Y"=   -1.043112E-03  Z"=    1.521373E-04
RUN4A
APPENDAGE = 0, BODY ANGLE = 15
 CP(1...36)=    0.111000       0.111000       0.107000
    9.799999E-02   0.107000       0.103000       0.101000
    0.108000       0.114000       0.117000       0.120000
    0.123000       0.119000       0.125000       0.125000
    0.127000       0.128000       0.126000       0.124000
    0.122000       0.119000       8.199999E-02   5.300000E-02
    5.000001E-02   3.799999E-02   5.200002E-02   5.400002E-02
    6.299999E-02   6.700000E-02   6.899998E-02   7.200000E-02
    9.199998E-02   9.600002E-02   0.108000       0.108000
    0.109000
 Y"=   -2.112905E-03  Z"=   -1.312740E-04
RUN5A
APPENDAGE = 0, BODY ANGLE = 15
 CP(1...36)=    0.115000       0.115000       0.116000
    0.105000       0.112000       0.114000       0.108000
    0.113000       0.122000       0.124000       0.127000
    0.127000       0.127000       0.126000       0.131000
    0.134000       0.136000       0.133000       0.127000
    0.131000       0.124000       8.899999E-02   6.099999E-02
    4.699999E-02   4.800001E-02   5.800000E-02   5.700001E-02
    7.099998E-02   7.300001E-02   7.999998E-02   8.399999E-02
    9.700000E-02   0.106000       0.117000       0.118000
    0.119000
 Y"=   -2.082680E-03  Z"=   -3.919010E-05
RUN6A
APPENDAGE = 0, BODY ANGLE = 18
 CP(1...36)=    9.100002E-02   9.000000E-02   8.899999E-02
    9.599999E-02   8.699998E-02   7.700002E-02   8.200002E-02
    8.299997E-02   8.999997E-02   0.102000       0.105000
    0.105000       0.103000       0.101000       0.106000
    0.107000       0.115000       0.112000       0.108000
    0.104000       7.699999E-02   3.900000E-02   1.899999E-02
    1.199999E-02   1.300001E-02   2.800000E-02   3.300002E-02
    4.299998E-02   4.200000E-02   4.200000E-02   3.299999E-02
    3.999999E-02   5.200002E-02   7.400000E-02   8.199999E-02
    8.700001E-02
 Y"=   -2.704611E-03  Z"=   -1.899212E-04
RUN7A
APPENDAGE = 0, BODY ANGLE = 18
 CP(1...36)=    9.900001E-02   9.700000E-02   9.299999E-02
    9.799999E-02   8.699998E-02   9.100002E-02   8.100000E-02
    9.099999E-02   9.700000E-02   0.102000       0.109000
    0.106000       0.107000       0.115000       0.114000
    0.119000       0.123000       0.114000       0.110000
    0.108000       9.399998E-02   4.899999E-02   1.899999E-02
    1.600000E-02   1.800001E-02   3.200001E-02   3.900000E-02
    4.999998E-02   4.899999E-02   4.899999E-02   4.599997E-02
    5.300000E-02   6.000000E-02   8.899999E-02   8.999997E-02
    9.700000E-02
 Y"=   -2.594750E-03  Z"=   -1.409689E-04
RUN9A
APPENDAGE = 0, BODY ANGLE = 17.5
 CP(1...36)=    8.600000E-02   8.899999E-02   8.499998E-02
    9.500000E-02   9.099999E-02   9.700000E-02   9.800002E-02
```

X'=0.925

```
    0.104000        0.112000        0.116000        0.120000
    0.121000        0.120000        0.122000        0.125000
    0.129000        0.128000        0.132000        0.128000
    0.127000        0.107000        6.700000E-02    3.400001E-02
    3.099999E-02    3.299999E-02    4.600000E-02    4.700002E-02
    6.199998E-02    6.000000E-02    6.299999E-02    6.199998E-02
    6.700000E-02    7.400000E-02    9.399998E-02    0.104000
    0.104000
 Y"=   -2.451211E-03  Z"=   -5.874883E-04
RUN10A
APPENDAGE = 0, BODY ANGLE = 17.5
 CP(1...36)=    8.800000E-02   8.800000E-02   8.399999E-02
    8.899999E-02    7.799998E-02    7.700002E-02    7.000002E-02
    8.600000E-02    8.600000E-02    9.500000E-02    0.100000
    0.104000        0.103000        0.108000        0.109000
    0.111000        0.116000        0.113000        0.101000
    0.102000        7.900000E-02    4.400000E-02    2.100000E-02
    1.199999E-02    9.999990E-03    2.500001E-02    2.900001E-02
    4.200000E-02    4.200000E-02    4.400000E-02    4.200000E-02
    4.799998E-02    6.000000E-02    7.499999E-02    8.399999E-02
    8.700001E-02
 Y"=   -2.529494E-03  Z"=   -2.553509E-04
RUN12A
APPENDAGE = 0, BODY ANGLE = 17.5
 CP(1...36)=    0.102000        0.100000        0.103000
    0.103000        9.299999E-02    9.299999E-02    9.400001E-02
    9.799999E-02    0.109000        0.106000        0.113000
    0.109000        0.112000        0.108000        0.108000
    0.116000        0.121000        0.116000        0.115000
    0.116000        0.103000        5.700001E-02    3.299999E-02
    2.500001E-02    1.600000E-02    4.500002E-02    4.300001E-02
    5.399999E-02    5.500001E-02    6.199998E-02    3.599998E-02
    5.800000E-02    6.700000E-02    9.299999E-02    9.899998E-02
    0.103000
 Y"=   -2.506023E-03  Z"=   -4.921755E-05
RUN14A
APPENDAGE = 0, BODY ANGLE = 12.5
 CP(1...36)=    9.500000E-02   9.599999E-02   9.099999E-02
    9.099999E-02    9.099999E-02    9.200001E-02    9.100002E-02
    9.500000E-02    9.899998E-02    0.100000        9.800002E-02
    0.102000        0.104000        0.104000        0.104000
    0.108000        0.110000        0.107000        0.102000
    0.109000        0.104000        8.899999E-02    6.799999E-02
    6.000000E-02    3.999999E-02    5.500001E-02    4.600000E-02
    5.899999E-02    6.400001E-02    6.599998E-02    5.899999E-02
    7.799998E-02    8.500001E-02    9.799999E-02    9.599999E-02
    9.700000E-02
 Y"=   -1.501599E-03  Z"=   -1.984033E-04
RUN15A
APPENDAGE = 0, BODY ANGLE = 5
 CP(1...36)=    3.300002E-02   3.200001E-02   3.299999E-02
    3.200001E-02    3.299999E-02    3.400001E-02    3.300002E-02
    3.700000E-02    3.599998E-02    3.200001E-02    3.400001E-02
    3.199998E-02    3.400001E-02    3.199998E-02    3.000000E-02
    3.100002E-02    3.200001E-02    3.100002E-02    2.700001E-02
    3.000000E-02    3.599998E-02    3.099999E-02    2.399999E-02
    2.399999E-02    1.300001E-02    2.200001E-02    1.900002E-02
    2.599999E-02    2.599999E-02    2.899998E-02    2.199998E-02
    2.899998E-02    2.900001E-02    3.099999E-02    2.699998E-02
    3.200001E-02
 Y"=   -3.895195E-04  Z"=    9.465335E-05
RUN16A
APPENDAGE = 0, BODY ANGLE = 2.5
```

X'=0.925

```
 CP(1...36)=    5.700001E-02   6.099999E-02   6.200001E-02
    6.399998E-02   6.000000E-02   6.200001E-02   6.100002E-02
    6.299999E-02   6.299999E-02   5.599999E-02   5.800000E-02
    6.099999E-02   5.900002E-02   5.499998E-02   5.699998E-02
    6.100002E-02   6.400001E-02   6.100002E-02   5.700001E-02
    6.000000E-02   6.199998E-02   5.899999E-02   5.700001E-02
    5.700001E-02   5.200002E-02   5.700001E-02   5.300000E-02
    5.899999E-02   5.500001E-02   5.699998E-02   5.300000E-02
    5.399999E-02   5.200002E-02   5.599999E-02   5.599999E-02
    5.800000E-02
 Y"=   -2.109386E-04  Z"=   -2.115713E-05
RUN17A
APPENDAGE = 0, BODY ANGLE = 7.5
 CP(1...36)=    9.400001E-02   9.299999E-02   9.399998E-02
    9.399998E-02   9.399998E-02   9.200001E-02   8.900002E-02
    9.199998E-02   9.399998E-02   9.400001E-02   9.500000E-02
    9.399998E-02   9.500000E-02   9.299999E-02   9.099999E-02
    9.600002E-02   9.500000E-02   9.800002E-02   9.299999E-02
    9.400001E-02   9.699997E-02   9.099999E-02   8.199999E-02
    7.400000E-02   6.099999E-02   7.100001E-02   6.800002E-02
    8.199999E-02   8.000001E-02   8.299997E-02   8.100000E-02
    9.299999E-02   9.100002E-02   9.399998E-02   9.199998E-02
    9.299999E-02
 Y"=   -6.011560E-04  Z"=    9.805239E-05
RUN1B
APPENDAGE = 10, BODY ANGLE = 0
 CP(1...36)=    2.400002E-02   2.899998E-02   2.800000E-02
    2.699998E-02   2.699998E-02   2.800000E-02   2.500001E-02
    2.699998E-02   2.699998E-02   2.000001E-02   2.100000E-02
    2.399999E-02   2.800000E-02   2.499998E-02   2.500001E-02
    2.600002E-02   2.899998E-02   2.700001E-02   2.800000E-02
    2.900001E-02   3.799999E-02   2.899998E-02   3.099999E-02
    2.900001E-02   2.800000E-02   3.100002E-02   3.200001E-02
    3.099999E-02   3.400001E-02   3.299999E-02   2.699998E-02
    3.299999E-02   2.700001E-02   3.099999E-02   2.699998E-02
    2.800000E-02
 Y"=    2.506397E-04  Z"=   -3.195305E-05
RUN2B
APPENDAGE = 10, BODY ANGLE = 0
 CP(1...36)=    4.200000E-02   4.200000E-02   4.200000E-02
    4.600000E-02   4.200000E-02   4.200000E-02   4.200003E-02
    4.299998E-02   4.699999E-02   4.100001E-02   4.300001E-02
    4.200000E-02   4.699999E-02   4.200000E-02   4.499999E-02
    4.900002E-02   4.800001E-02   4.700002E-02   4.300001E-02
    4.700002E-02   5.199999E-02   5.000001E-02   5.200002E-02
    5.200002E-02   4.500002E-02   5.200002E-02   4.700002E-02
    5.100000E-02   5.000001E-02   5.100000E-02   4.799998E-02
    4.899999E-02   4.700002E-02   5.199999E-02   4.799998E-02
    4.800001E-02
 Y"=    2.763394E-04  Z"=   -9.653390E-05
RUN4B
APPENDAGE = 15, BODY ANGLE = 0
 CP(1...36)=    2.100000E-02   1.999998E-02   1.999998E-02
    1.999998E-02   1.999998E-02   1.600000E-02   1.500002E-02
    1.699999E-02   1.899999E-02   1.100001E-02   1.300001E-02
    1.299998E-02   1.699999E-02   1.599997E-02   1.600000E-02
    2.000001E-02   2.000001E-02   1.800001E-02   1.600000E-02
    2.500001E-02   2.399999E-02   2.300000E-02   2.500001E-02
    2.100000E-02   2.100000E-02   2.300000E-02   2.300000E-02
    2.699998E-02   2.100000E-02   1.999998E-02   1.799998E-02
    1.899999E-02   1.900002E-02   2.100000E-02   1.799998E-02
    1.400000E-02
 Y"=    2.522670E-04  Z"=   -6.499159E-05
```

X'=0.925

RUN5B
APPENDAGE = 20, BODY ANGLE = 0
CP(1...36)= 2.800000E-02 2.899998E-02 2.699998E-02
2.699998E-02 2.599999E-02 2.300000E-02 2.000001E-02
1.999998E-02 2.300000E-02 1.699999E-02 1.600000E-02
1.699999E-02 1.800001E-02 1.699999E-02 1.600000E-02
2.400002E-02 2.700001E-02 2.200001E-02 2.300000E-02
2.400002E-02 3.199998E-02 3.000000E-02 3.400001E-02
3.200001E-02 2.700001E-02 3.500000E-02 3.200001E-02
3.599998E-02 3.500000E-02 3.399998E-02 3.199998E-02
3.199998E-02 3.100002E-02 3.200001E-02 3.000000E-02
2.900001E-02
Y"= 5.721229E-04 Z"= 1.441206E-04
RUN6B
APPENDAGE = 5, BODY ANGLE = 0
CP(1...36)= 3.600001E-02 3.999999E-02 4.099998E-02
4.200000E-02 4.299998E-02 3.900000E-02 3.800002E-02
3.999999E-02 4.099998E-02 3.400001E-02 3.500000E-02
3.599998E-02 3.999999E-02 3.799999E-02 3.799999E-02
4.000002E-02 4.100001E-02 3.900000E-02 3.500000E-02
3.900000E-02 4.299998E-02 4.200000E-02 4.200000E-02
4.300001E-02 3.900000E-02 4.100001E-02 3.800002E-02
4.099998E-02 4.100001E-02 4.099998E-02 3.799999E-02
4.099998E-02 3.900000E-02 4.200000E-02 3.999999E-02
3.999999E-02
Y"= 8.977187E-05 Z"= 1.759684E-05

Appendix 3

Papers by the author accepted for open publication.

1. Dynamic Effects on Rudders and Hydroplanes
   B Ward. The Naval Architect July/August 1991.
   pp E364-E365

2. Experiments to Improve Predictions of Submarine Manoeuvres
   B Ward. Manoeuvring and Control of Marine Craft. Proceedings of the Second International Conference, held at the University of Southampton, 14-17 July 1992. pp 247-260.

3. Experiments to Investigate Vortex Separation on an Appended Body
   B Ward, P A Wilson. Manoeuvring and Control of Marine Craft. Proceedings of the Second International Conference, held at the University of Southampton, 14-17 July 1992. pp 519-532.

4. Forces on a Body of Revolution in a Vortex Flow Field
   B Ward, P A Wilson. RINA Written Transactions Part B 1992.

Dynamic effects on rudders and hydroplanes

B Ward, from the Maritime Division of the Defence Research Agency (ARE Haslar) obtained some peculiar results from recent experiments.

IN recent years the use of mathematical models as early stage design tools for ships and submarines has become the norm. Work continues at ARE Haslar into the prediction of motions and manoeuvres of marine vehicles using such methods. In support of this work it was decided to examine the dynamic effects on lift forces for low aspect ratio rudders and hydroplanes. A thorough literature search was carried out; much previous work on oscillating hydroplanes was at very high frequencies more appropriate, say, to helicopters. It was therefore decided to perform some dedicated experiments (Ref 1) to obtain the required data.

Experiment

Three NACA 0020 sections of different aspect ratios were used (Fig 1).

The experiment was conducted in the Circulating Water Channel at ARE Haslar. The DATS computer package (Ref 2) was used for both data acquisition and data analysis.

Static and oscillating runs were carried out. The oscillating runs were carried out at frequencies from 0.055Hz to 0.386Hz. Frequencies were chosen to correspond to full scale angular rates in the region of 5deg/sec (Fig 2).

Results and discussion

Stall angle varied with aspect ratio. No significant variation of C_L with frequency was noted over the range examined.

Fig 3 shows a plot of phase angle against $\frac{\omega c}{U}$ for an aspect ratio of 1.5. The phase angles are positive indicating that lift leads incidence. Note the linear trend in the data. Little variation was apparent between the three aspect ratios tested.

Fig 4 shows continuous plots of C_L against incidence for two oscillating runs with aspect ratio 2 at different frequencies. Incidence amplitude is 35.5 degrees in both cases (above the static stall angle). Stall is evident at the lower frequency. At the higher frequency the lift coefficient is higher at zero angle corresponding to greater phase lead. Stalling does not seem to occur at the high frequency.

Fig 5 shows the results of three ramping motion experiments to an incidence of 41 degrees at 6 degrees/sec for an aspect ratio of 1.5. In each case the lift coefficient follows the angle of incidence to well above the maximum static value. In other words the hydroplane does not immediately stall. After some time flow separation occurs, the hydroplane stalls and the lift collapses to the stall value. High lift is maintained for an apparently arbitrary time.

Conclusions

The experiment to examine dynamic effects on oscillating hydroplanes showed the effects to be small but worth noting. Phase angles were small but may be significant in terms of autopilot design.

The most interesting aspect of the experiment was the delayed stall noted during the ramping motion runs.

Hydrodynamic stall is a complex phe-

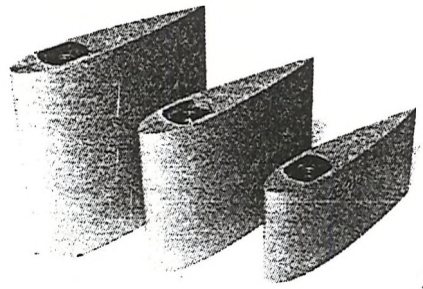

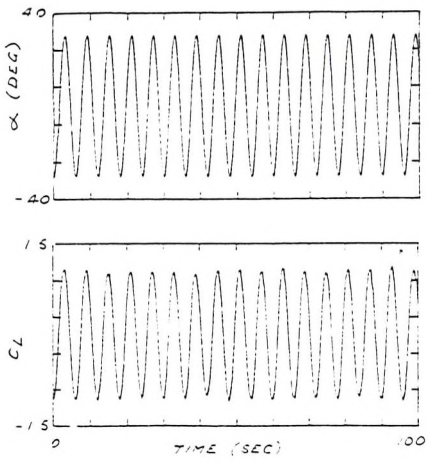

Fig·1 (above left). Three NACA 0020 sections.

Fig 2 (left). Dynamic time history from a typical oscillating run.

Fig 3 (below). Phase angle-aspect ratio 1.5.

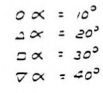

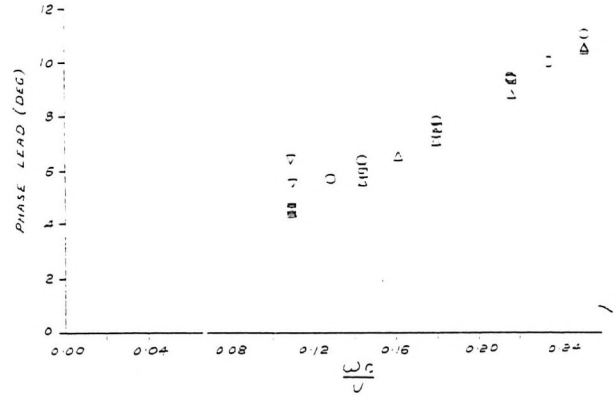

Fig 4 (below). Aspect ratio 2, incidence 35.5deg.

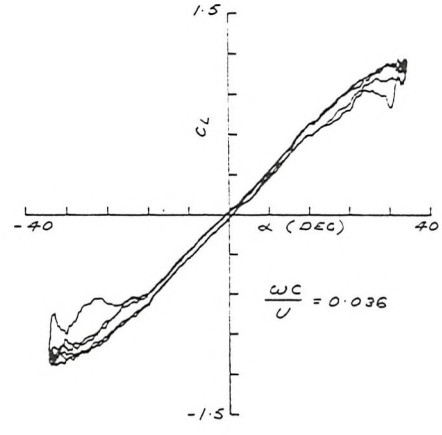

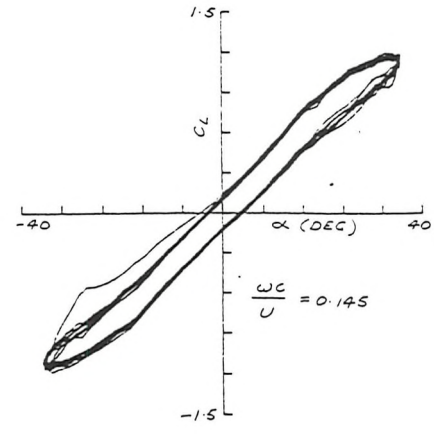

Notation

c	Chord length	metres
C_L	Lift coefficient	—
U	Freestream velocity	metres/sec
a	Angle of incidence: positive nose to port	degrees
ω	Frequency	radians/sec

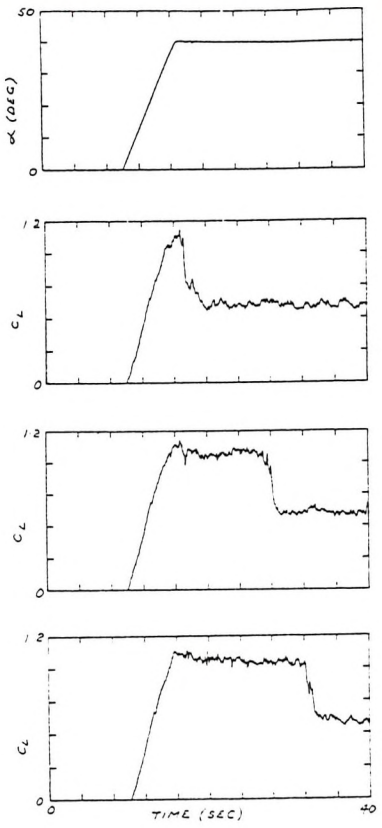

Fig 5. Example of delayed stall with aspect ratio 1.5, incidence 41deg, angular rate 6deg/sec.

nomenon with the loading dependent on many parameters, including Reynolds number, leading-edge radius and thickness.

The delayed stall experienced in these experiments may be the leading edge stall described in Ref 3. This form of stall is related to the formation of a small separation bubble near the leading edge. At some angles of attack, the bubble bursts and the flow separates from the entire upper surface of the hydroplane, resulting in a sudden loss in lift.

No turbulence stimulator was used in these experiments. Perhaps this caused the flow to remain laminar around the curved nose for the arbitary period. Air bubbles which are present in the open channel eventually break down the separation bubble mentioned above causing stall. The Reynolds number at which the experiment was conducted was 0.3×10^6 (basing Reynolds number on chord). This is below the critical value where laminar flow becomes turbulent. This may also have been a factor.

The author has not been able to find any previous record of the type of delayed stall shown in Fig 5. Was this observation something quite peculiar to the experiment or is it a phenomenon that exists in the real world?

References

1. B Ward, A R J M Lloyd. *Experiments on low-aspect ratio hydroplanes to measure lift under static and dynamic conditions.* ARE TM(UHR) 90306. March 1990.
2. DATS User Manual. PROSIG Computer Consultants Ltd.
3. G B McCulloch, D E Gault. *Examples of three representative types of airfoil-section stall at low speed.* NACA TN 2502. September 1951.

Experiments To Improve Predictions of Submarine Manoeuvres

B Ward
Ship and Submarine Dynamics Section
DRA Haslar

ABSTRACT

A knowledge of hydrodynamic forces is necessary to determine the manoeuvring characteristics of a submarine design. Computer models have been used for this purpose using derivative data from model experiments. A computer model has been developed at DRA Haslar over the last decade which requires no input derivative data and hence avoids the need to carry out model experiments for each design in the early stages.

This computer model uses a semi-empirical approach which combines classical theory and empirical equations. The empirical equations determine parameters such as forces and moments on the hull, lift forces on control surfaces and positions and strengths of body vortices. Over the last five years various experiments have been conducted to acquire the necessary empirical data and also to gain a greater understanding of how the flow around the submarine affects the manoeuvring characteristics.

Recent validations have shown the predictions of submarine manoeuvring characteristics such as turning circle, speed loss and yaw rate in the turn and vertical pulse manoeuvres to be good. However predictions of depth changes during turns are unsatisfactory.

This paper discusses the experiments to obtain the empirical data.

INTRODUCTION

The prediction of the manoeuvring behaviour of submarines has become more important in recent years whether it is for the early designing of depth and course autopilots or for optimizing appendage sizes. A necessary prerequisite

to simulating submarine manoeuvres is a knowledge of hydrodynamic forces and moments which act on the body of the submarine in accordance with momentary velocities, accelerations and appendage positions. Scaled model tests have usually determined hydrodynamic coefficients which are used in a Taylor series or curve approximation to formulate the motion equation in accordance with the Newton Axiom.

Lloyd[1] described a new mathematical model, SUBSIM, which predicts the manoeuvring characteristics of submersible bodies. Subsequent developments were reported in Lloyd[2]. The SUBSIM program is effectively an intermediate step between the traditional derivative approach to the prediction of manoeuvring characteristics and the intensive computational fluid dynamics approach to estimating the force on a body. The purpose of SUBSIM is not to quantify forces exactly but to determine gross manoeuvring characteristics. The use of experiment data to determine empirical functions is a convenient approach to use and overcomes deficiencies in the theoretical methods and the expense of model tests on a particular design. The designer can use SUBSIM at an early stage and arrive at a design before any physical model testing is required. This paper describes some of the experiments used to collect the empirical data.

FORCES AND MOMENTS ON A BODY OF REVOLUTION

Conventional submarines have tended to be near bodies of revolution with pointed tails. It is appropriate for those scientists and engineers involved in submarine design to investigate methods of predicting forces on such shapes. The estimation of forces on a body of revolution has been a problem in the aerodynamics world for much of this century. Early methods such as Munk[3] and Von Karman[4] were unreliable. More recent developments Mendenhall[5] and Tinker[6] tend to be highly computational and therefore time consuming. Lloyd[1,2] opted for a quick empirical approach.

In SUBSIM the forces and moments on the hull are represented by

$$Z' = [Z'_{W} + Z'_{W|W|}\sin\alpha]\sin\alpha \qquad (1)$$

$$M' = [M'_{W} + M'_{W|W|}\sin\alpha]\sin\alpha \qquad (2)$$

where Z'_W , $Z'_{W|W|}$, M'_W and $M'_{W|W|}$ are functions of L/D and C_P . The functions were derived by fitting equations to data from 1950's David Taylor

Research Centre (DTRC) data. It was decided that a series of experiments in which fineness ratio was varied from 7.5 to 13 would enhance the database allowing better formulae to be derived as well as verifying the DTRC data. Experiments to measure forces and moments on bodies of revolution were conducted in No 2 Ship Tank (a large towing tank mainly used for submerged body experiments) at DRA Haslar (formerly ARE Haslar).

The model hull consisted of three main sections; nose,tail and middle body. Two identical sections were inserted either side of the middle body to lengthen the model. Diameter was constant at 0.526 metres. Dimensions and other details are given in Table 1.

Table 1

Model	Length(m)	L/D	C_P
DRE1	3.948	7.5	0.64
DRE2	4.210	8	0.66
DRE3	4.736	9	0.7
DRE4	5.264	10	0.73
DRE5	5.790	11	0.756
DRE6	6.316	12	0.776
DRE7	6.842	13	0.793

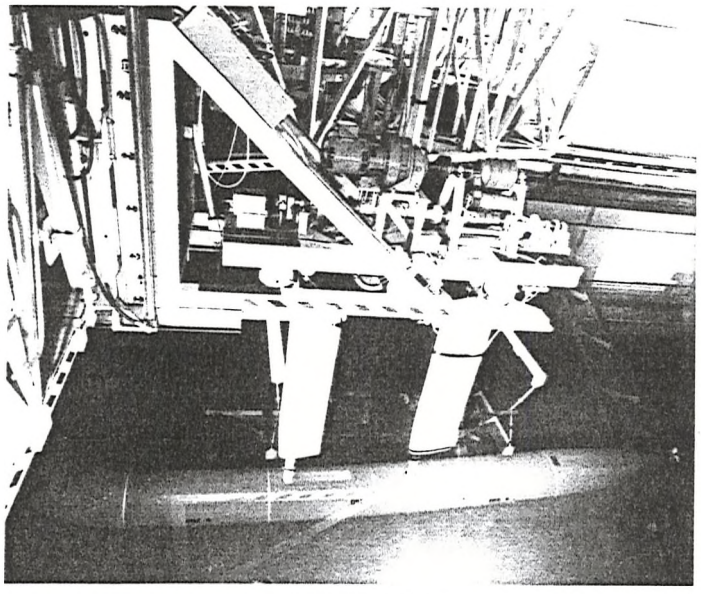

Figure 1 : Model below No 2 Ship Tank carriage

Two swords held the model below the No 2 Ship Tank carriage as shown in Figure 1. The model was pitched over a range of angles from -16 degrees to +16 degrees. Speed was maintained at 2.5 m/s which gives a Reynolds number of 1.15×10^6 (basing R_e on diameter); this is above the critical R_e of 1.0×10^6.

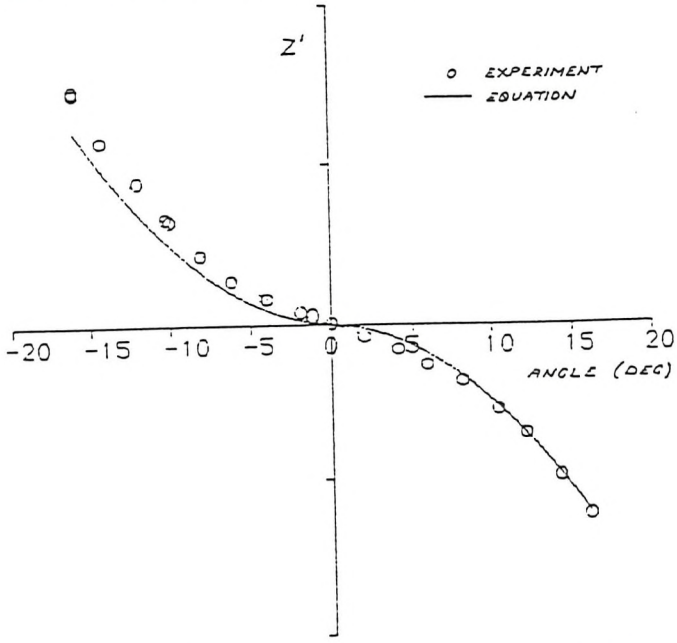

Figure 2 : Model DRE1, L/D=7.5, C_P=0.64

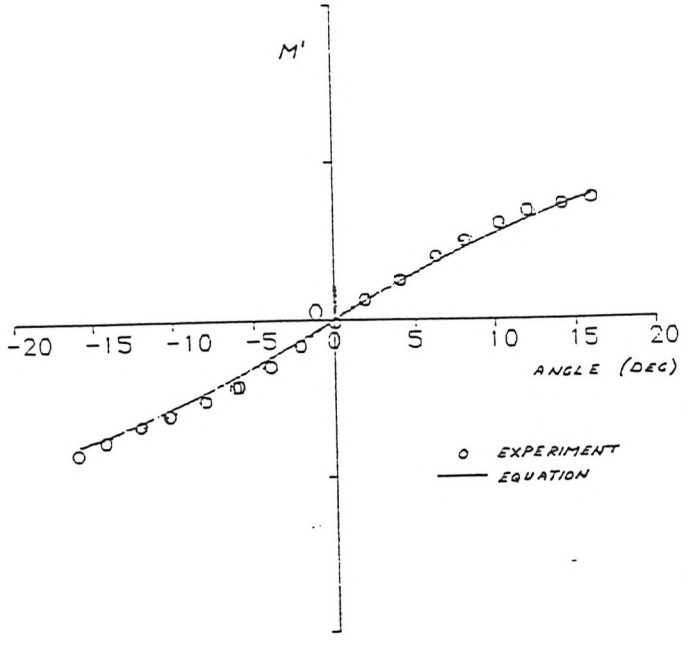

Figure 3 : Model DRE4, L/D=10, C_P=0.73

Regression polynomials of the second degree were fitted to each set of data to yield the four coefficients Z'_w ,$Z'_{w|w|}$,M'_w and $M'_{w|w|}$. Figures 2 and 3 show examples of the resulting curve fits to the No 2 Ship Tank data. It was concluded that the data from No 2 Ship Tank and the DTRC data are in good agreement generally.

Further experiments on the rotating arm facility will provide data from which rotary derivatives can be derived.

LIFT ON LOW ASPECT RATIO HYDROPLANES UNDER STATIC AND DYNAMIC CONDITIONS

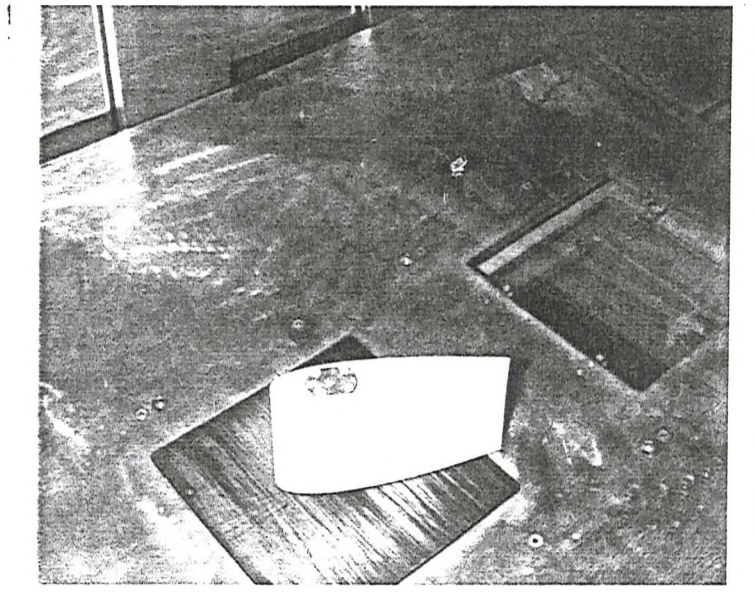

Figure 4 : Hydroplane experiment in Circulating Water Channel

It was decided that there was a need for data on dynamic effects on lift forces for low aspect ratio hydroplanes. A thorough literature search was carried out; previous papers usually described two dimensional experiments at much higher frequencies than those of relevant interest. It was therefore decided to perform some dedicated experiments to obtain the required data.

Three NACA 0020 hydroplanes were used of aspect ratios 1, 1.5 and 2. Each hydroplane had a chord length of 0.26m and span of 0.13m, 0.195m and 0.26m respectively. A strain gauged stock at the quarter chord position of the hydroplane was attached to a servo to oscillate the hydroplane. Strain gauge bridges on the stock were calibrated to give normal and tangential forces.

The experiment was conducted in the Circulation Water Channel (Figure 4) at DRA Haslar. The horizontal flow velocity was maintained at 2.5 m/s.

Figure 5 shows a plot of non dimensional lift C_L against angle of incidence for aspect ratio 2.

Oscillating runs were carried out at frequencies from 0.055 Hz to 0.386 Hz corresponding to $\omega c/U$ values from 0.036 to 0.252. Frequencies were chosen to correspond to full scale angular rates in the region of 5 degs/sec. An example plot is shown in Figure 6.

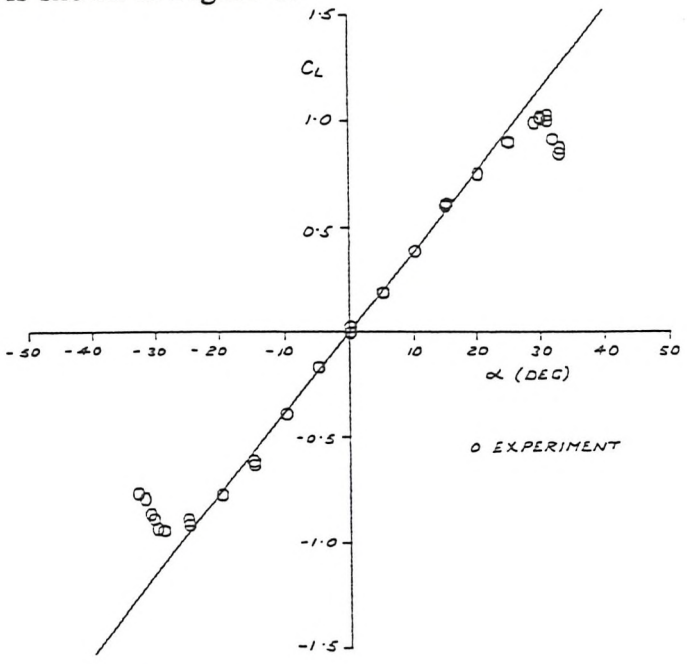

Figure 5 : Lift coefficient - aspect ratio 2, static condition

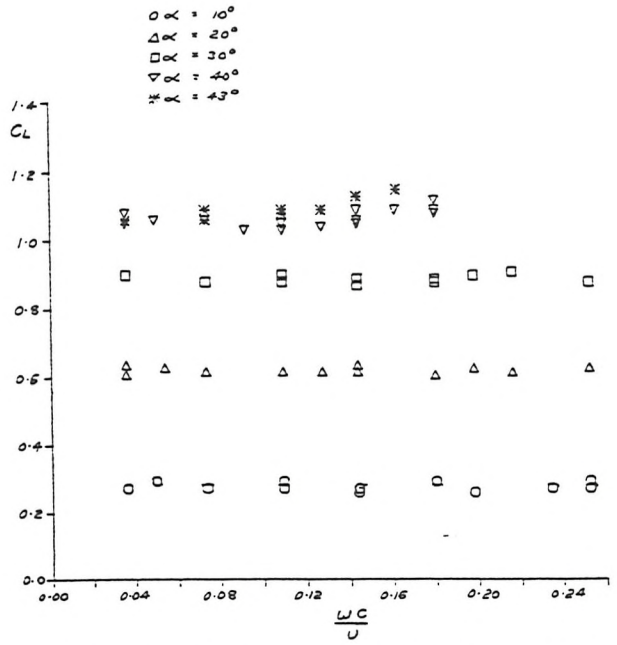

Figure 6 : Lift coefficient - aspect ratio 1, dynamic condition

The experiment showed the dynamic effects to be small but worth noting. No significant variation in C_L was noted over the range of frequencies examined. Phase angles were small; a phase lead of approximately 10 degrees occurs at the highest frequency of 0.386Hz ($\omega c/U = 0.252$).

It was concluded that it was not necessary to model the dynamic effects as they are insignificant at the angular rates likely to be encountered.

VORTICITY AROUND A BODY OF REVOLUTION IN CURVED FLOW

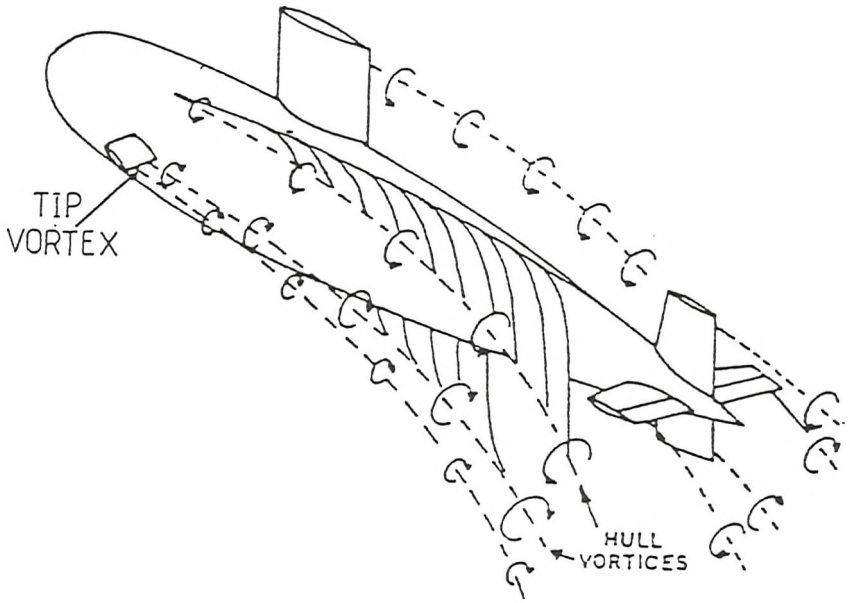

Figure 7 : A typical pattern of vortices around a manoeuvring submarine

The flow around a manoeuvring submarine is dominated by vortices which are shed from the appendages and the hull (Figure 7). The strength and position of appendage vortices may be predicted by lifting line theory (Glauert[7]). The body vortices are affected by incidence and rate of turn of the submarine. The SUBSIM computer program makes use of empirical formulae to represent the positions and strengths of body vortices.

The experiments (discussed in Lloyd[8,9]) were conducted on the rotating arm facility (Figure 8) in the manoeuvring tank at DRA Haslar. They were performed by the Wolfson Unit for Marine Technology and Industrial Aerodynamics (University of Southampton) working under contract.

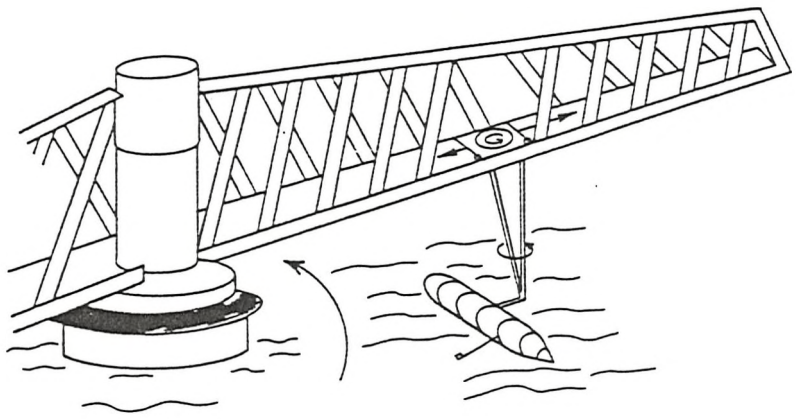

Figure 8 : The rotating arm experiment

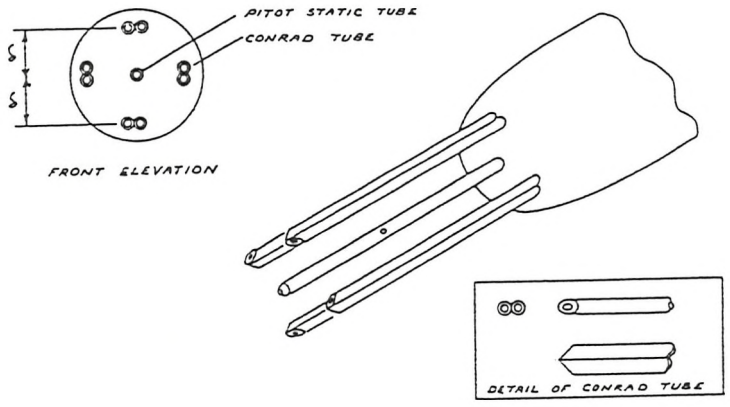

Figure 9 : The Freestone vorticity probe

A 5 metre body of revolution was used with fineness ratio L/D of 8.5. To measure vorticity a Freestone[10] probe (Figure 9) was used which was mounted on a stayed circular strut which could be positioned at one of three locations along the length of the model (x'=0.7,0.85,0.925). The probes' radial and angular location could be adjusted. Runs were conducted over a range of angles of incidence and turn rates at the three stations. Measurements were taken at 10 degree angular intervals at 25 mm radial steps from the body surface.

During the analysis of vorticity traverses (Figure 10). A number of salient features were apparent;
a. The peak value was probably missed due to the limited number of data values.
b. The physical dimensions of the probe precluded any measurements close to the local body surface.

c. The traverses appeared to come down to a 'plateau' as the radius increases, whereas it would have been expected that they would decrease smoothly to zero at the 'edge' of the vortical flow. This is probably associated with zero errors in the Freestone probe. It was found during the experiment that the probe gave small levels of 'vorticity' in uniform flow when no vorticity was expected and that these zero errors were functions of the flow direction at the probe. A simple correction was devised based on the results obtained at the outer limits of the strut, and this was applied to each traverse, forcing the vorticity at r=1.5 x D to be zero. However, the flow direction changes as the probe is moved towards the body and this will affect the zero error correction. No simple method of quantifying this effect has been devised.

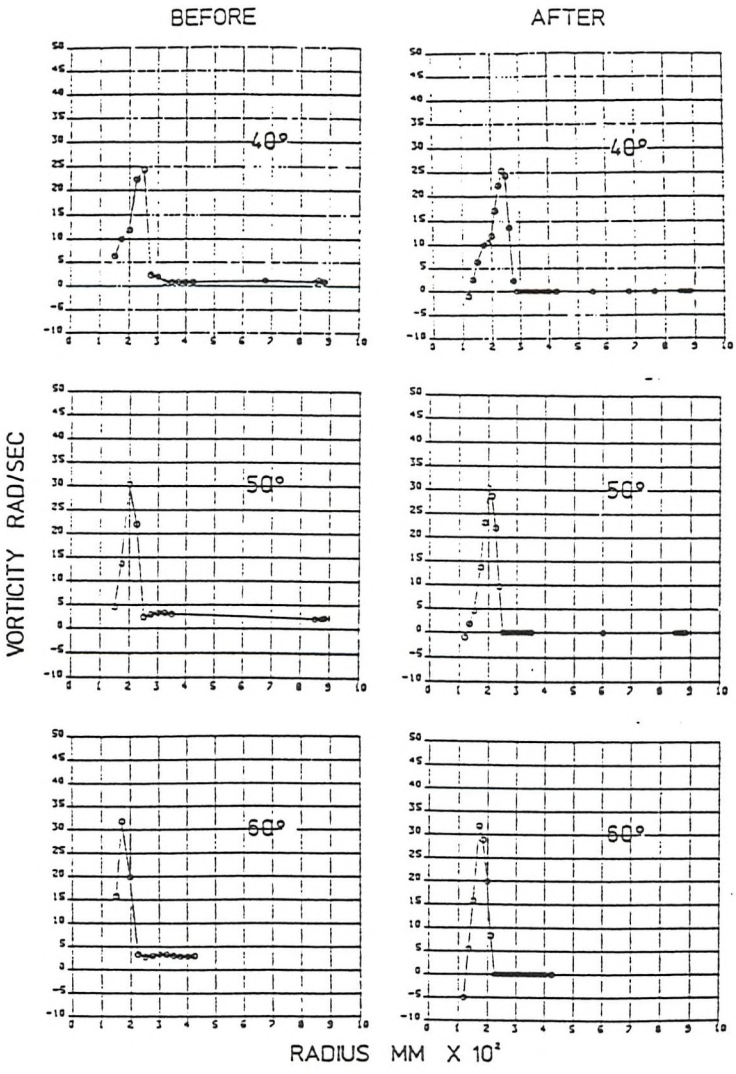

Figure 10: Vorticity traverses - before and after fairing
(x'=0.925, r'=0.3, α=7.5)

To overcome these shortcomings the data were faired to a more expected form; ensuring smooth variations as each of the parameters was varied. This involved;

a. Inserting estimated additional points close to the local radius of the body.
b. Interpolating extra points throughout the curve including, at times, a point for peak vorticity.
c. Bringing traverses down to zero at the apparent edge of the vortical flow.
d. Ensuring that the estimated peak vorticity increased smoothly with strut angle. Examples of fairing are shown in Figure 10.

The faired data was reanalysed by the author and new empirical equations were derived for circulation density, centre of circulation and vortex core radius. These equations are functions of angle of incidence, turn parameter etc.

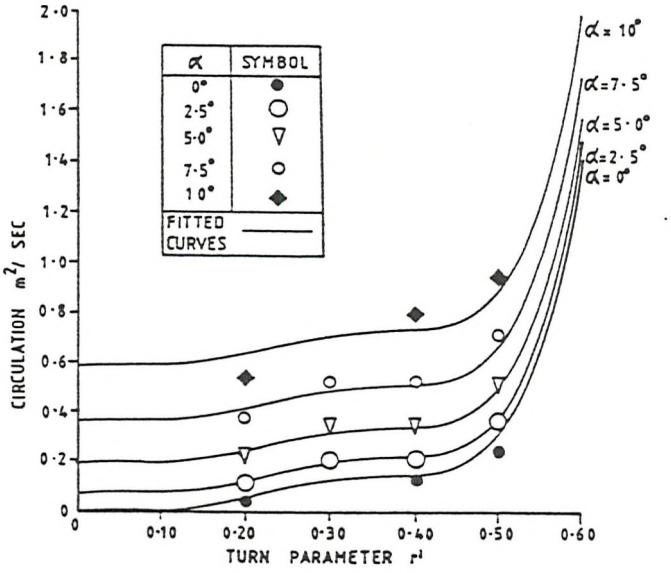

Figure 11 : Total circulation against turn parameter for varying values of incidence angle

The total circulation was estimated from

$$\Gamma = \int_0^{\pi/2} \Gamma_\theta \theta d\theta \qquad (3)$$

Results for all test conditions at x'=0.925 are shown in Figure 11.

Equations were incorporated into SUBSIM and an extensive validation was carried out. Computed predictions were compared with full-scale trials results. Predictions of turning circle, yaw rate and speed loss in the turn were

consistently good. Figure 12 shows plots of tactical diameter for three submarines and as shown for a variety of speeds and rudder angles the SUBSIM predictions of tactical diameter are very good. However, prediction of depth change in the turn is poor. This problem has led to further experimental work to examine the flow over an appended body.

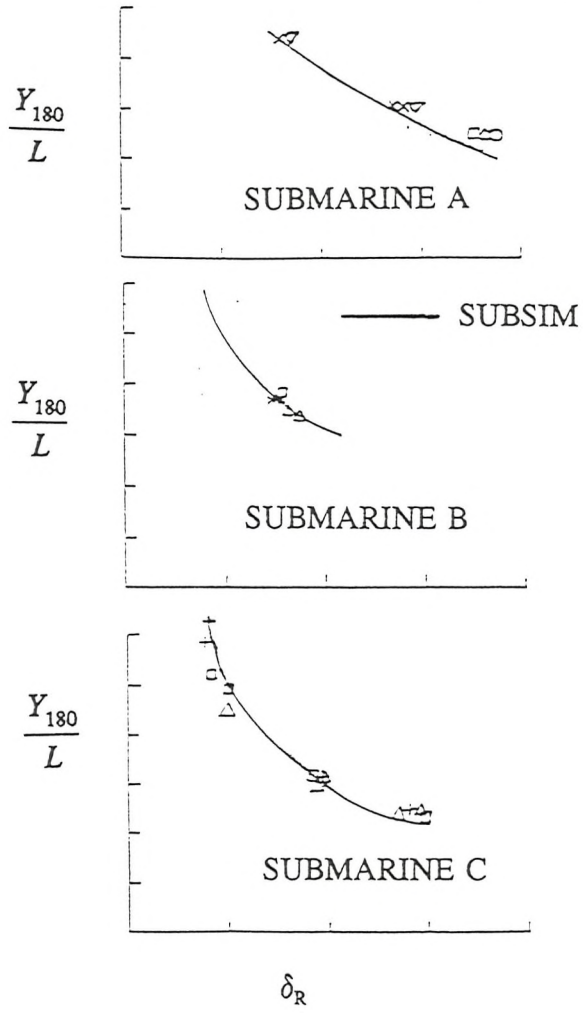

Figure 12 : Computer prediction of tactical diameter

VORTICITY AND PRESSURE ON AN APPENDED BODY OF REVOLUTION

A one metre appended body of revolution was used in the Circulating Water Channel. This is the subject of Ward, Wilson[11]. Vorticity and pressure were measured under various static conditions. It was concluded that the appendage, which is representative of a submarine bridge fin, creates an asymmetry in the flow which leads to an asymmetry in pressure distribution as shown in Figure 13.

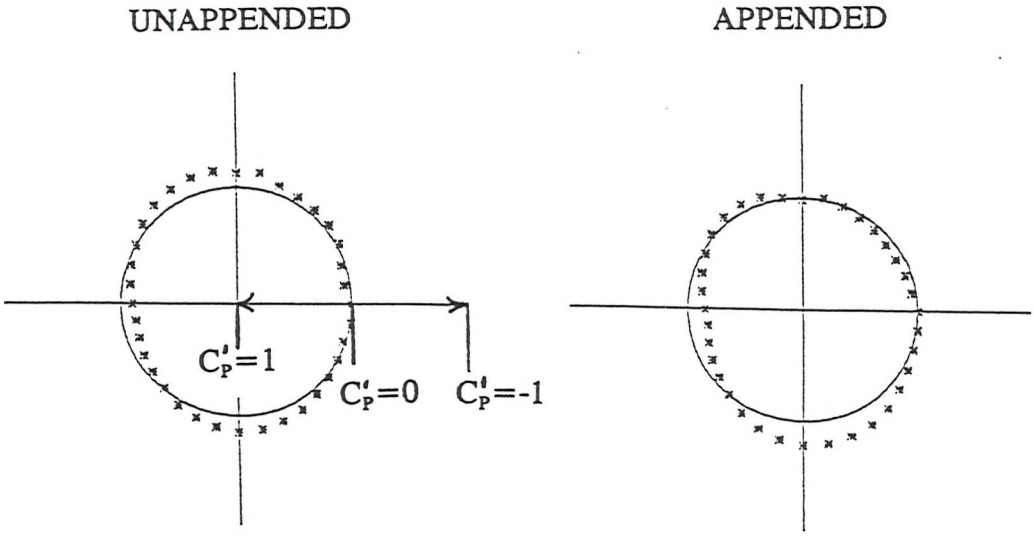

Figure 13 : Pressure coefficients, x'=0.4, α=17.5 degrees

CONCLUSIONS

A description has been given in this paper of various experiments conducted at DRA Haslar to support a programme of research into the prediction of submarine manoeuvres. The experiments conducted were to examine hydrodynamic effects such as dynamic effects on oscillating hydroplanes and the shedding of vortices from the hull of a submerged body. Empirical data was collected in order to obtain estimates of forces and moments on a hull, lift on hydroplanes and positions and strengths of vortices.

ACKNOWLEDGEMENTS

This work has been carried out with the support of the Procurement Executive of the Ministry of Defence.

REFERENCES

1. Lloyd A R J M. Progress Towards a Rational Method of Predicting Submarine Manoeuvres. RINA Symposium on Naval Submarines. 1983.
2. Lloyd A R J M. Developments in the Prediction of Submarine Manoeuvres. Undersea Defence Technology. 1988.
3. Munk M M. The Aerodynamic Forces on Airship Hulls. NACA Report 184. 1924.
4. Von Karman T. Calculation of Pressure Distribution on Airship Hulls. NACA TM No 574. 1930.
5. Mendenhall M R, Spangler S B, Perkins S C. Vortex Shedding From Circular and Non-circular Bodies at High Angles of Attack. AIAA Paper 79-0026. 1979.

6. Tinker S J. A Discrete Vortex Model of Separated Flow Over Manoeuvring Submersibles. Advances in Underwater Technology, Ocean Science and Offshore Engineering. Volume 15: Technology Common to Aero and Marine Engineering. 1988.
7. Glauert H. The Elements of Airfoil and Airscrew Theory. Cambridge University Press. 1947.
8. Lloyd A R J M, Campbell I F. Experiments to Investigate Vortices Shed from a Submarine-like Body of Revolution. 59th Meeting of the AGARD Fluid Dynamics Panel Symposium, Monterey, California, USA. Aerodynamic and Related Hydrodynamic Studies Using Water Facilities. AGARD-CCP 413. October 1986.
9. Lloyd A R J M. Experiments to Investigate the Vorticity Shed by a Body of Revolution in Curved Flow. Advances in Underwater Technology, Ocean Science and Offshore Engineering. Volume 15: Technology Common to Aero and Marine Engineering. 1988.
10. Freestone M M. Vorticity Measurement by a Pressure Probe. The Aeronautical Journal of the Royal Aeronautical Society. January 1988.
11. Ward B, Wilson P A. Experiments to Investigate Vortex Separation from an Appended Body of Revolution. MCMC Conference. University of Southampton. July 1992.

Notation

A	Maximum cross-sectional area of hull	m^2
c	Chord length	m
C_L	Lift coefficient	
C_P	Prismatic coefficient of hull : $\frac{V}{AL}$	
C'_P	Pressure coefficient : $\frac{P}{\frac{1}{2}\rho U^2}$	
D	Diameter of body of revolution	m
L	Length of hull	m
M	Total pitch moment : positive bow up	kNm
M'	$M' = \frac{M}{\frac{1}{2}\rho U^2 L^3}$	

M'_w	Non-dimensional linear pitch moment/ heave velocity co-efficient for hull	
$M'_{w\|w\|}$	Non-dimensional second order pitch moment/ heave velocity coefficient for hull	
P	Pressure	Nm^{-2}
r	Radius from body axis to position of probe	m
r'	Non-dimensional rate of turn or turn parameter ; L/S	
r_*	Core radius of vortex	m
R_e	Reynolds number : $\frac{UD}{\upsilon}$	
S	Arm radius ; radius of turn	m
U	Flow velocity	m/sec
V	Volume of hull	m^3
w	Velocity in z direction	m/sec
x	Longitudinal distance from nose of body ; positive aft	m
x'	Non-dimensional distance from nose to body ; x/L	
Y_{180}	Tactical diameter of submarine turning circle	m
z	Vertical scale	m
Z	Total force in z direction : positive down	kN
Z'	$Z' = \frac{Z}{\frac{1}{2}\rho U^2 L^2}$	
Z'_w	Non-dimensional linear heave force/ heave velocity coefficient for hull	
$Z'_{w\|w\|}$	Non-dimensional second order heave force/ heave velocity coefficient for hull	
Γ	Circulation	m^2/sec
Γ_θ	Circulation density at a given angle	$m^2/sec/rad$
α	Angle of Incidence	deg
δ	Freestone probe 'radius'	m
δ_R	Angle of deflection of rudder	deg
ζ	Vorticity	rad/sec
ρ	Density of fresh water	1.0 tonnes/m^3
θ	Angle of strut	deg or rad
υ	Kinematic viscocity of fresh water	1.14 x 10^{-5} m^2/sec
ω	Frequency	rad/sec

Experiments to Investigate Vortex Separation on an Appended Body of Revolution

by B Ward
Ship and Submarine Dynamics Section, DRA Haslar
and P A Wilson
Department of Ship Science, University of Southampton

ABSTRACT

A knowledge of hydrodynamic forces is necessary to determine the manoeuvring characteristics of a submarine design. Computer models have been used for this purpose using derivative data from model experiments. A computer model has been developed at DRA Haslar over the last decade which requires no input derivative data and hence avoids the need to carry out model experiments for each design in the early stages.

Recent validations have shown the prediction of submarine manoeuvring characteristics such as turning circle, speed loss and yaw rate in the turn, and vertical pulse manoeuvres to be good. However, predictions of depth change during turns are unsatisfactory. This is certainly due to the estimation of the out-of-plane forces which are related to the circulation around the hull.

Experiments were conducted to examine vortex separation and the pressure distribution around a submerged body of revolution with and without an appendage.

INTRODUCTION

If a body is at a moderate angle of incidence and turn rate the boundary layer on the leeward surface separates as shown in Figure 1. Vorticity shed from the boundary layer is convected away and coalesces to form a diffuse pair of vortices with cores almost parallel to the body axis. The strength of the vortices increases towards the tail of the body as more vorticity is added.

Determination of the point of separation on bodies of revolution has been a problem in fluid dynamics for sometime. The use of an empirical estimate from experimental results has tended to be the more common solution. Lloyd[1,2]

described a mathematical model, SUBSIM, which predicts the manoeuvring characteristics of submarines. The model uses a combination of classical theory and empirical equations. The empirical equations are derived from model experiments as described in Ward[3].

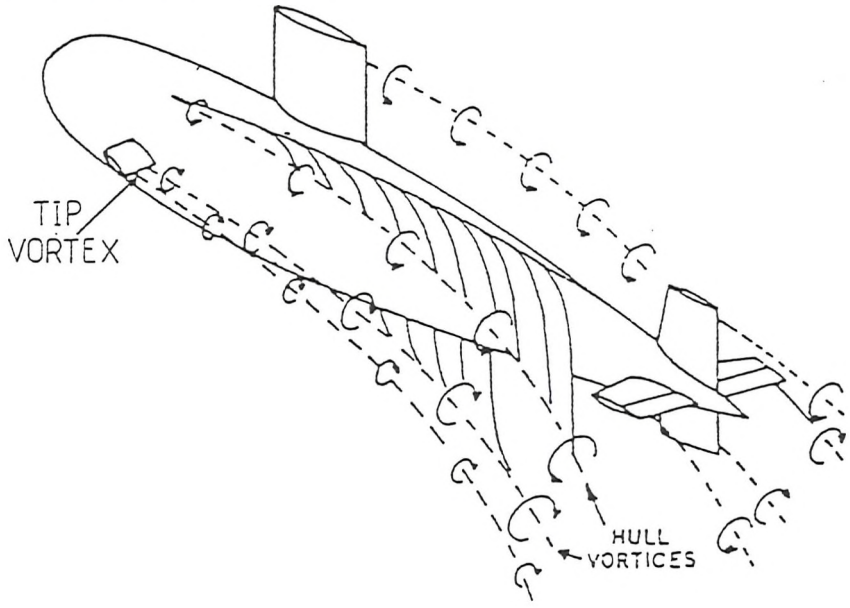

Figure 1 : A typical pattern of vortices on a manoeuvring submarine

PREVIOUS EXPERIMENTS TO INVESTIGATE VORTEX FLOW

Lloyd [4,5] described experiments to measure vortex strengths and positions. The aim was to acquire data from which empirical estimates of vorticity could be derived. The author became involved in the subsequent analysis of experiments which measured body vortices in curved flow.

The experiments were conducted on the rotating arm facility in the manoeuvring tank at DRA Haslar (formerly ARE Haslar). They were performed by the Wolfson Unit for Marine Technology and Industrial Aerodynamics (University of Southampton) working under contract.

A 5 metre body of revolution was used with fineness ratio L/D of 8.5. A Freestone[6] probe was used to measure vorticity. The probe was mounted on a stayed circular strut which could be positioned at one of three locations along the length of the model ($x'=0.7, 0.85, 0.925$). The probes radial and angular location could be adjusted.

EXPERIMENTAL PROCEDURE AND RESULTS

Runs were conducted over a range of angles of incidence and turn rates at the three stations.

A typical faired traverse is shown in Figure 2.

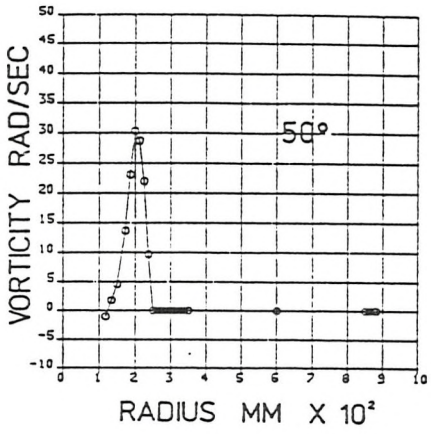

Figure 2 : A typical vorticity traverse

Measurements were taken at 10 degree angular intervals (taking 0 degrees with the strut parallel to the surface of the tank on the leeward side of the model and 90 degrees with the probe vertical above the model) at 25 mm radial steps from the body surface.

The local circulation density is

$$\Gamma_\theta = \int_0^\infty \zeta r dr \qquad (1)$$

A graph of circulation density against angle was plotted for each experiment condition and an example is shown in Figure 3. An empirical curve was derived from all results. Other equations were derived to determine positions of vortices and core radii. Figure 4 shows a representation of the flow as two symmetrical sets of vortices.

VALIDATION

The equations were incorporated into the SUBSIM computer program. The modified program was then validated by comparing predictions of submarine manoeuvres with full-scale trials results. Figure 5 is typical of a turning circle prediction where control deflections have been replicated exactly as on the trial. It can be seen that the trajectory in the lateral plane, heading and speed loss in the turn simulations are all very good. However, there are problems in predicting depth change during turns.

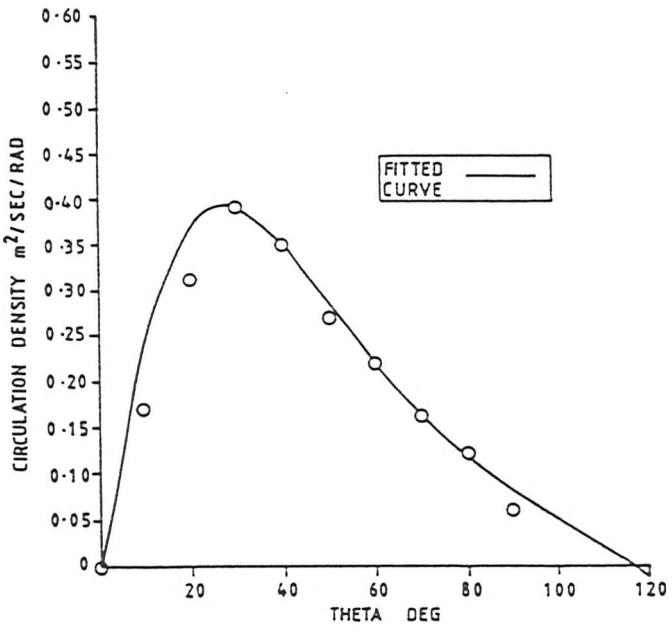

Figure 3 : Circulation density against strut angle
(x'=0.925, r'=0.4, α=5 degrees)

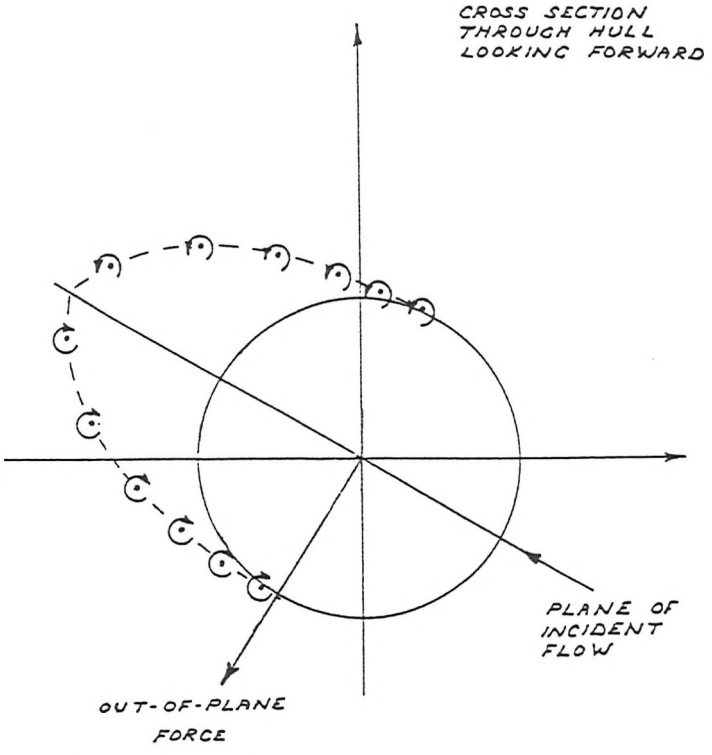

Figure 4 : Location of body vortices and out-of-plane force

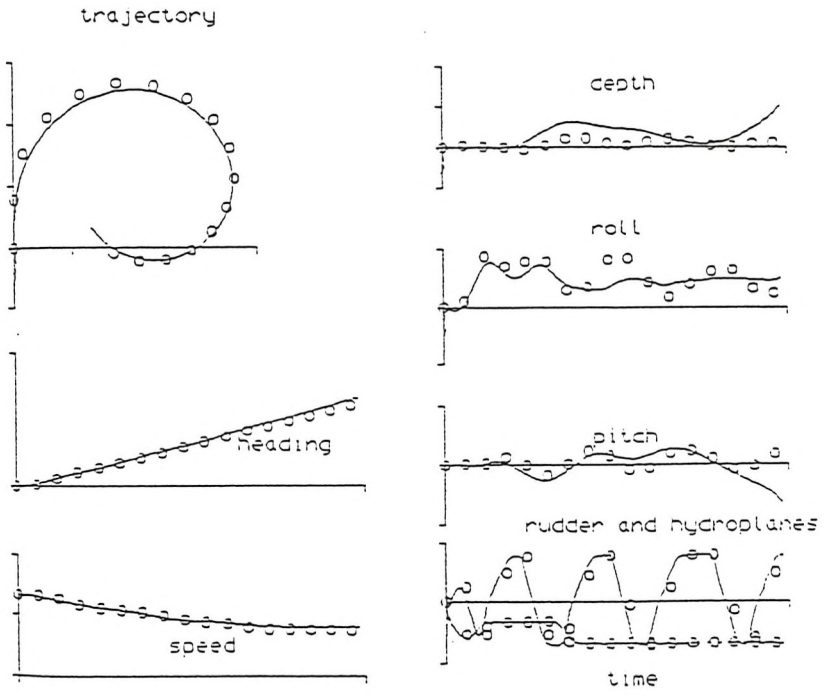

Figure 5 : Typical submarine turning circle

The reason for poor prediction of depth change in the turn is almost certainly due to unsatisfactory estimation of the out-of-plane force (Figure 4). This force is related to body vortices and as noted earlier the vortices are modelled as symmetrical pairs. This modelling would be correct in dealing with an unappended body of revolution as was the case in the experiments described above. In reality, if a change in separation point occurred on one side of the body then an asymmetry would occur in the force. This phenomenon occurs in the presence of an appendage. On a submarine the most forward appendages are the bow hydroplanes and the bridge fin. The bow hydroplanes are relatively small in relation to the submarine hull but bridge fins are usually substantial. This has caused some problems in the prediction of submarine manoeuvres.

MEASUREMENTS OF VORTICITY AND PRESSURE DISTRIBUTIONS

It was decided to conduct experiments on a body of revolution with an appendage and examine the vortical flow and pressure distribution at various cross-sections. The Freestone probe was again used to measure vorticity as in the rotating arm experiments.

MODEL HULL DESIGN

The model hull was a 1 metre body of revolution made of glass-reinforced plastic and had a fineness ratio L/D of 8.

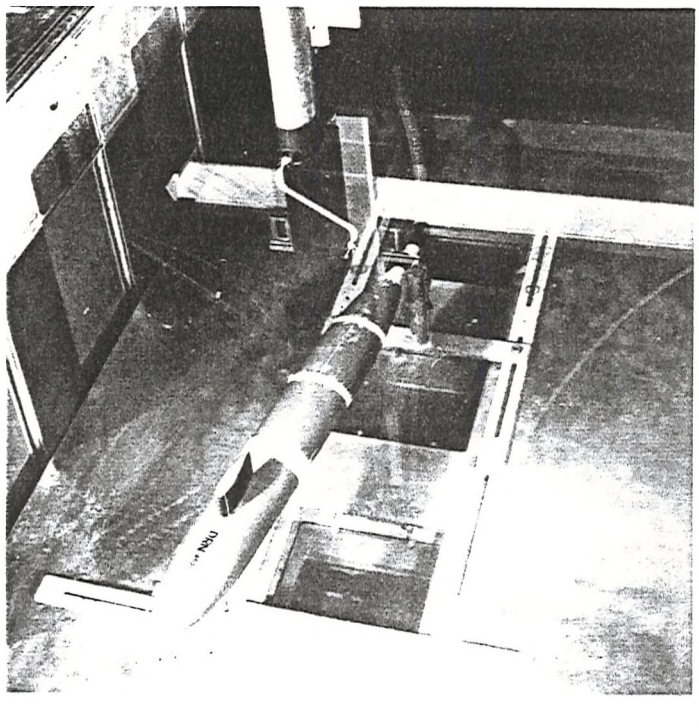

Figure 6 : Model and traverse rig

Metal rings were positioned at four stations flush with the surface of the hull with 36 pressure tappings drilled accurately at 10 degree intervals. The model had a detachable NACA 0020 wing with chord length 0.1125 metres and span 0.09 metres.

EXPERIMENTAL PROCEDURE

The experiments were conducted in the Circulating Water Channel (Figure 6) at DRA Haslar in two stages during 1990 and 1991. The model hull was tested at various conditions to explore the relationship between the vortex characteristics, angle of incidence and pressure distribution at particular cross-sections along the body. All angles of incidence were measured with the model's nose to starboard. Speed was constant at 2.5 m/s.

A traverse rig was specially designed for these experiments and was used to position the Freestone probe. For the second stage of the experiment the rig was controlled by stepper motors that gave 0.5mm positional accuracy. A single computer program was also used during the second stage to control the rig, acquire data and perform the arithmetic operations to calculate vorticity.

RESULTS

1990 RESULTS

The rig was traversed in the horizontal direction taking readings at 10mm intervals. If a fine peak was suspected say in the case of the appendage vortex a more refined mapping at 1mm intervals was carried out over the area of maximum vorticity. Horizontal traverses were made at 10mm intervals in the vertical direction. Searches at shorter step sizes were conducted in order to find the peak values for appendage vortices.

The horizontal traverses were integrated using a simple trapezoidal rule to give the circulation density. The circulation density values were then integrated (Equation 2) in the vertical direction to give the total circulation in that area of the body.

$$\Gamma = \int_{-\infty}^{\infty}\int_{-\infty}^{\infty} \zeta_x dy dz \qquad (2)$$

The results are presented in Table 1.

Table 1

x'	Body α	Fin α	Γ_D	Γ_K	Γ_D/UD	Γ_K/UD
0.575	10	0	0.001	-0.034	0.005	-0.11
0.75	10	0	0.004	-0.034	0.013	-0.11
0.925	10	0	0.009	-0.072	0.029	-0.25

Figure 7 shows a body vortex contour plot at x'=0.925. This plot is of vorticity values measured with body incidence of 10 degrees and the appendage at 0 degrees to the body.

1991 RESULTS

Vorticity was measured at x'=0.575 (with appendage) and x'=0.925 (with and without appendage) with body incidence 5, 10 and 15 degrees.

Pressure meassurements were taken at x'=0.4, 0.575, 0.75 and 0.925 with and without an appendage. The body was yawed up to an angle of 17.5 degrees. A Scanivalve was used to scan round the 36 pressure tappings at each station.

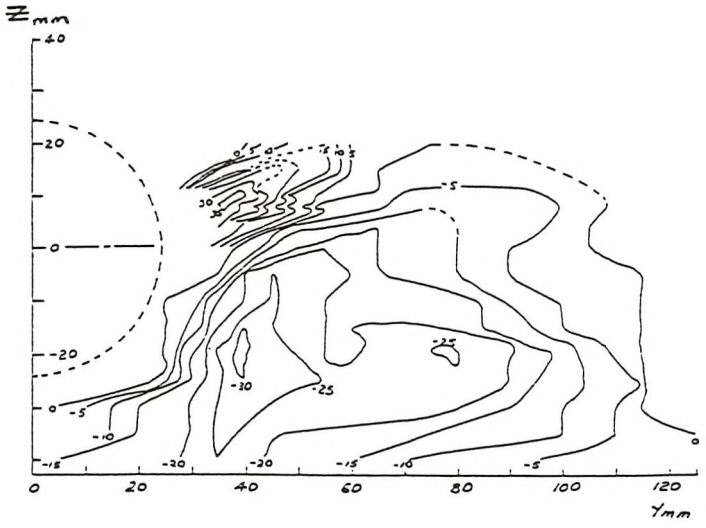

Figure 7 : Body vortex contours, ζ_x, rad/sec
body 10 degrees, appendage 0 degrees, x'=0.925

The probe used in the 1990 experiments was damaged during the rigging of the 1991 experiments and a new probe had to be manufactured. It became apparent that there were considerable offsets in the 1991 results compared with 1990. Attempts were made to correct for discrepancies but in the end no reliable method could be achieved and therefore no circulation values could be calculated. The offsets are certainly due to imperfection in the production of the new probe. On reflection it was felt that the contour plots of the 1991 results do give a qualitative feel for the circulation around the body under particular conditions. An example is given in Figure 8.

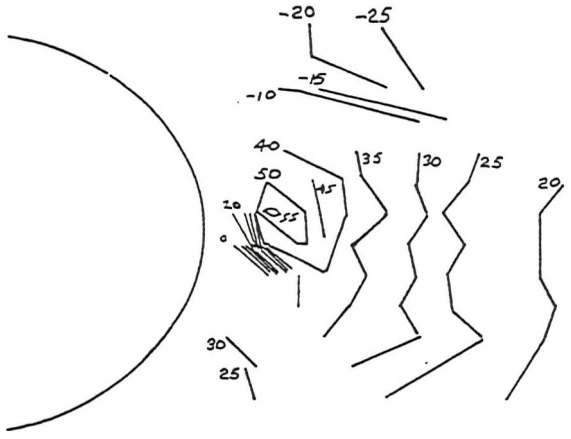

Figure 8 : Body vortex contours, ζ_x, rad/sec
body 10 degrees, appendage 0 degrees, x'=0.575

Pressure coefficients were calculated from the pressure measurements.

Figure 9 shows plots of pressure coefficients for unappended and appended bodies. Note the suction on the top of the body for the unappended case at high angles; this does not occur with the presence of the appendage.

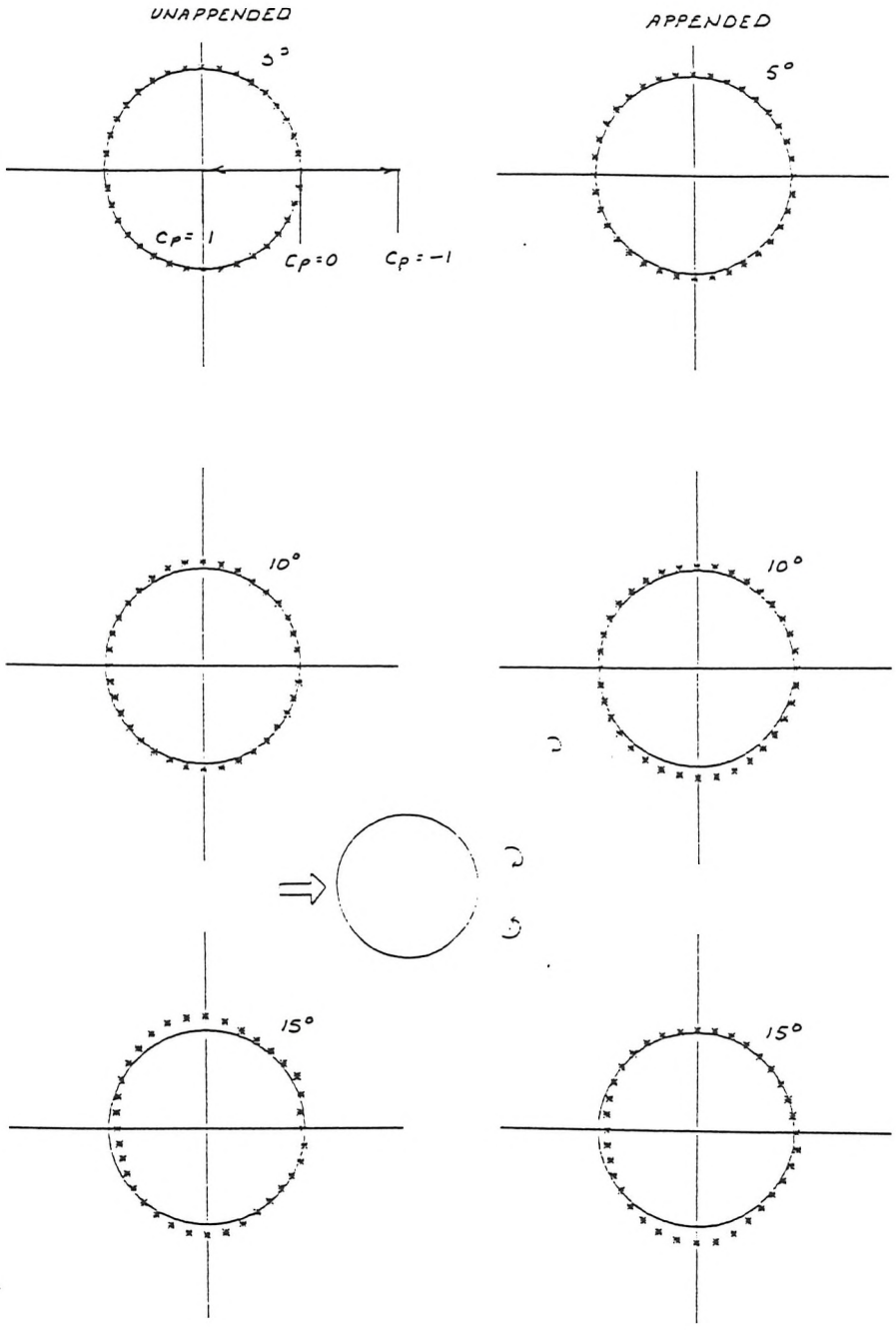

Figure 9 : Pressure coefficients, x'=0.575

Pressure coefficients were integrated to give force per unit length in both the Y and Z plane as given in equations 3 and 4.

$$F'_Y = -\frac{2\pi R}{36}\sum C_P \sin\theta_P \qquad (3)$$

$$F'_Z = \frac{2\pi R}{36}\sum C_P \cos\theta_P \qquad (4)$$

Integrated values (Figure 10) show that the distribution of side force along the body changes with the presence of an appendage.

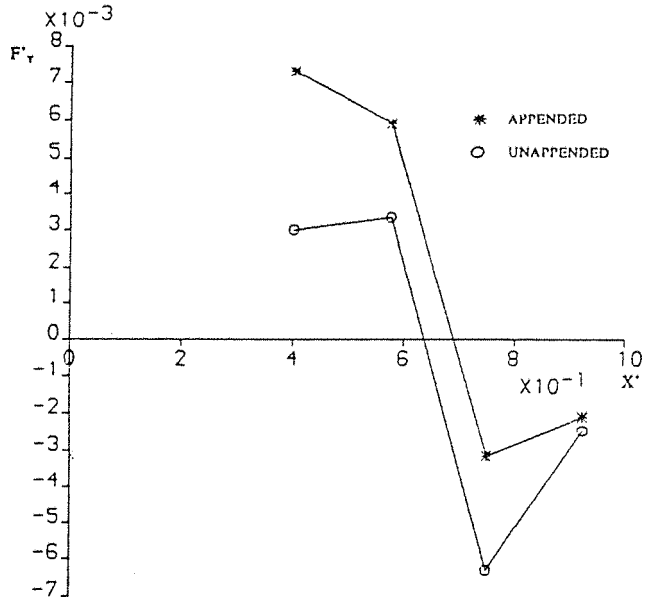

Figure 10 : Side force distribution at 15 degrees yaw

Figure 11 shows Z force distribution for the appended case. There is a significant downward force on the model which gets higher as the model is yawed to higher angles.

The body was held fixed at zero incidence with the appendage at an angle. The force on the body due to the isolated vortex was then examined. These values were small but variations did exist between station and angle. There is less significant effect on the body due to an isolated vortex compared with the change in pressure distribution for a body yawed at a high incidence. However, the presence of the appendage does change the pressure distribution around the body when the body is yawed.

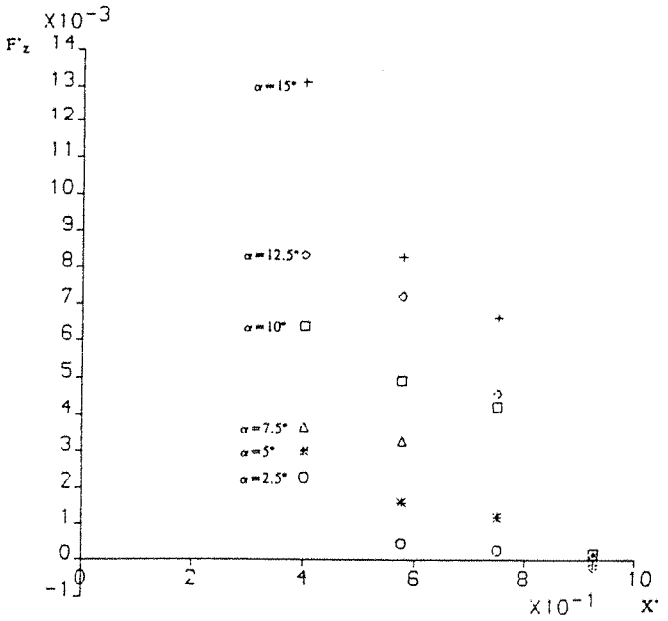

Figure 11 : Z force distribution for appended body

DISCUSSION OF VORTEX RESULTS

From the vorticity contour plots an asymmetry between the deck and the keel vortices is apparent i e the keel vortex covers a much larger area. The values for circulation in Table 1 confirm this. Vorticity contours for x'=0.575 show there appears to be a single vortex certainly shed from the keel side of the body. For x'=0.925 there is evidence of two distinct vortices.

Table 1 shows at x'=0.575 Γ_D=0.001 which builds up to 0.009 at x'=0.925. Hence there is evidence of a deck vortex at x'=0.575.

The SUBSIM model at present assumes no separation until x'=0.65 and then two identical sets of vortices are created which as mentioned earlier is not the case in reality.

The change in circulation around the aft end of the body is not caused by the vortex from the tip of the fin but the presence of the fin itself. The fin acts as a spoiler and delays the longitudinal point of separation hence the reduced strength of the upper body vortex (Figure 12).

With the fin at 0 degrees aligned to the body and the body yawed at 10 degrees, the circulation from the fin was found to be Γ_F=0.07 which makes the total circulation approximately zero, as predicted by Stokes' theorem. Perhaps this factor could point the way to modelling the reduced strength of the upper body vortex. Taking the whole body as one closed system the circulation will add up to zero as shown in Figure 12.

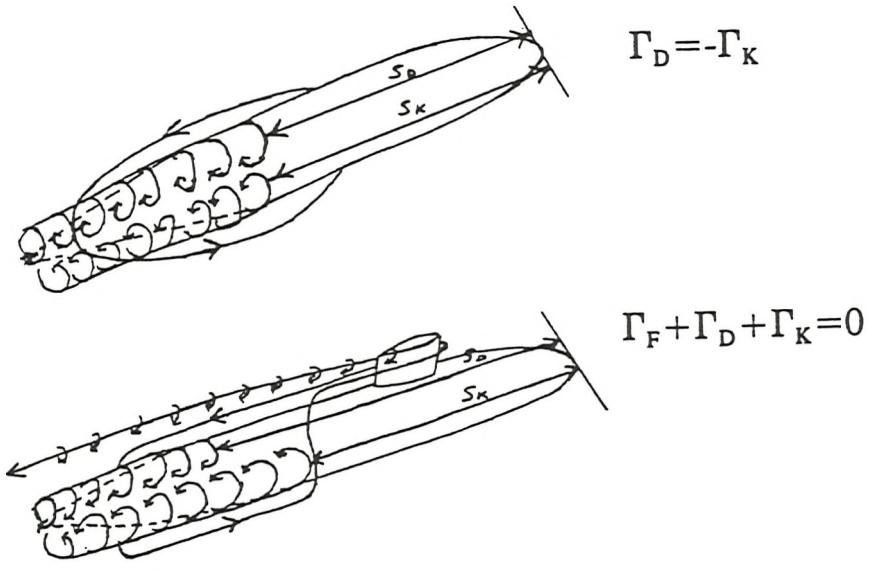

Figure 12 : Separation point and distribution of circulation

CONCLUSIONS

This paper has described experiments to examine the flow around an appended body of revolution. The model was tested over a range of angles with and without an appendage. The effects of the appendage on circulation around the body and pressure around the hull are evident from the results.

The findings of these experiments suggest that the method of calculating the out-of-plane forces in SUBSIM is unsatisfactory. At present the method only accounts for appendage vortices and the interaction between appendage vortices and body vortices. No account is taken of body vortices since they are modelled as symmetrical pairs and it has been assumed that they do not contribute to the out-of-plane force. However, it is necessary to model the body vortices correctly to account for the change the appendage makes to the circulation around the body. It may be sufficient to calculate the force on the body due to these modified body vortices alone. Further work is required to acquire more accurate data, perhaps in a towing tank with a larger model.

ACKNOWLEDGEMENTS

This work has been carried out with the support of the Procurement Executive of the Ministry of Defence.

REFERENCES

1. Lloyd A R J M. Progress Towards a Rational Method of Predicting Submarine Manoeuvres. RINA Symposium on Naval Submarines. London 1983.
2. Lloyd A R J M. Developments in the Prediction of Submarine Manoeuvres. Undersea Defence Technology. 1988.
3. Ward B. Experiments to Improve the Predictions of Submarine Manoeuvres. MCMC Conference. University of Southampton. July 1992.
4. Lloyd A R J M, Campbell I F. Experiments to Investigate Vortices Shed from a Submarine-like Body of Revolution. 59th Meeting of the AGARD Fluid Dynamics Panel Symposium, Monterey, California, USA. Aerodynamics and Related Hydrodynamic Studies Using Water Facilities. AGARD-CCP 413. October 1986.
5. Lloyd A R J M. Experiments to Investigate the Vorticity Shed by a Body of Revolution in Curved Flow. Advances in Underwater Technology, Ocean Science and Offshore Engineering. Volume 15: Technology Common to Aero and Marine Engineering. 1988.
6. Freestone M M. Vorticity Measurements by a Pressure Probe. The Aeronautical Journal of the Royal Aeronautical Society. January 1988.

Notation

C_P	Pressure coefficient ; $P/0.5\rho U^2L$	
D	Diameter of hull	m
F'_Y	Side force per unit length/$0.5\rho U^2L$: positive to starboard	
F'_Z	Downward force per unit length/$0.5\rho U^2L$: positive down	
K	Calibration factor for Freestone probe	
L	Length of hull	m
P	Pressure	Nm^{-2}
r	Radius from body axis to position of probe	m
r'	Non-dimensional rate of turn or turn parameter ; L/S	
R	Radius of model at cross-section	m
S	Arm radius ; radius of turn	m
S_D	Longitudinal point of separation - deck side of body	m
S_K	Longitudinal point of separation - keel side of body	m
U	Flow velocity	m/s
x	Longitudinal distance from nose of body : positive aft	m
x'	Non-dimensional distance from nose to body ; x/L	
y	Lateral distance from body centre : positive starboard	mm
z	Vertical distance from body centre	mm
Γ	Circulation	m^2/s
Γ_θ	Circulation density at a given angle	$m^2/s/rad$

Γ_D	Circulation from body - deck side : positive clockwise looking forward	m^2/s
Γ_F	Circulation from fin : positive clockwise looking forward	m^2/s
Γ_K	Circulation from body - keel side : positive clockwise looking forward	m^2/s
α	Angle of incidence	deg
ζ	Vorticity	rad/s
ρ	Mass density of fresh water	tonnes/m^3
θ	Angle of strut	deg
θ_P	Angular location of pressure tapping 0 degrees pointing up, positive clockwise looking forward	deg